Statistical Model of Sonic Boom Structural Damage

Booz-Allen Applied Research, Inc.

July 1976

Report No. FAA-RD-76-87

STATISTICAL MODEL OF SONIC BOOM STRUCTURAL DAMAGE

Robert L. Hershey

Thomas H. Higgins

July 1976

Final Report

Prepared for

U.S. DEPARTMENT OF TRANSPORTATION

FEDERAL AVIATION ADMINISTRATION

Systems Research & Development Service

Washington, D.C. 20590

TECHNICAL REPORT STANDARD TITLE PAGE

1. Report No.	2. Government Accession No.	3. Recipient's Catalog No.
FAA-RD-76-87		

4. Title and Subtitle	5. Report Date
STATISTICAL MODEL OF SONIC BOOM STRUCTURAL DAMAGE	July 197
	6. Performing Organization Code

7. Author(s)	8. Performing Organization Report No.
Robert L. Hershey and Thomas H. Higgins	

9. Performing Organization Name and Address	10. Work Unit No.
Booz, Allen Applied Research 4733 Bethesda Avenue Bethesda, Maryland 20014	11. Contract or Grant No. DOT-FA72WA-2823

12. Sponsoring Agency Name and Address	13. Type of Report and Period Covered
Department of Transportation Federal Aviation Administration Systems Research and Development Service Washington, D.C. 20590	Final Report
	14. Sponsoring Agency Code ARD-5[illegible]

15. Supplementary Notes

16. Abstract

The probabilities of structural damage from sonic booms were estimated for various susceptible structural elements using a statistical modeling technique. The breakage probabilities were found to vary widely with the specific material configuration, but to consistently increase with increasing nominal overpressures. The ranges of breakage probabilities at a nominal overpressure of 1 psf for typical configurations of susceptible materials were as follows: windows—4×10^{-6} to 3×10^{-8}, plaster—3×10^{-4} to 5×10^{-7}, bric-a-brac—1×10^{-6} to 1×10^{-8}, brick walls—6×10^{-7} to 1×10^{-9}. The results of the modeling tend to agree well with sonic boom claims experience.

17. Key Words		18. Distribution Statement
Sonic Boom	Statistical Simulation	Document is available to the public through the National Technical Information Service, Springfield, Virginia 22161.
Plaster	Random Loading	
Brick	Bric-a-Brac	
Glass	Impact	

19. Security Classif. (of this report)	20. Security Classif. (of this page)	21. No. of Pages	22. Price
Unclassified	Unclassified	142	6.00/2.25

Form DOT F 1700.7 (8-69)

PRICES SUBJECT TO CHANGE

The contents of this report reflect the views of Booz, Allen Applied Research which is responsible for the facts and the accuracy of the data presented herein. The contents do not necessarily reflect the official views or policy of the Department of Transportation. This report does not constitute a standard, specification or regulation.

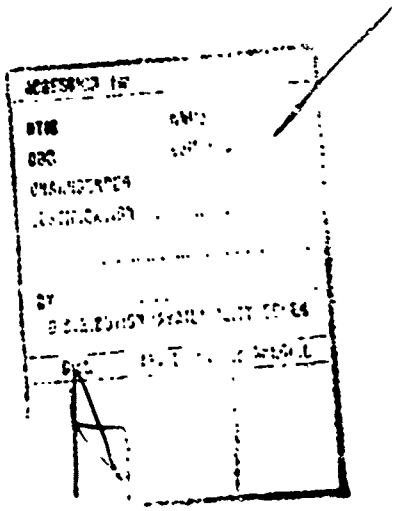

METRIC CONVERSION FACTORS

Approximate Conversions to Metric Measures

Symbol	When You Know	Multiply by	To Find	Symbol
	LENGTH			
in	inches	*2.5	centimeters	cm
ft	feet	30	centimeters	cm
yd	yards	0.9	meters	m
mi	miles	1.6	kilometers	km
	AREA			
in^2	square inches	6.5	square centimeters	cm^2
ft^2	square feet	0.09	square meters	m^2
yd^2	square yards	0.8	square meters	m^2
mi^2	square miles	2.6	square kilometers	km^2
	acres	0.4	hectares	ha
	MASS (weight)			
oz	ounces	28	grams	g
lb	pounds	0.45	kilograms	kg
	short tons (2000 lb)	0.9	tonnes	t
	VOLUME			
tsp	teaspoons	5	milliliters	ml
Tbsp	tablespoons	15	milliliters	ml
fl oz	fluid ounces	30	milliliters	ml
c	cups	0.24	liters	l
pt	pints	0.47	liters	l
qt	quarts	0.95	liters	l
gal	gallons	3.8	liters	l
ft^3	cubic feet	0.03	cubic meters	m^3
yd^3	cubic yards	0.76	cubic meters	m^3
	TEMPERATURE (exact)			
°F	Fahrenheit temperature	5/9 (after subtracting 32)	Celsius temperature	°C

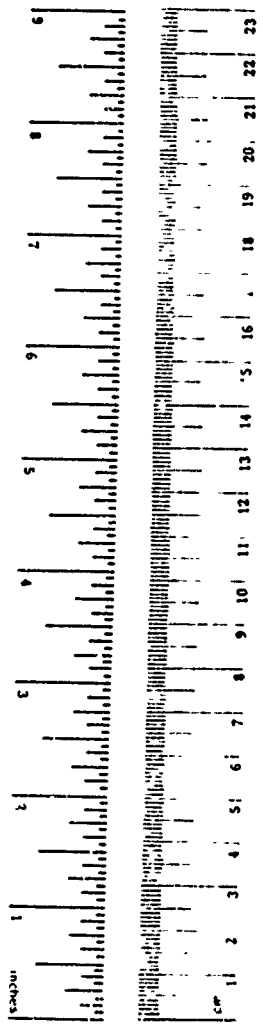

Approximate Conversions from Metric Measures

Symbol	When You Know	Multiply by	To Find	Symbol
	LENGTH			
mm	millimeters	0.04	inches	in
cm	centimeters	0.4	inches	in
m	meters	3.3	feet	ft
m	meters	1.1	yards	yd
km	kilometers	0.6	miles	mi
	AREA			
cm^2	square centimeters	0.16	square inches	in^2
m^2	square meters	1.2	square yards	yd^2
km^2	square kilometers	0.4	square miles	mi^2
ha	hectares (10,000 m^2)	2.5	acres	
	MASS (weight)			
g	grams	0.035	ounces	oz
kg	kilograms	2.2	pounds	lb
t	tonnes (1000 kg)	1.1	short tons	
	VOLUME			
ml	milliliters	0.03	fluid ounces	fl oz
l	liters	2.1	pints	pt
l	liters	1.06	quarts	qt
l	liters	0.26	gallons	gal
m^3	cubic meters	35	cubic feet	ft^3
m^3	cubic meters	1.3	cubic yards	yd^3
	TEMPERATURE (exact)			
°C	Celsius temperature	9/5 (then add 32)	Fahrenheit temperature	°F

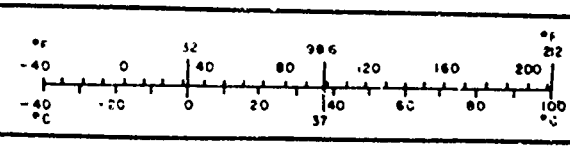

PREFACE

The advice and assistance of associates at Booz, Allen Applied Research was sincerely appreciated: Mr. John Wing. Mr. David Weiss. Dr. Russ Kevala, and Mrs. Sharon Burns Holcombe.

The authors would like to thank all those individuals and organizations who provided data for this study and for our predecessor study on glass upon which this one is based:

National Bureau of Standards:
Dr. Edward B. Magrab
Mr. E. V. Lyndecker
Mr. James Gross
Mr. James Cliston
Mr. Webster Capps
Dr. Sheldon M. Wiederhorn
Mr. James R. Clifton

National Concrete Masonry Association:
Mr. Thomas Redmond

National Gypsum Company:
Mr. David Bieri

Gypsum Association:
Mr. Herbert B. Carlson
Mr. C. M. Hedlund

U. S. Gypsum Company
Mr. J. M. Sommerfield

Brick Institute of America:
Mr. Alan Yorkdale

National Lime Association:
Mr. Kenneth Gutschick

NASA Langley:
Dr. Harvey H. Hubbard
Mr. Domenic J. Maglieri
Mr. Harry W. Carlson
Mr. Arnold W. Mueller

John A. Blume and Associates:
Mr. Lloyd Lee

Wyle Laboratories:
Mr. Robert White

Libbey-Owens-Ford Company

PPG Industries:
Mr. Robert W. McKinley

Corning Glass Works:
Dr. John S. McCartney
Dr. John Munier

Alfred University:
Dr. Charles H. Greene
Dr. Harry Stevens

Air Force Office of Research:
Mr. Mathew J. Kerper

Naval Research Laboratory:
Dr. Steve Freiman

Virginia Polytechnic Institute:
Dr. Robert Heller

University of Southhampton:
Dr. G. M. Lilley

Royal Aircraft Establishment:
Mr. David R.B. Webb

TABLE OF CONTENTS

INDEX OF FIGURES

INDEX OF TABLES

I. INTRODUCTION

There is a considerable body of data on sonic boom structural damage effects from various experiments that have been conducted over the past fifteen years. Experiments have shown that there is a small but finite probability of sonic booms breaking especially susceptible items such as windows, plaster, and bric-a-brac. The probability of breakage was consistently found to increase with higher overpressure sonic booms. The results of the experiments have in general agreed with the Air Force's experience in reimbursing damage claims from the public from supersonic overflights. The claims most frequently substantiated and reimbursed have been for damage to glass, plaster, and bric-a-brac.

Window glass is generally the most susceptible element in a house to sonic boom damage. Our previous work [1, 2, 3, 4] has determined the probability of breakage of various window configurations as a function of sonic boom overpressure. It was calculated from our statistical model that for a typical window population there would be 1.1 breaks per million panes in good condition boomed at a nominal overpressure of 1 pound per square foot (psf). This estimate agreed well with sonic boom claims data.

The statistical modeling method which was used in the previous studies of glass breakage is a method we call "the response probability density function technique." This technique, which will be described in detail in another chapter, combines the probability density function (pdf) of the sonic boom stress with the pdf of the material strength. The resultant pdf readily yields the probability of structural failure.

Since the response pdf technique was first applied to sonic booms on glass in 1972-73 we have made substantial progress in extending it to other structural response applications. It was applied to estimating the probability of air terminal window breakage from the noise from taxiing aircraft in 1974 [5]. Then in 1975 it was applied in the Concorde environmental impact statement to determine the breakage probabilities of windows, plaster ceilings, stone bridges, and brick chimneys to noise from subsonic overflights. On the basis of the success of the technique for these cases, this study extends the method to prediction of sonic boom breakage for plaster, bric-a-brac, and brick. Thus, with the glass previously accounted for and the three items considered in this study, there is now a comprehensive treatment for predicting the probability of breakage for the vast majority of sonic boom structural damage cases.

II. SONIC BOOM LOADING

The basic problem in sonic boom breakage prediction is one of finding the stress created by a transient overpressure. The overpressure caused by a sonic boom is usually an N-wave (see Figure 1). Those small variations in the wave shape that make some individual waves more peaked or more rounded than the ideal N-wave have little influence on the results derived here. These variations are accounted for in the fact that the present statistical model's parameters were derived from actual field data which represented the typical waveforms encountered. The paragraphs which follow review the definitions of the parameters shown in Figure 2.

1. NOMINAL OVERPRESSURE, p_o

Adequate methods presently exist for calculating a predicted peak sonic boom overpressure value based on aircraft's altitude, speed, weight, and dimensions [7]. This calculated value is called the nominal overpressure, p_o. Its value is generally in the range of 1 psf to 4 psf for typical supersonic aircraft operations. It is desired to predict P, the probability of a window being broken by a given boom, as a function of p_o.

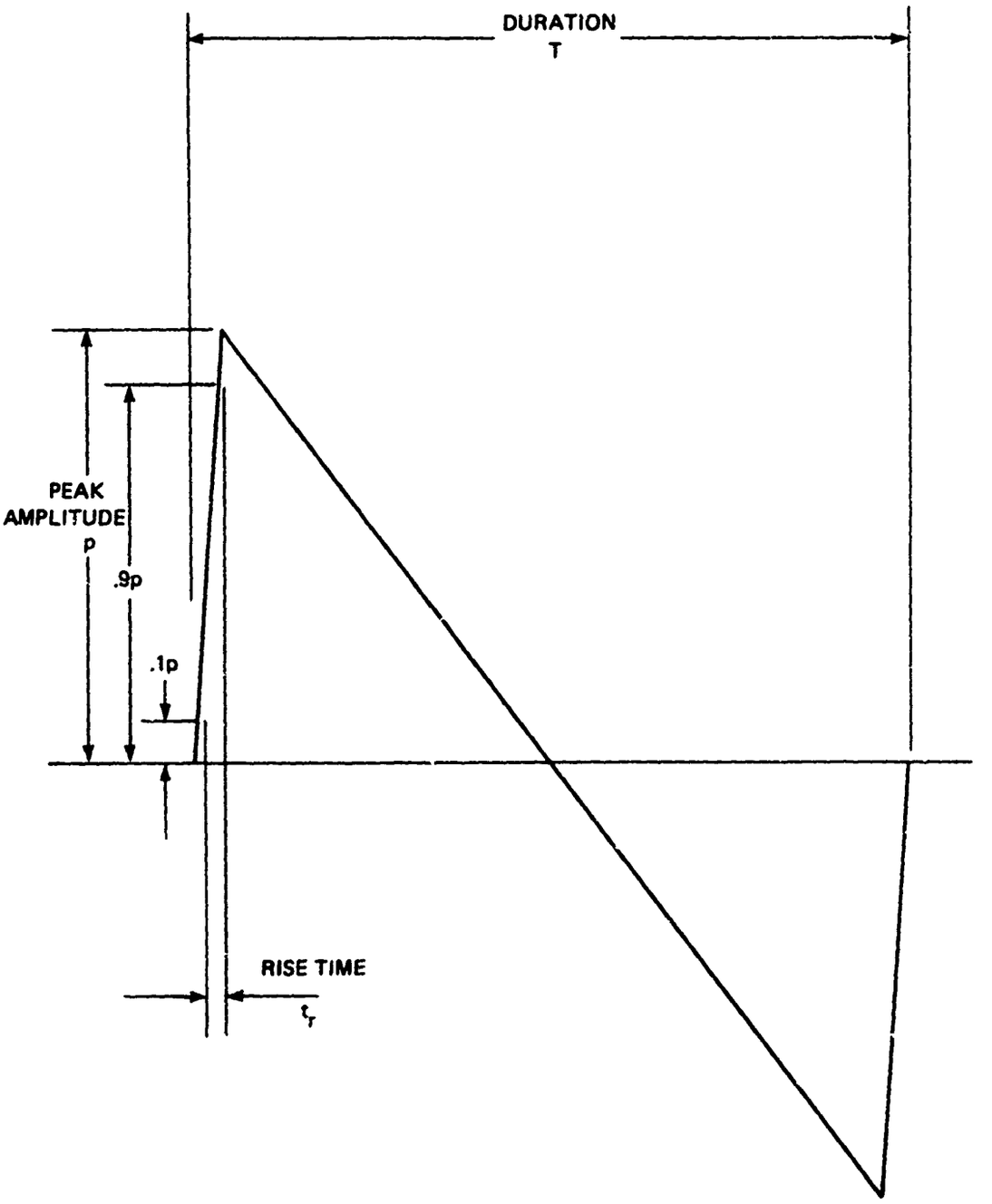

Figure 1. Typical N-Wave

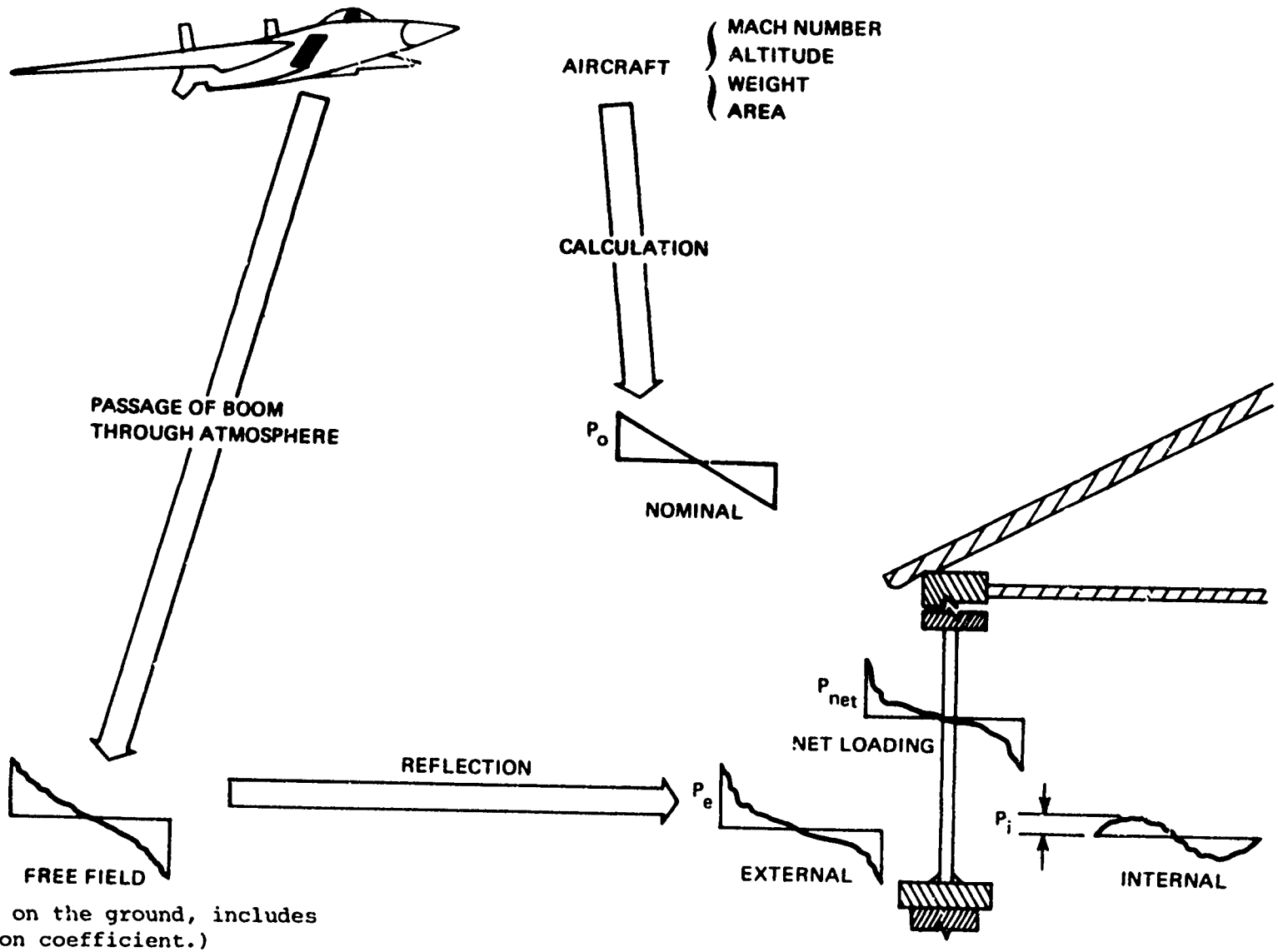

Figure 2. Evolution of Sonic Boom Load

2. FREE FIELD OVERPRESSURE, p_f

The sonic boom suffers various attenuation and focusing effects in passing through the atmosphere to the ground. The random inhomogeneities in the atmosphere cause a spread in the range of values of the peak free field overpressure (p_f) that is measured on the ground. By convention, the value of p_f is measured with a microphone mounted on the ground, usually on a plywood board. This method of measurement results in a pressure doubling effect from the ground reflection being included in the value of p_f. Thus the measured value, p_f, is not really a free field pressure as the term is commonly used in acoustics, but it is conventionally called this in the sonic boom community. Similarly, the calculation of p_o, the nominal pressure, includes a conventional value of the ground reflection coefficient of 1.9. In general, the mean value of p_f will be very close to p_o, but individual values of p_f will exhibit considerable spread. This random effect results from the atmospheric inhomogeneities and from differences in the aircraft operating parameters from those used for calculating p_o.

3. EXTERNAL OVERPRESSURE, p_e

When a sonic boom having a free field peak overpressure p_f impinges on a structure it creates an external overpressure waveform having a peak value p_e. The value of p_e will depend on the angle the

incoming wave makes with the structure, the reflection coefficient of the structure surface, and whether the wave combines with other waves reflected off other structures or the ground. For instance, it has generally been observed in experiments [8, 9] that the side of a house exposed to a head-on sonic boom wave exhibits a much higher overpressure than the opposite side. There have been some attempts [10, 11, 12] to obtain analytical solutions for p_c in terms of p_f by modeling the acoustical scattering. These attempts, however, involved complicated computer solutions which were applicable only to a single structure geometry and wave angle. For practical engineering situations, the relation between p_f and p_e would seem to be best treated by statistical methods.

4. INTERNAL OVERPRESSURE, p_i

The waveform of the overpressure inside a structure depends on the transmissibility of the structure to sound as a function of its geometry. The solution for the internal waveform is quite complicated and differs for each structure [13, 14]. It is generally observed [13, 14] that the internal overpressure waveform is sinusoidal with a period the same as that of the N-wave and a peak value p_i which is some fraction of the external peak overpressure p_e. Subtracting the waveform of the internal pressure from that of the external pressure gives the net loading waveform acting on the window (see the top of Figure 3).

p_e = peak external pressure
p_i = peak internal pressure
q = p_i/p_e internal pressure ratio

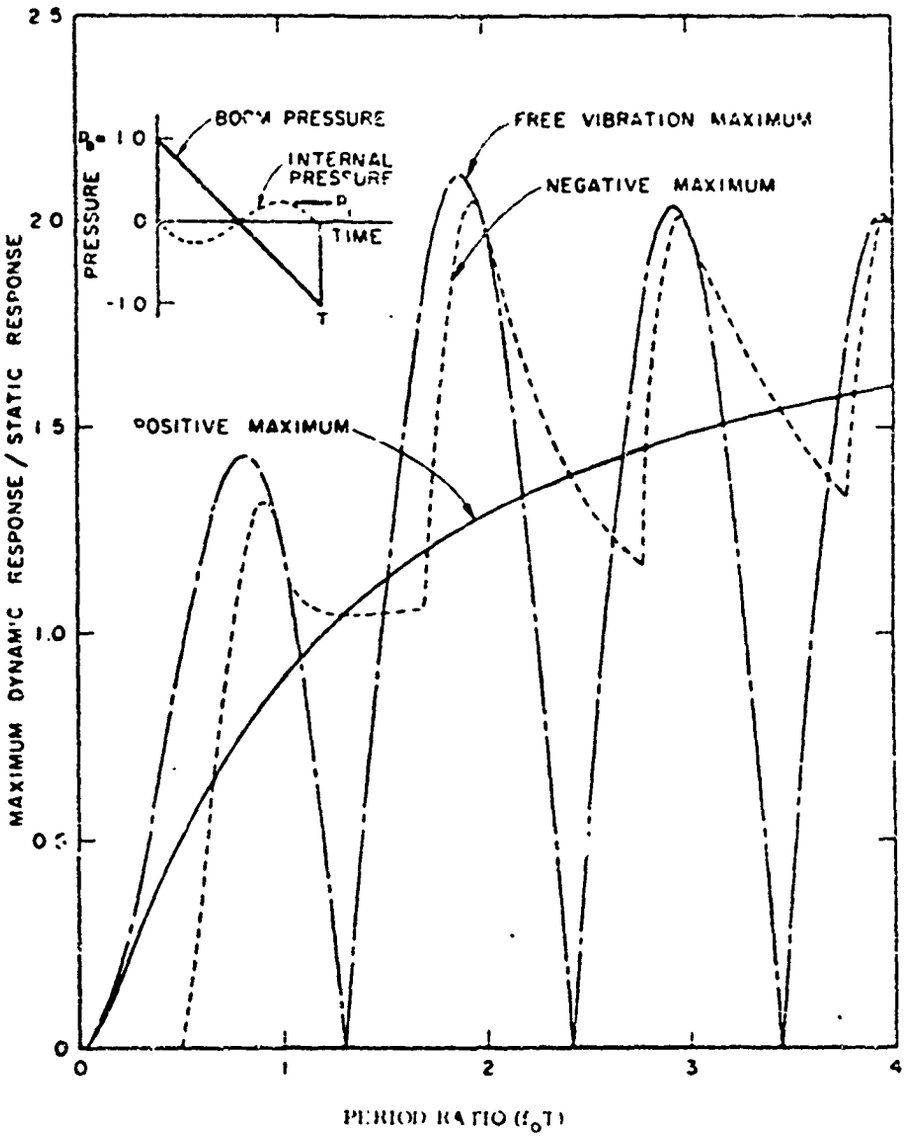

Figure 3. Dynamic Amplification Factor for First Mode Deflection of a Square Plate to Boom and Internal Pressure: q = 0.25

5. STATIC STRESS

The analysis of the loading of a structure by a sonic boom has been a problem that has attracted much interest in the past fifteen years [9, 14-21]. Generally these analyses have included a comparison with loading under uniform static pressure. This is because most structural elements are designed to static wind loading, and hence static pressure design data are much more readily available than sonic boom loading data.

A window configuration, for instance, is usually assumed to be a rectangular plate simply supported at all four edges; which has been found to agree with experimental studies of static window loading [22]. For small deflections, the stress is a linear function of the static pressure and is given by the well-known formula [23]

$$\sigma_s = \frac{p_s a^2 b^2}{2h^2(a^2+b^2)} \tag{1}$$

where σ_s is the extreme fiber stress at the center of the plate, p_s is the static pressure, a is the longer side of the rectangle, b is the shorter side, and h is the thickness of the plate.

6. DYNAMIC AMPLIFICATION FACTOR (DAF)

Since windows are usually designed to static load requirements, it is desirable to compare sonic boom loads to such static loads. This

is accomplished by finding the dynamic amplification factor (DAF) defined by

$$DAF = \frac{\sigma_m}{\sigma_d}. \tag{2}$$

The numerator of the DAF is the maximum stress in the plate and the denominator is the dynamic stress defined by

$$\sigma_d = \frac{p_e a^2 b^2}{2h^2(a^2+b^2)} = p_e F \tag{3}$$

where F is a stress factor. Note that σ_d is the stress that would be produced by a static pressure equal in magnitude to the peak external pressure p_e.

Throughout the literature there are various definitions of DAF. Some definitions use a ratio of deflections rather than stresses, and others use the peak value of the net loading waveform p_{net} rather than p_e, the peak value of the external pressure waveform. Since the problem at hand is one of rupture and not deflection the current definition was deemed more appropriate. In the definition of σ_d of (3) it was decided to use p_e rather than p_{net} because (a) p_e is more easily measured, (b) p_e is very nearly equal to p_{net} as can be seen from the top of Figure 3, (c) the available overflight data base contains only values of p_e, and (d) it was found by statistical analysis that the internal pressure does not correlate well with window stress.

7. SONIC BOOM STRESS ANALYSIS

According to theory, when a thin plate such as a window is loaded to the extent that its deflection exceeds one half its thickness, nonlinear effects start to come into play. This results because membrane stresses become comparable in magnitude to the bending stresses. Because of this effect, the stress will be somewhat lower than that predicted by Equation 1 once the deflection starts to exceed one half the thickness. The nonlinear differential equations for large deflections have been solved in recent years [24, 25] and the results have been presented as a series of graphs for rectangles having various aspect ratios [26].

Unfortunately the stresses in glass plates correlate very poorly with large deflection theory [14]. Although the center deflections of the plates follow the nonlinear theory fairly well the stresses do not. Thus what some authors [14-16] have done is to calculate DAF's on the basis of deflection using dynamic analysis with the nonlinear theory. It can be seen from Figures 3 and 4 from the linear theory and Figure 5 from the nonlinear theory that the envelopes of the DAF curves seem to range between 1 and 2 whether the linear or nonlinear theory is used. The curves in Figures 3 and 4 were developed by Seaman [14] using the conventional approach of modeling the window as a linear single degree of freedom system, finding its impulse response, and convolving with the excitation to find the maximum excursion. The slight difference

p_e = peak external pressure
p_i = peak internal pressure
q = p_i/p_e internal pressure ratio

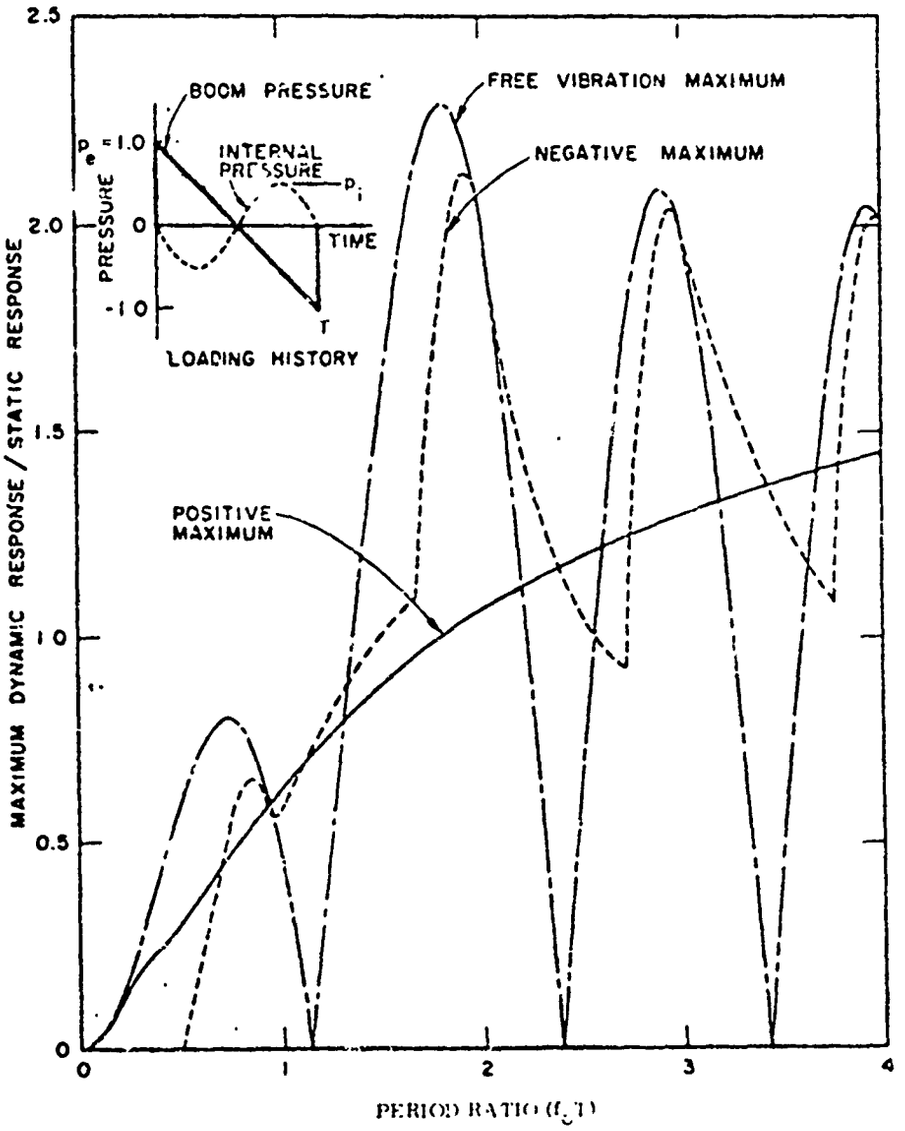

Figure 4. Dynamic Amplification Factor for First Mode Deflection of a Square Plate to Boom and Internal Pressure: $q = 0.50$

between the curves in Figures 3 and 4 results from the fact that Figure 3 uses an internal pressure ratio $q = \frac{p_i}{p_e} = .25$ and Figure 4 has $q = .5$. Since these figures resulted from linear analysis the deflection DAF's shown are numerically equal to stress DAF's. Seaman then went through a large deflection analysis which resulted in the curve in Figure 5. The other references cited [15-21] all displayed results similar to Seaman's. These three curves are introduced here to point out two striking similarities which hold regardless of whether deflection is assumed linear or nonlinear and no matter how great the value of q:

1. Most of the values of the DAF are between 1 and 2.
2. The values of the DAF below 1 occur only for small values of the period ratio, for cases where a structural element with a low resonant frequency f_o is excited by a short duration boom with a small value of T.

The second point above emphasizes that the structural element's frequency can be important in some cases. Assuming linear deflection and simple support around all four edges of a plate, its natural frequency is [27]

$$f_o = \frac{\pi h}{2}\sqrt{\frac{Y}{12\rho(1-\nu^2)}}\left(\frac{1}{a^2} \quad \frac{1}{b^2}\right) \tag{4}$$

where Y is Young's modulus, ρ is the mass density, and ν is Poisson's ratio. A case of a low period ratio can occur when an F-104 aircraft

h = thickness of plate

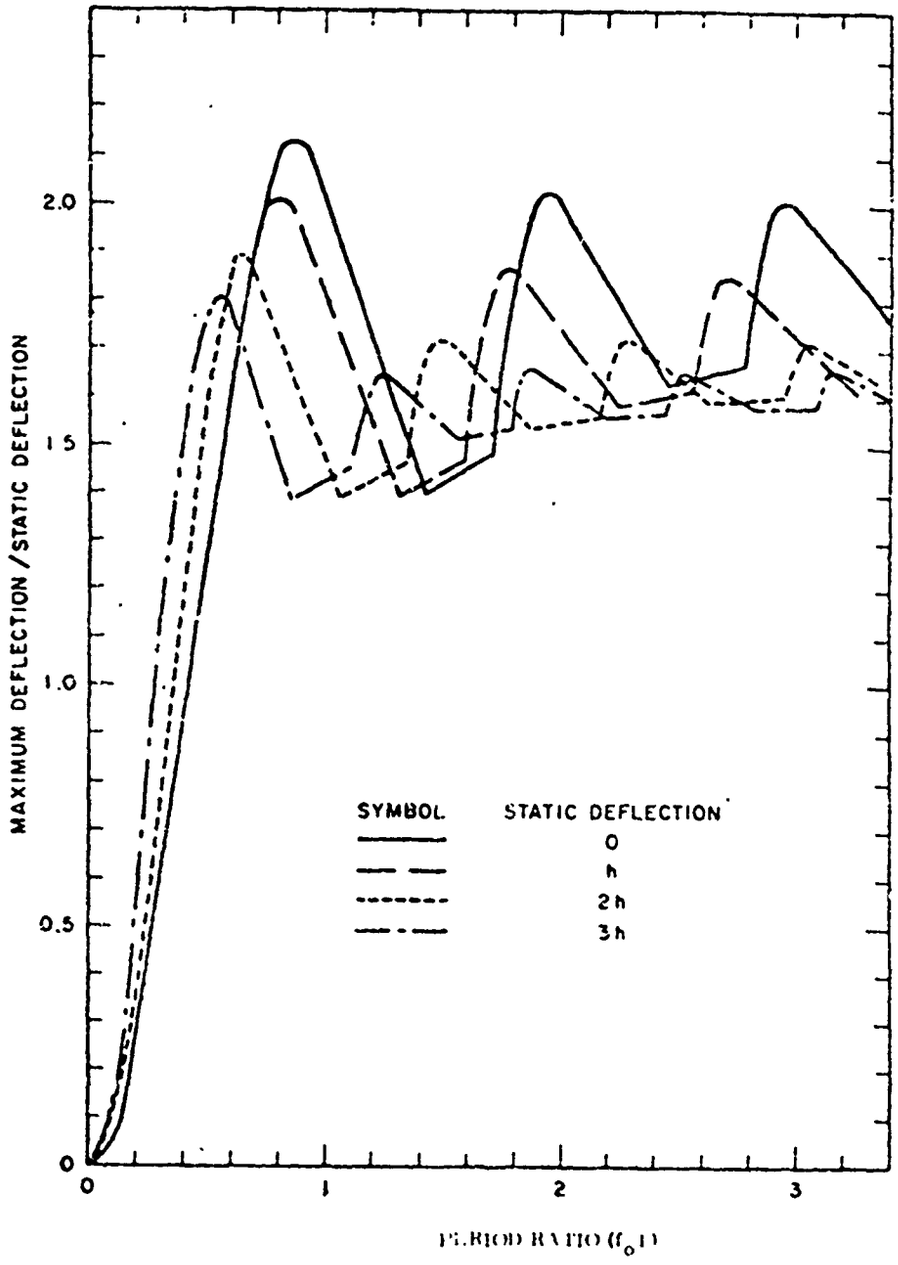

Figure 5. Summary of Nonlinear First Mode Deflection of a Square Plate to a Boom Loading

with T = .067 sec booms a large storefront window with f_o = 4Hz. In this case, the window suffers minimal deflection because the excitation is considerably above the window's natural frequency.

In the present study the linear stress theory of Equation (1) is used exclusively. The reasons for disregarding the large deflection theory here are the following:

1. The DAF measurements used in the present study were at small deflections in the linear range.
2. The large deflection theory gives poor results for predicting breaking stress.
3. The coefficient relating stress to pressure in Equation (1) will be seen to cancel out later in the analysis anyway. In effect we will be working only with boom pressure and breaking pressure, assuming the relation between stress and pressure to be linear between the sonic boom test pressures and the structural element breaking pressures. This allows the use of linear transformations.

Having surveyed the problem of sonic boom loading, the discussion will now review the data from sonic boom structural response experiments.

III. SONIC BOOM EXPERIMENTS

A large data base consisting of over 70,000 readings from various experiments of the past twelve years has been utilized in this study. The experiments which generated this data were the following:

1. Oklahoma City Sonic Boom Tests performed by FAA and NASA in 1964 [28].
2. White Sands Sonic Boom Structural Reaction Tests performed by FAA in 1965 [29,30].
3. Edwards Air Force Base Sonic Boom Tests performed by FAA and NASA in 1966 [31,32].

Each of these experiments will now be described, together with the contribution of its data to the present study.

1. OKLAHOMA CITY TESTS

The sonic boom tests conducted in the Oklahoma City area from April to July 1964 were primarily to determine community response. In addition to surveying how acceptable the booms were to the public, the tests also included measurements of ground overpressure. The

overpressures measured were values of p_f, the peak free field overpressure. Over 3500 sonic boom signatures were recorded during this test series. These signatures form the basis of the present analysis of the relation between peak nominal pressure p_o and peak free field pressure p_f.

The aircraft used to produce the Oklahoma City sonic booms were the F-104, F-101, F-106, and B-58 shown in Figure 6. These were planes whose characteristics had been thoroughly analyzed by NASA, and they were able to calculate a nominal overpressure p_o for each flight. The values of p_o ran from .64 psf to 2.17 psf for the F-101 and F-104 flights. Only the F-101 and F-104 data are analyzed here since there were an insufficient number of readings from F-106's and B-58's to be statistically meaningful.

The flight track for the test series is shown in Figure 7. Note that there were three ground measurement stations at various distances from the flight track: Station 1, Station 3, and Station 4. A test building was located at each station with a microphone shock mounted inside. These inside microphones which measured p_i were at the center of the room 5 ft from the floor level. Outside microphones, which

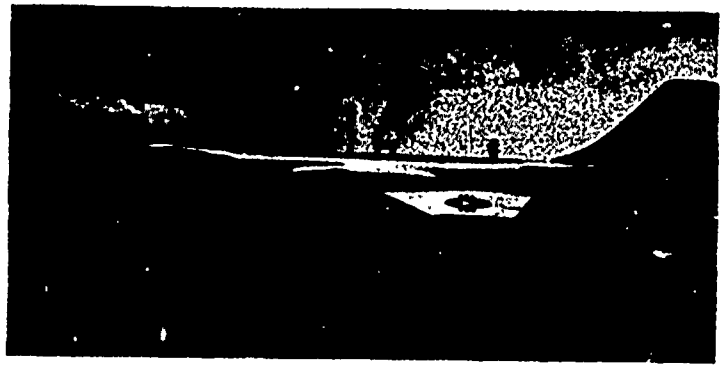

(a) Airplane A, F-104

(b) Airplane B, F-101

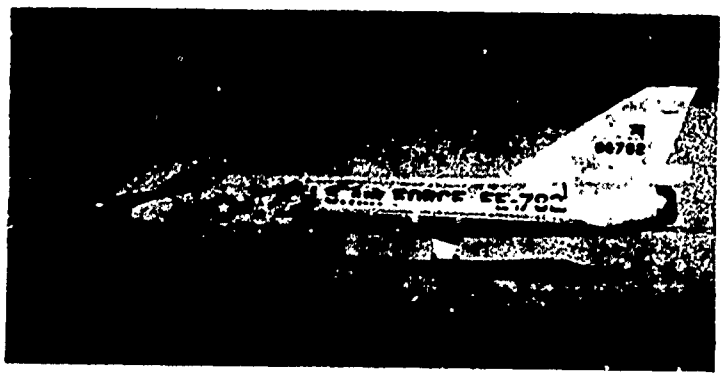

(c) Airplane C, F-106

(d) Airplane D, B-58

Figure 6. Airplanes Used in Test Program

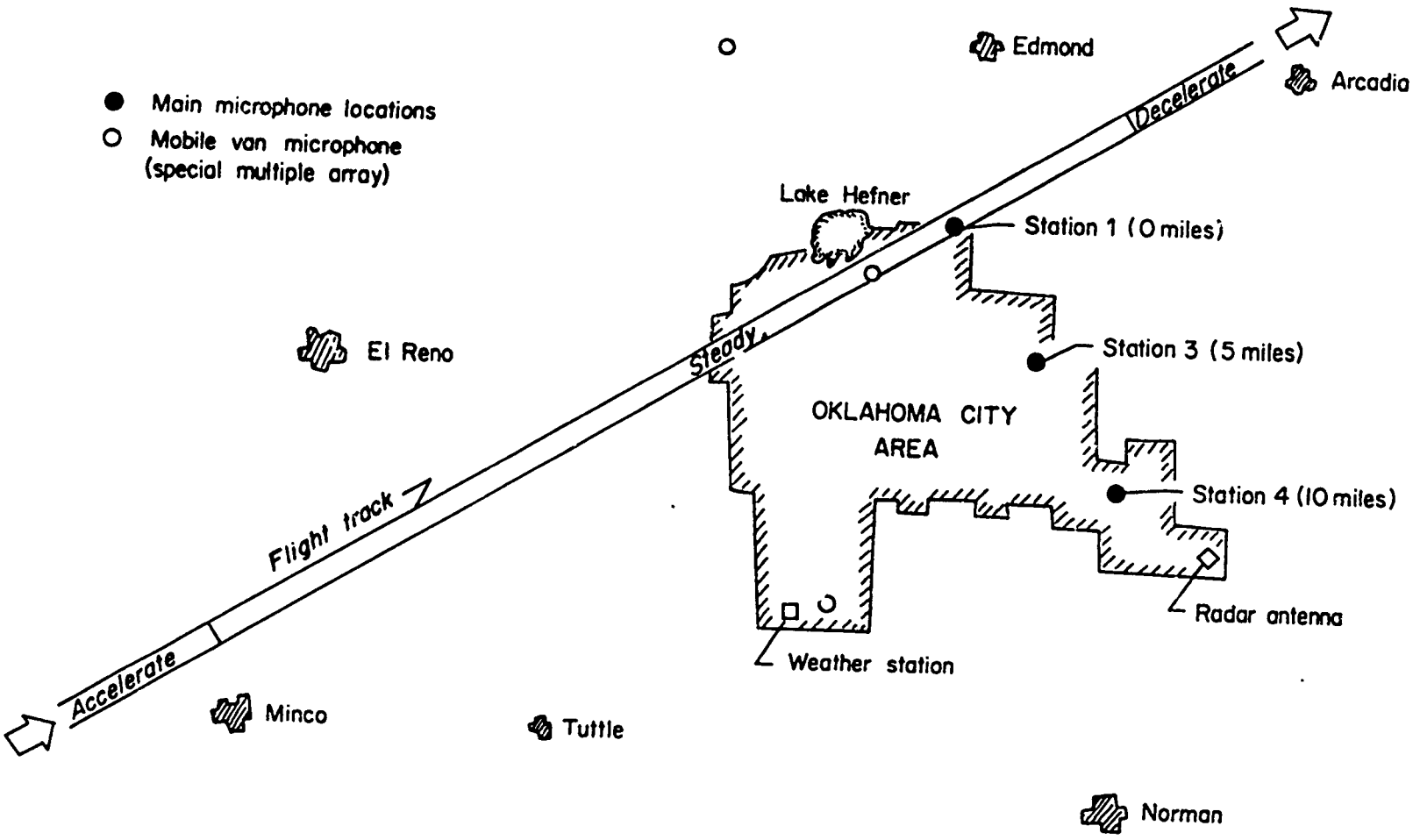

Figure 7. Planview Sketch of Test Area Showing Flight Track, Measuring Stations, and Facilities

measured p_f were shock-mounted at ground level on the surface of a plywood reflecting board. NASA obtained strip charts of internal and free field overpressure for each boom at each station. From these strip charts NASA determined the peak values p_f and p_i and the positive duration $T/2$ and positive impulse $I/2$ for each boom. A representative page of Oklahoma City data is shown in Table 1. Note that Δp_o, Δp_i, Δt_opos, and $I_o$pos of the column headings are p_f, p_i, $T/2$, and $I/2$, respectively, in the present notation. The nominal overpressure values for each station have been added at the bottom of each station set for comparison.

In its analysis of the data NASA calculated the ratio p_f/p_o for each boom measured. Histograms of this ratio were then plotted by NASA for each station's readings for the F-101 and F-104. These six histograms are shown in Figures 8-13 In the present notation $\Delta P_{o\,meas} / \Delta P_{o\,calc}$ of the abscissas is p_f/p_o. Each figure also includes a cumulative probability plot of the data on a lognormal scale. Note from the straight lines shown for comparison that the data do appear to be distributed lognormal. As will be discussed later this lognormal probability density leads to a simplification of the analysis.

Table 1. Typical Oklahoma City Data
Summary of Sonic-Boom Data for Various Flights of Airplane A for an Altitude of 32,000 Feet

Operating conditions				Weather				Sonic-boom pressure signature data													
								Station 1					Station 3					Station 4				
Date	Flight	Time	Mach	Surface temp., °F	Surface wind, knots	Cloud cover	Precipitation	Δp_o, lb/sq ft	Δp_1, lb/sq ft	Δt_o, pos., sec	I_o, pos., lb-sec/sq ft	Wave shape	Δp_o, lb/sq ft	Δp_1, lb/sq ft	Δt_o, pos., sec	I_o, pos., μsec, lb-sec/sq ft	Wave shape	Δp_o, lb/sq ft	Δp_1, lb/sq ft	Δt_o, pos., sec	I_o, pos., lb-sec/sq ft	Wave shape
2-10-64	3/28	930	1.5	41	010/12	●	None	1.10	0.41	0.047	0.0234	N	1.46	0.33	0.045	0.0229	P	0.73	0.27	0.046	0.0191	N
2-10-64	4/29	1008	1.5	43	020/17	◐	None	1.34	.42	.048	.0254	NP	1.24	.37	.046	.0269	C	1.03	.28	.052	.0192	NP
2-10-64	5/30	1326	1.5	52	350/18	○	None	.77	.35	.053	.0210	R	2.29	.30	.046	.0258	P	1.02	.31	.049	.0225	NP
2-10-64	6/31	1358	1.5	52	010/18	◐	None	1.02	.44	.056	.0276	NP	1.11	.33	.049	.0247	NP	.91	.28	.048	.0210	N
2-10-64	7/32	1602	1.5	51	340/14	○	None	.91	.36	.069	.0298	NR	1.11	.34	.050	.0248	NP	.93	.29	.044	.0199	NR
2-10-64	8/33	1631	1.5	51	340/14	•	None	.72	.33	.053	.0219	R	1.33	.36	.047	.0288	NP	.91	.29	.052	.0197	N
2-11-64	1/35	701	1.5	26	110/10	•	None	1.10	.47	.044	.0269	N	.97	.37	.042	.0314	N	.61	.29	.051	.0182	NR
2-11-64	2/36	731	1.5	27	130/10	•	None	----	----	------	-------	---	.99	.34	.040	.0227	N	.81	.30	.047	.0190	NR
2-11-64	3/37	930	1.5	34	150/15	•	None	.97	.34	.045	.0252	NR	1.04	.38	.049	.0299	NR	.89	.23	.050	.0174	NP
2-11-64	4/38	1000	1.5	37	150/15	◐	None	1.12	.39	.043	.0275	N	1.30	.43	.040	.0263	NP	.92	.36	.051	.0235	N
2-11-64	5/39	1328	1.8	47	150/14	●	None	1.19	.36	.043	.0263	N	1.15	.39	.042	.0261	N	.90	.29	.042	.0148	NR
2-11-64	6/40	1359	1.8	48	160/15	•	None	.81	.33	.045	.0288	R	1.15	.43	.037	.0239	N	.65	.23	.048	.0198	NR
2-12-64	1/43	705	1.5	45	160/20	●	None	.68	.28	.053	.0199	R	----	----	------	-------	---	.24	.10	.086	.0117	R
2-12-64	2/44	729	1.5	45	160/20	●	None	.87	.29	.045	.0191	R	----	----	------	-------	---	.57	.22	.046	.0151	R
2-12-64	3/45	928	1.5	43	170/19	●	-L, F	.68	.26	.042	.0173	R	----	----	------	-------	---	.49	.16	.051	.0133	R
2-12-64	4/46	959	1.5	43	170/18	•	-L, F	1.40	.35	.041	.0276	P	----	----	------	-------	---	.79	19	.043	.0134	NP
2-13-64	1/47	700	1.5	33	030/10	●	None	.81	.35	.047	.0257	R	.66	.25	.056	.0165	R	----	----	------	-------	---
2-13-64	2/48	728	1.5	33	030/10	•	None	1.02	.38	.045	.0284	R	.87	.38	.042	.0239	R	----	.36	------	-------	---
2-13-64	7/53	1559	1.5	48	020/19	○	None	1.12	----	.043	.0272	R	1.22	.35	.041	.0257	NP	1.12	.29	.045	.0183	NP
2-13-64	8/54	1630	1.5	48	020/9	•	None	1 25	----	.043	.0287	NR	.92	.29	.047	.0208	NR	.70	.30	.050	.0169	NR
2-14-64	1/34	701	1.5	28	150/12	○	None	.96	----	------	-------	---	1.18	.33	.041	.0302	N	.88	.34	.043	.0215	NP
2-14-64	2/55	729	1.5	28	150/12	•	None	----	----	------	-------	---	1.23	.34	.039	.0208	N	.96	.35	.039	.0176	NP
2-14-64	3/56	928	1.5	36	150/12	•	None	1.07	----	------	-------	---	.85	.32	.054	.0253	NR	.73	.31	.044	.0160	NR
2-14-64	4/57	1003	1.5	39	150/18	•	None	1.37	.28	.041	.0238	NP	.70	.27	.039	.0135	N	.71	.28	.042	.0155	NR
2-14-64	5/58	1329	1.5	51	150/25	•	None	1.33	.39	.043	.0259	NR	----	----	------	-------	---	1.39	.30	.042	.0219	P
2-14-64	6/59	1357	1.5	52	150/20	◐	None	1.22	.34	.042	.0296	NR	----	----	------	-------	---	1.44	.36	.050	.0219	P
2-14-64	7/60	1558	1.5	51	140/22	●	None	1.04	.35	.043	.0253	NR	.82	.30	.040	.0190	NR	.62	.28	.051	.0178	---
2-14-64	8/61	1627	1.5	50	140/22	•	None	.87	.35	.043	.0249	NR	.83	.28	.046	.0198	NR	.47	.18	.077	.0172	---
2-15-64	1/63	701	1.5	37	280/20	•	None	1.24	.30	.050	.0271	NP	1.33	.32	.042	.0260	NP	.47	.23	.050	.0121	NR
2-15-64	2/64	731	1.5	29	310/27	•	-R	1.11	.36	.047	.0227	NR	1.12	.32	.044	.0254	N	.70	.22	.047	.0173	NR
2-15-64	3/65	1329	1.5	41	330/26	•	None	1.94	.37	.045	.0273	P	1.19	.36	.041	.0239	N	.48	.22	.060	.0141	R
2-15-64	5/67	1559	1.5	39	330/17	●	None	.81	.21	.046	.0232	R	.52	.20	.048	.0149	R	.30	.12	.059	.0128	R
2-15-64	6/68	1630	1.5	39	310/20	•	None	.58	.26	.056	.0195	R	.67	.27	.050	.0225	R	.66	.17	.049	.0112	NP
2-16-64	2/70	730	1.5	21	120/8	○	None	1.15	.39	.047	.0331	NR	.90	.29	.042	.0228	NR	.54	.20	.050	.0157	NR
2-16-64	3/71	930	1.5	28	290/8	•	None	1.25	.36	.047	.0325	NR	.89	.29	.045	.0249	NR	.56	.21	.050	.0146	NR
2-16-64	4/72	959	1.5	28	320/6	•	None	1.27	.32	.047	.0325	NP	.86	.29	.040	.0195	NR	.53	.18	.050	.0171	NR
2-17-64	2/78	730	1.5	31	150/15	•	None	1.32	.33	.055	.0295	NP	.92	.28	.040	.0204	N	.92	.22	.050	.0188	N
Nominal Overpressures, p_o:								1.18					1.02					.76				

*For these two readings nominal overpressures were: Station 1, p_o = 1.27; Station 3, p_o = 1.09; Station 4, p_o = .81.

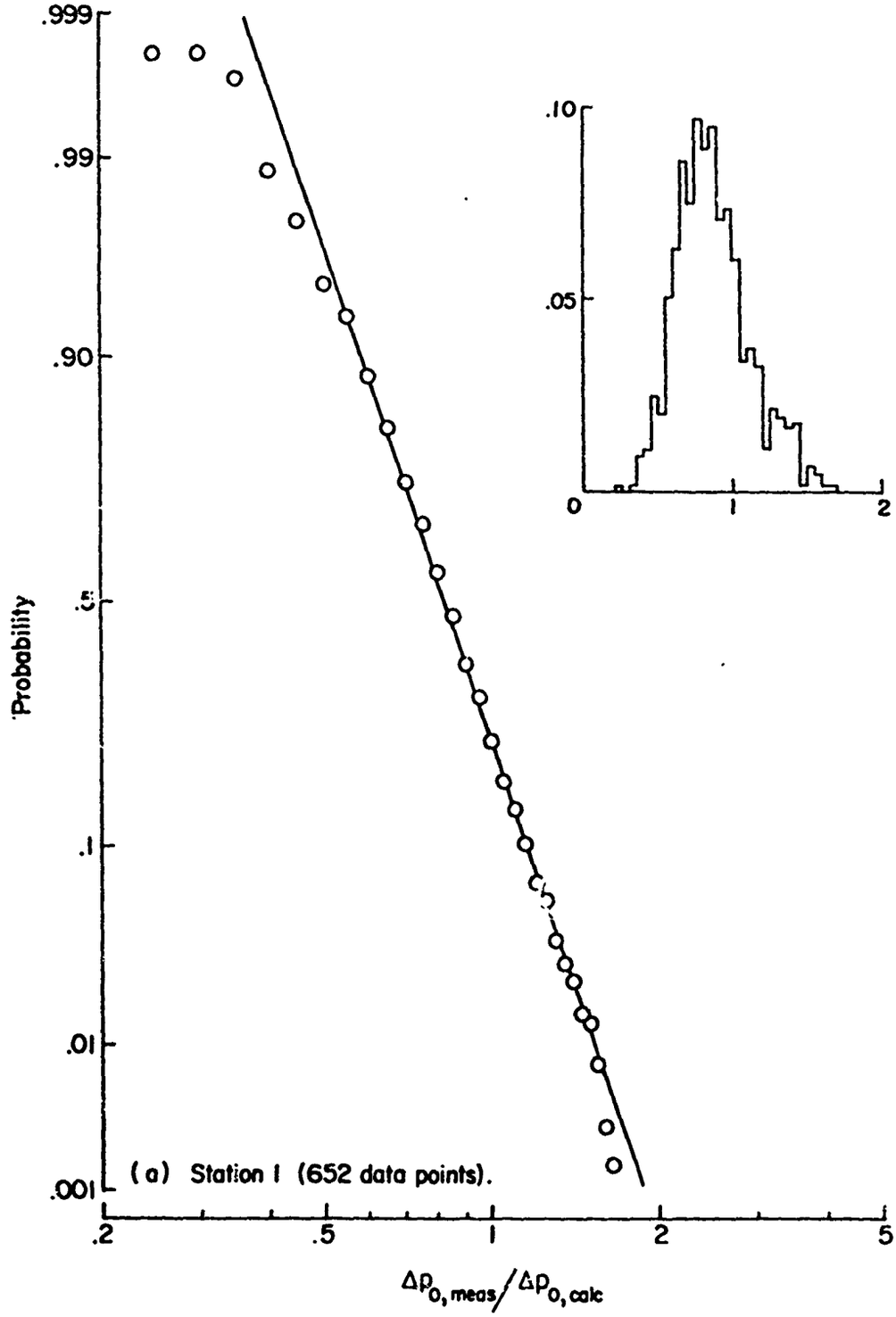

Figure 8. Probability of Equaling or Exceeding a Given Value of the Ratio of Measured to Calculated Overpressures for Airplane A at Station 1

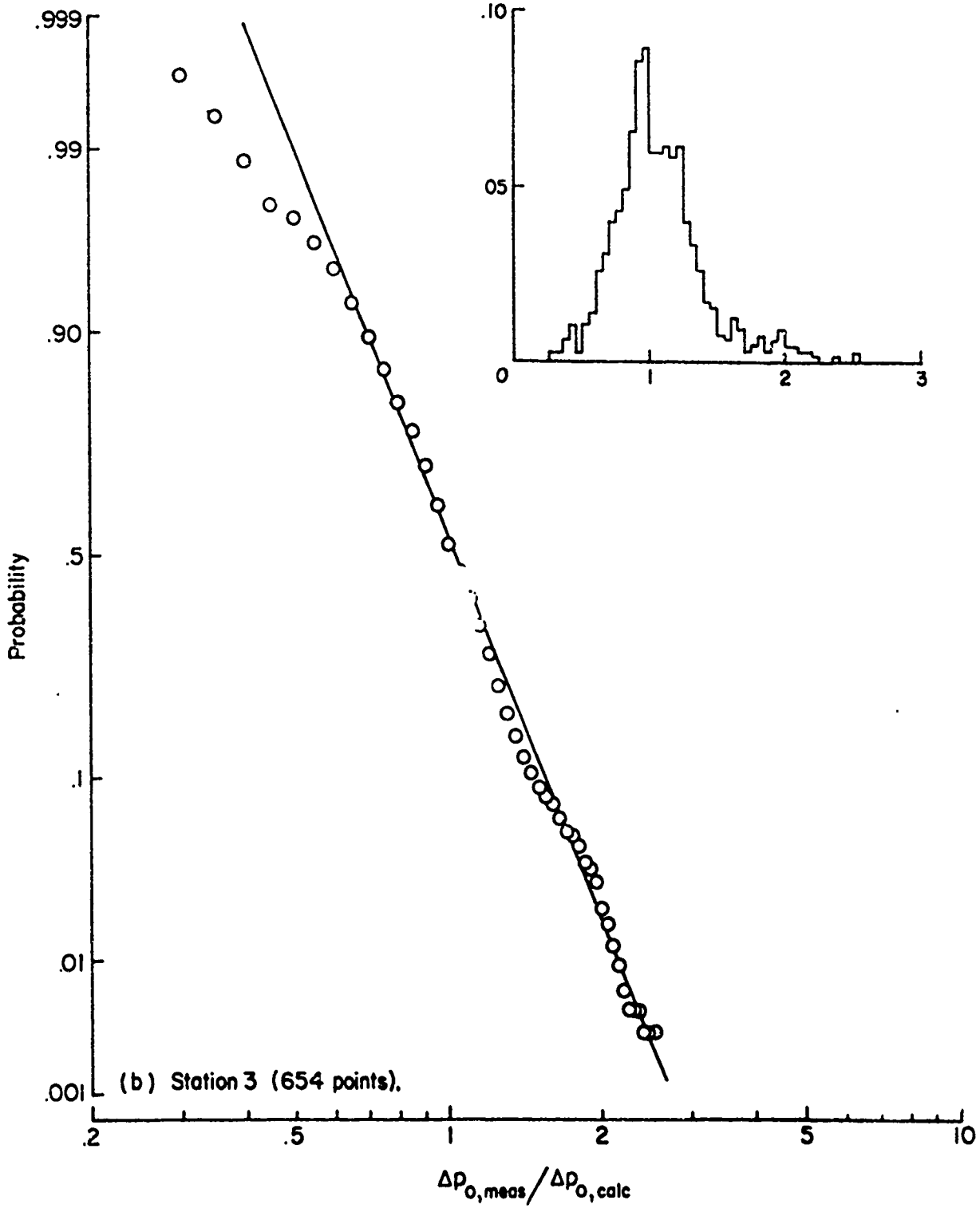

Figure 9. Probability of Equaling or Exceeding a Given Value of the Ratio of Measured to Calculated Overpressures for Airplane A at Station 3

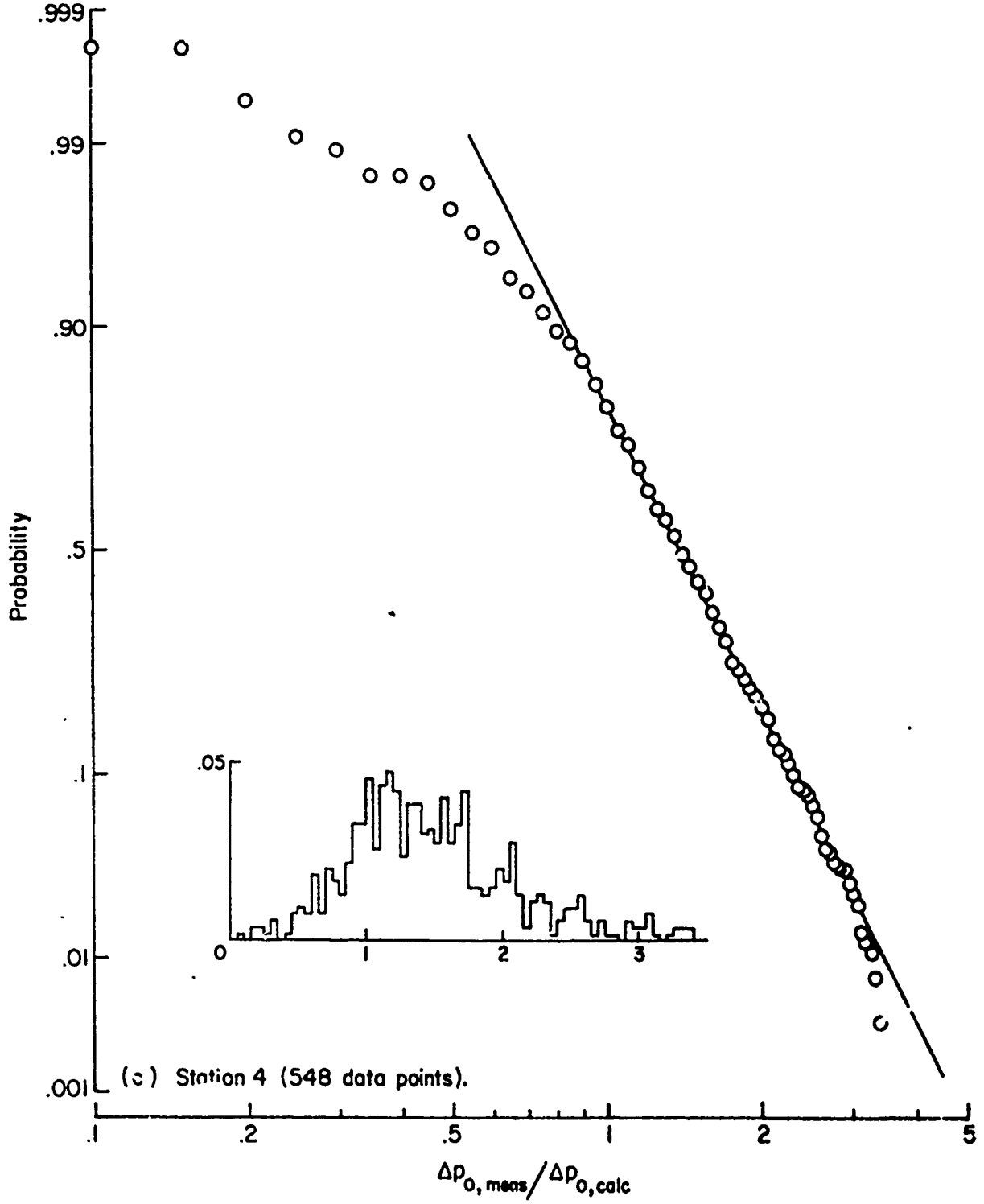

Figure 10. Probability of Equaling or Exceeding a Given Value of the Ratio of Measured to Calculated Overpressures for Airplane A at Station 4

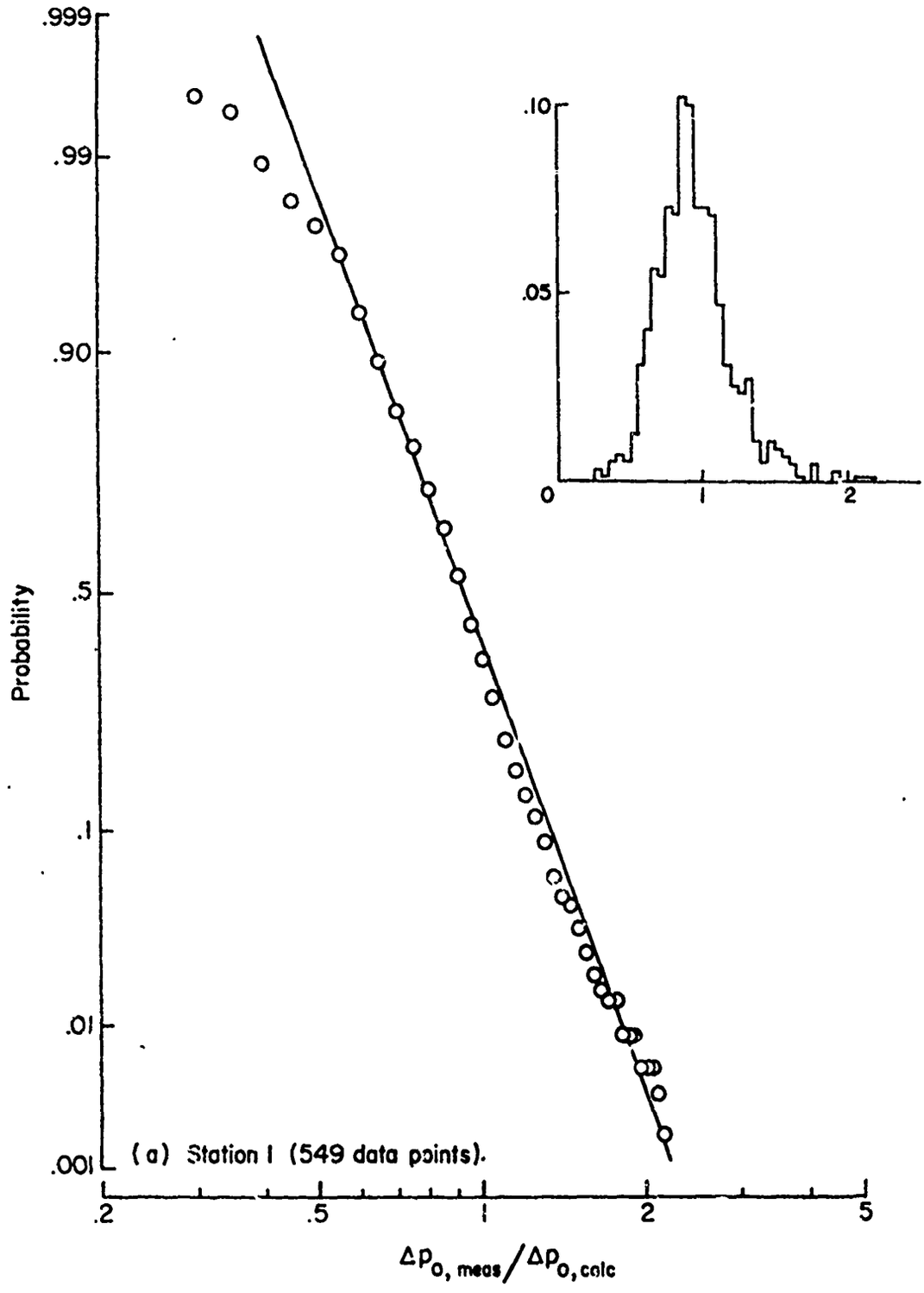

Figure 11. Probability of Equaling or Exceeding a Given Value of the Ratio of Measured to Calculated Overpressures for Airplane B at Station 1

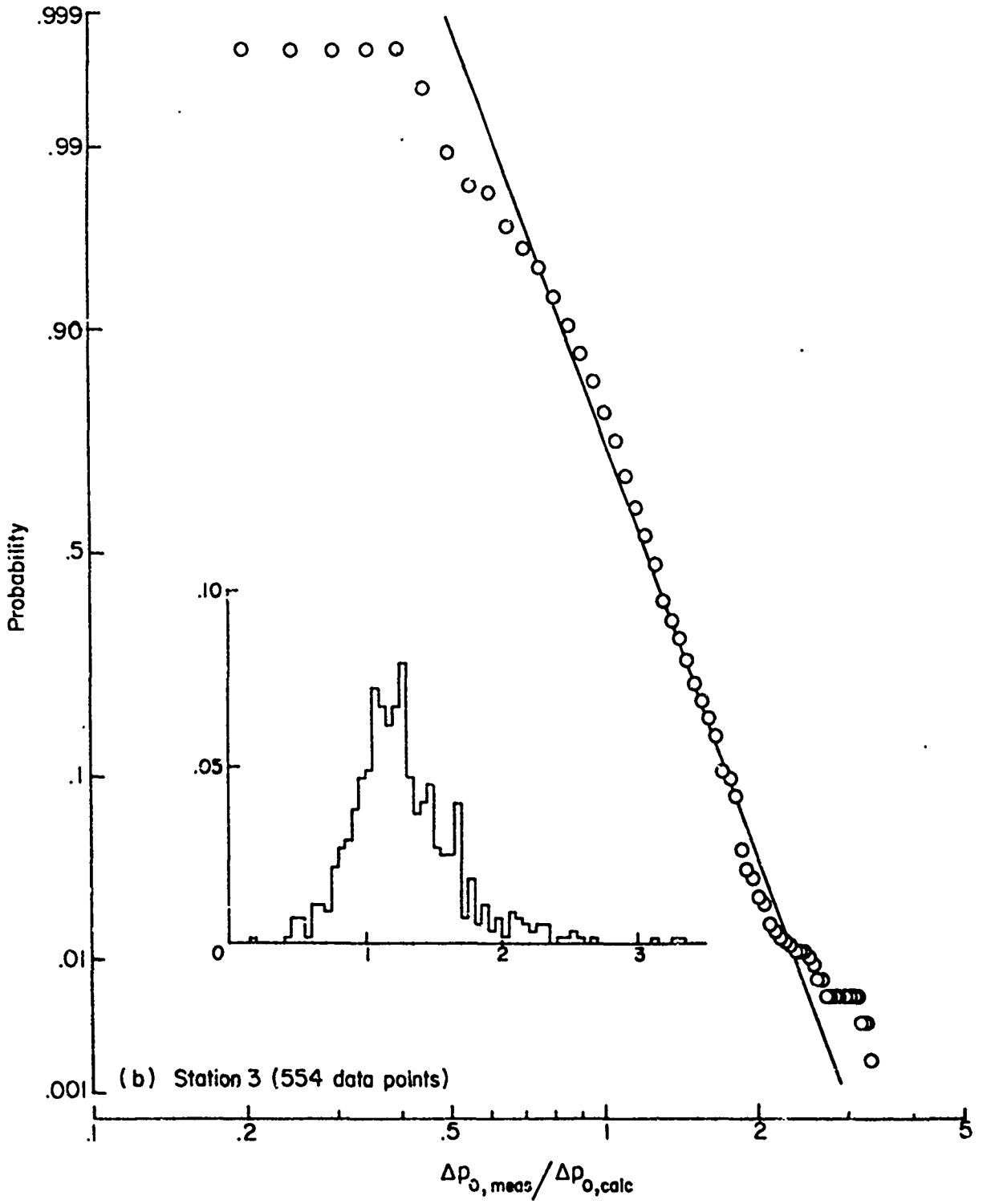

Figure 12. Probability of Equaling or Exceeding a Given Value of the Ratio of Measured to Calculated Overpressures for Airplane B at Station 3

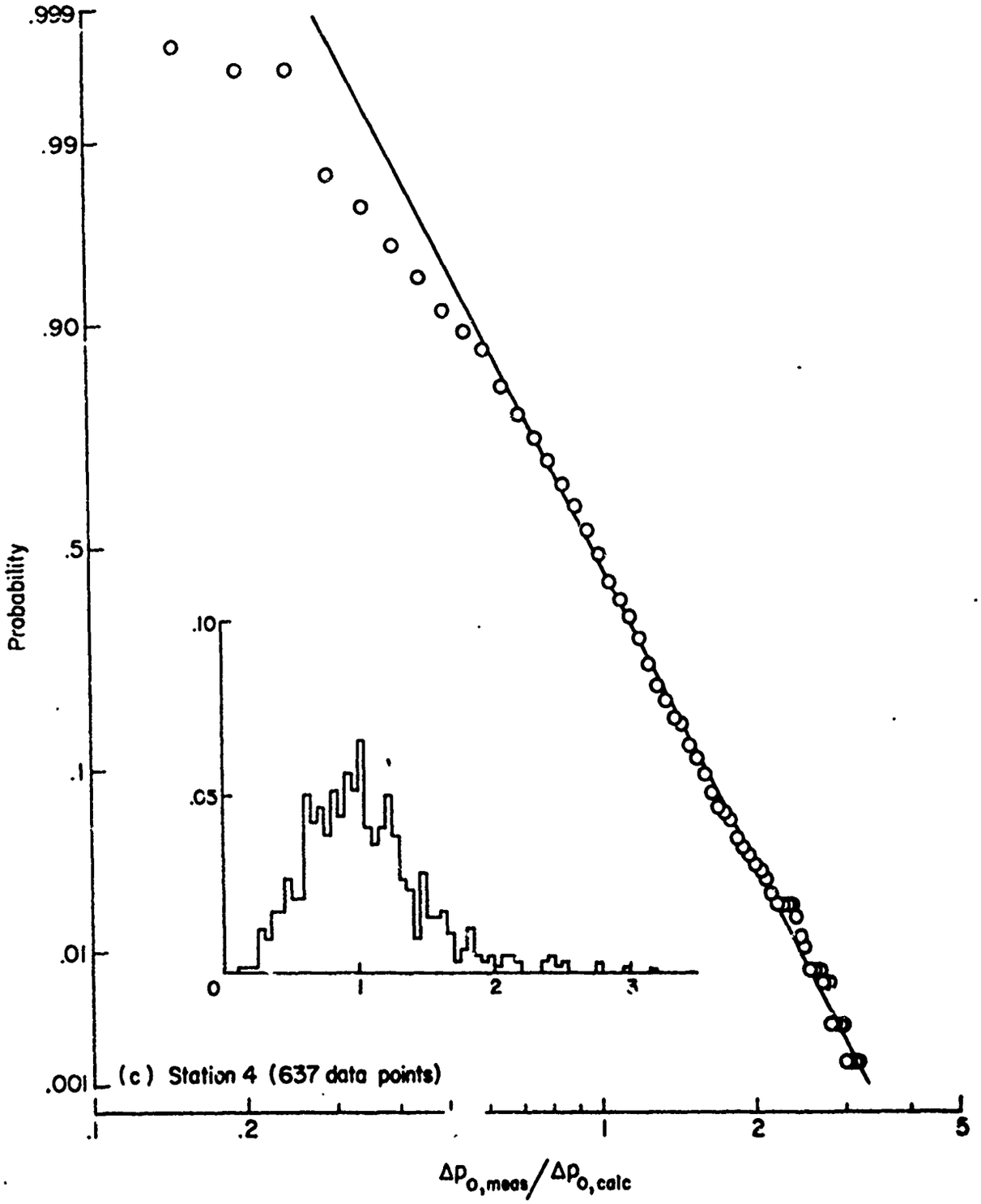

Figure 13. Probability of Equaling or Exceeding a Given Value of the Ratio of Measured to Calculated Overpressures for Airplane B at Station 4

2. WHITE SANDS TESTS

The main purpose of the White Sands, N. M., tests of 1965 was to measure structural reactions to sonic booms. These tests were conducted by FAA at the White Sands test range. Several structures were equipped with microphones on various external walls to measure external pressure p_e. In addition there were also microphones outside on the ground for measuring p_f and inside at the centers of rooms for measuring p_i. For measuring the structural reactions there were strain gauges, scratch gauges, and accelerometers attached to windows, walls, and roofs.

The aircraft used in the White Sands tests were F-104's and B-58's as shown in Figures 6a and 6d. These aircraft were flown over the uninhabited test structures at much lower altitude than for normal operations to deliberately create high overpressures. While typical sonic booms from normal aircraft operations are of the order of 1-4 psf, those in this test series were often in the 10-20 psf range. These high overpressures were necessary to cause the large structural responses necessary to explore damage conditions.

The particular structure which provided the data used in the present study was designated W4. The instrumentation on this structure, shown in Figure 14, consisted of strain gauges (labeled R), microphones (labeled M), velocimeters (labeled V), and accelerometers (labeled A). In addition to the instrumentation shown there were also an interior microphone M-7 and an exterior ground-mounted free field microphone M-16. The readings from the instrumentation which were utilized in the present study are shown in Tables 2-5 [33]. In each case the table values of strain and pressure are the peak values for the tape recorded sequence. Note that the column headed "vector" has the letters A-H. These correspond to eight possible angles of sound wave incidence in 45^{o} increments as keyed to Table 6.

In addition to the foregoing strain gauge data from building W-4, there was also another series of 484 external pressure reading sets from this same building. These readings formed the basis of the present statistical analysis of the effect of the angle of incidence. The first 30 of these sets of readings are shown in Table 7 as printed out by the computer, including some transformed values. The fourth column contains the cosines of the angles between the incoming sound rays and the normal to the surface. Note from the values of the cosines that as in Table 6 all angles have been approximated as the nearest 45^{o} multiple. Columns 5 and 7 contain the ratio p_e/p_f for the north and south walls,

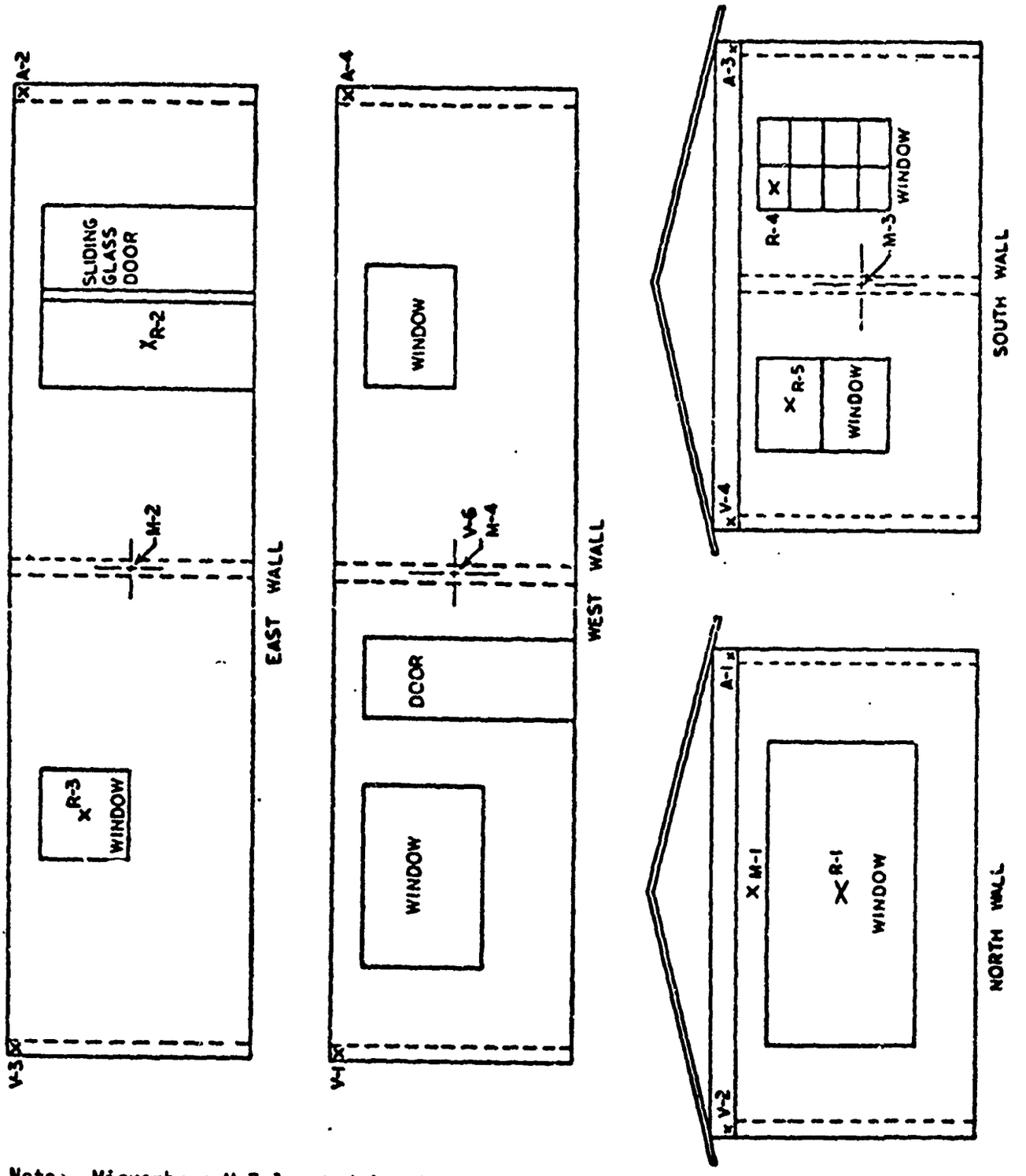

Note: Microphone M-7 located in middle of room interior; 9 feet behind R-1 and R-2.

Figure 14. Instrument Locations for White Sands Test Structure W4

Table 2. White Sands Strain Readings Rosette R-1, November 27, 1964

Run	Mach	Alt. x 1,000	Vector	Strain μ in./in. a	b	c	Recorded Pressures - psf M-1	M-7	M-16
1-145	1.40	13.5	D	57	35	NR	NR	NR	NR
2-146	1.43	14.0	H	54	29	NR	3.1	1.9	3.5
3-147	1.32	13.5	D	NR	NR	NR	2.4	2.7	3.9
4-148	1.30	14.0	E	40	26	NR	1.4	0.9	3.9
5-149	1.30	14.0	B	80	48	NR	NR	NR	NR
6-150	1.30	14.0	E	69	42	NR	1.9	0.9	3.9
7-151	1.39	15.0	F	40	26	NR	1.8	0.9	3.4
8-152	1.34	13.0	A	66	42	NR	5.5	1.1	3.4
9-153	1.38	14.0	F	46	29	NR	1.9	1.3	3.1
10-154	1.40	14.0	G	52	29	NR	2.2	0.9	3.9
11-155	1.40	14.3	C	43	29	NR	1.8	1.8	3.9
12-156	1.38	14.0	G	NR	NR	NR	NR	NR	NR
13-157	1.30	14.0	H	86	48	NR	3.6	1.4	2.0
14-158	1.36	14.0	D	66	35	NR	2.5	2.2	3.4
15-159	1.36	14.0	H	57	42	NR	3.2	1.4	1.9
16-160	1.25	13.5	A	66	35	NR	5.0	2.2	7.4
17-161	1.30	14.0	F	63	36	NR	1.7	2.2	3.7
18-162	1.30	14.0	A	89	52	NR	3.2	1.2	2.7
19-163	1.20	14.0	B	100	58	NR	3.2	1.9	2.5
20-164	1.38	15.0	E	60	36	NR	1.5	1.0	1.9
21-165	1.34	14.0	B	83	45	NR	4.3	2.0	5.0
22-166	1.45	16.0	C	77	42	NR	NR	NR	NR
23-167	1.39	14.3	G	72	39	NR	NR	NR	NR
24-168	1.45	13.9	C	80	45	NR	NR	NR	NR
25-169	1.30	14.0	D	80	45	NR	4.1	2.7	3.9
26-170	1.30	14.0	H	117	65	NR	3.2	1.4	5.3
27-171	1.40	14.0	D	69	36	NR	2.3	1.8	3.9
28-172	1.35	14.0	E	34	19	NR	1.9	0.8	2.0
29-173	1.30	14.0	B	72	42	NR	4.5	1.4	3.2
30-174	1.33	14.0	E	23	13	NR	1.7	0.8	4.3

Table 3. White Sands Strain Readings Rosette R-2, November 27, 1964

Run	Mach	Alt. x 1,000	Vector	Strain μ in./in. a	b	c	Recorded Pressures - psf M-2	M-7	M-16
1-145	1.40	13.5	D	19	35	28	NR	NR	NR
2-146	1.43	14.0	H	11	9	NR	4.6	1.9	3.5
4-148	1.30	14.0	E	7	9	6	1.9	0.9	3.9
5-149	1.30	14.0	B	30	39	25	NR	NR	NR
6-150	1.30	14.0	E	11	13	6	2.3	0.9	3.9
7-151	1.39	15.0	F	11	13	9	3.5	0.9	3.4
8-152	1.34	13.0	A	19	22	31	4.5	1.1	3.4
9-153	1.38	14.0	F	11	26	19	4.6	1.3	3.1
10-154	1.40	14.0	G	22	30	28	1.5	0.9	3.9
11-155	1.40	14.3	C	7	13	9	1.9	1.8	3.9
13-157	1.30	14.0	H	33	44	46	3.3	1.4	2.0
14-158	1.36	14.0	D	22	22	22	3.6	2.2	3.4
15-159	1.36	14.0	H	19	35	31	2.5	1.4	..9
16-160	1.25	13.5	A	30	39	38	6.5	2.2	7.4
17-161	1.30	14.0	F	37	44	34	2.6	2.2	3.7
18-162	1.30	14.0	A	19	30	25	4.5	1.2	2.7
19-163	1.20	14.0	B	30	44	41	2.4	1.9	2.5
20-164	1.38	15.0	E	19	22	25	3.2	1.0	1.9
21-165	1.34	14.0	B	22	35	28	2.3	2.0	5.0
22-166	1.45	16.0	C	11	13	13	NR	NR	NR
23-167	1.39	14.3	G	19	26	28	NR	NR	NR
24-168	1.45	13.9	C	7	9	13	NR	NR	NR
25-169	1.30	14.0	D	11	13	9	2.9	2.7	3.9
26-170	1.30	14.0	H	26	49	44	5.6	1.4	5.3
27-171	1.40	14.0	D	7	9	13	2.0	1.8	3.9
28-172	1.35	14.0	E	7	9	9	1.8	0.8	2.0
29-173	1.30	14.0	B	30	39	34	6.0	1.4	3.2
30-174	1.33	14.0	E	7	9	9	2.3	0.8	4.3

Table 4. White Sands Strain Readings Rosette R-1, November 28, 1964

Run	Mach	Alt. x 1,000	Vector	Strain μ in./in. a	b	c	Recorded Pressures - psf M-1	M-7	M-16
2-176	1.30	11.9	A	109	61	NR	9.1	3.6	5.9
3-177	1.25	11.7	F	52	29	NR	4.5	1.1	4.0
4-178	1.25	11.4	H	80	25	NR	7.3	1.7	5.3
5-179	1.26	12.5	D	49	29	NR	6.4	2.0	3.8

Table 5. White Sands Strain Readings Rosette R-2, November 28, 1964

Run	Mach	Alt. x 1,000	Vector	Strain μ in./in. a	b	c	Recorded Pressures - psf M-2	M-7	M-16
2-176	1.30	11.9	A	NR	12	19	14.3	3.6	5.9
3-177	1.25	11.7	F	NR	39	34	16.2	1.1	4.0
4-178	1.25	11.4	H	NR	52	53	19.0	1.7	5.3
5-179	1.26	12.5	D	NR	26	22	4.8	2.0	3.8

Table 6. Angle of Incidence on Structure W4

Vector Letter	North Wall		East Wall		South Wall	
	θ	cos θ	θ	cos θ	θ	cos θ
A	0	1.0	90	0	180	-1.0
B	315	0.707	45	0.707	135	-0.707
C	45	0.707	135	-0.707	225	-0.707
D	90	0	180	-1.0	270	0
E	135	-0.707	225	-0.707	315	0.707
F	180	-1.0	270	0	0	1.0
G	225	-0.707	315	0.707	45	0.707
H	270	0	0	1.0	90	0

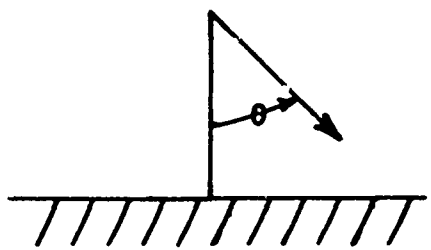

Table 7. External Pressures on Building W4 at White Sands

	P_f	P_{e_1} North Wall	P_{e_2} South Wall	cos ϑ	$\frac{P_{e1}}{P_f}$	$\frac{P_{e2}}{P_f}$	$\log_{10}\left(\frac{P_{e1}}{P_f}\right)$	$\log_{10}\left(\frac{P_{e2}}{P_f}\right)$
1	6.20000	3.40000	3.40000	-1.00000	.54839	.54839	-.26091	-.26091
2	4.80000	3.20000	4.60000	-.70700	.66667	.95833	-.17609	-.01848
3	5.60000	2.90000	3.00000	-.70700	.51786	.53571	-.28579	-.27107
4	5.30000	3.40000	2.30000	0.00000	.64151	.43396	-.19280	-.36255
5	5.30000	4.00000	2.30000	0.00000	.75472	.43396	-.12222	-.36255
6	7.00000	3.60000	2.70000	0.00000	.51429	.38571	-.28880	-.41373
7	5.90000	3.80000	6.70000	-1.00000	.64407	1.13559	-.19107	.05522
8	4.80000	6.70000	1.70000	1.00000	1.39583	.35417	.14483	-.45079
9	7.60000	6.80000	1.30000	.70700	.89474	.17105	-.04830	-.767
10	5.30000	3.00000	4.20000	-.70700	.56604	.79245	-.24715	-.10.13
11	7.00000	9.00000	1.30000	.70700	1.28571	.18571	.10914	-.73115
12	7.30000	6.50000	1.30000	.70700	.89041	.17808	-.05041	-.74938
13	6.50000	5.30000	1.10000	.70700	.81538	.16923	-.08864	-.77152
14	7.00000	4.00000	3.20000	0.00000	.65714	.45714	-.18234	-.33995
15	5.60000	4.00000	2.70000	0.00000	.71429	.48214	-.14613	-.31682
16	6.20000	3.40000	1.50000	0.00000	.54839	.24194	-.26091	-.61630
17	6.20000	3.40000	1.50000	0.00000	.54839	.24194	-.26091	-.61630
18	3.90000	2.90000	3.80000	-.70700	.74359	.97436	-.12867	-.01128
19	5.30000	6.30000	1.30000	.70700	1.18868	.24528	.07506	-.61033
20	3.90000	2.90000	4.60000	-.70700	.74359	1.17949	-.12867	.07169
21	5.60000	3.00000	3.20000	-1.00000	.53571	.57143	-.27107	-.24304
22	5.30000	7.60000	1.50000	1.00000	1.43396	.28302	.15654	-.54818
23	6.20000	3.20000	5.70000	-1.00000	.51613	.91935	-.28724	-.03652
24	5.10000	3.40000	3.80000	-.70700	.66667	.74510	-.17609	-.12779
25	7.90000	5.70000	1.30000	.70700	.72152	.16456	-.14175	-.78368
26	5.60000	3.00000	3.40000	-.70700	.53571	.60714	-.27107	-.21671
27	4.90000	5.80000	2.30000	0.00000	1.18367	.46939	.07323	-.32847
28	5.20000	6.00000	1.20000	0.00000	1.15385	.23077	.06215	-.63682
29	1.90000	3.10000	3.10000	-1.00000	1.63158	1.63158	.21261	.21261
30	6.00000	1.50000	2.00000	0.00000	.25000	.33333	-.60206	-.47712

respectively. Columns 6 and 8 contain the common logarithms of the ratios from Columns 5 and 7, respectively. It will be shown later how these ratios and logarithms are used in the present statistical model.

3. EDWARDS AIR FORCE BASE TESTS

The sonic boom tests conducted at Edwards Air Force Base, California, in June 1966 were for measurement of both human response and structural reaction. Like the previous tests, these were conducted under FAA sponsorship. Stanford Research Institute, under the direction of Karl Kryter, performed the human response studies and John A. Blume and Associates again performed the structural studies [31,34]. NASA also participated in reduction and analysis of the sonic boom data.

As part of the Edwards structural test two test houses, shown in Figures 15 and 16, were extensively instrumented. Of particular interest in the present study, five windows were instrumented with strain gauges and two indoor microphones were installed. There was also extensive instrumentation of walls and ceilings.

Between the Edwards tests and the White Sands tests, there were seven windows of various sizes instrumented. These are summarized in Table 8. The strain readings on these windows form the basis of the present statistical model of the dynamic amplification factor.

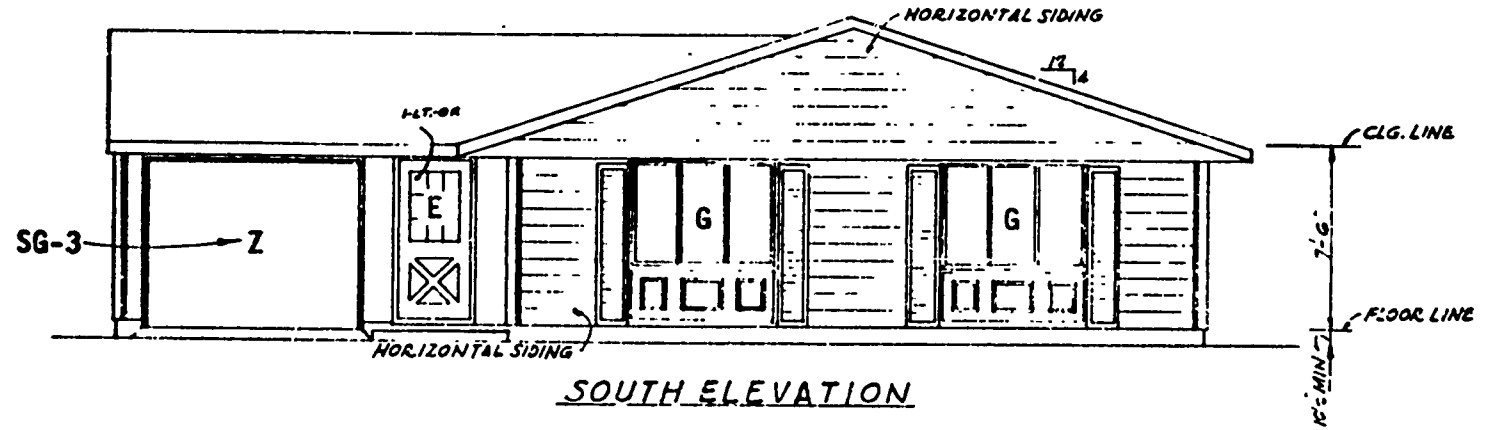

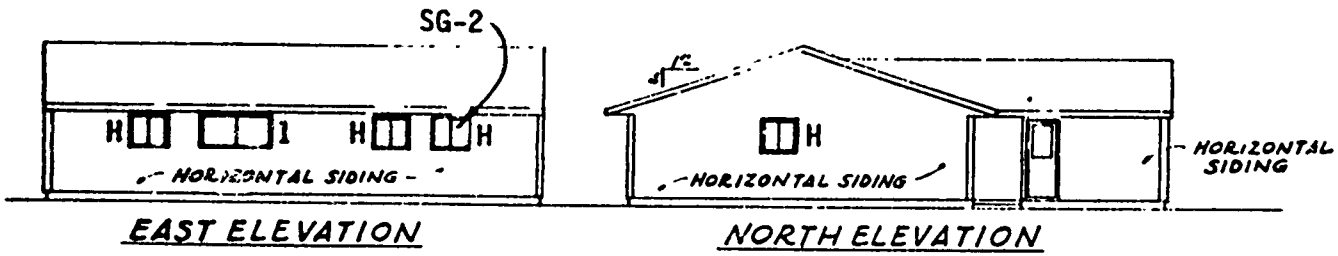

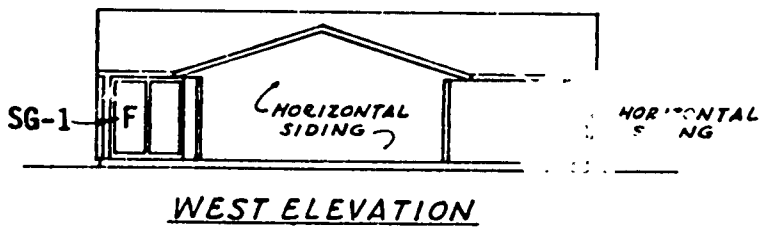

Window Schedule		
Code	Area ft^2	Nominal Dimensions LxH-inches
E	6.0	24 x 36
F	48.0	72 x 80
G*	12.0	48 x 36
H*	6.0	36 x 36
I*	12.0	72 x 36
Z	59.0	105 x 81

*Aluminum Sliding Windows

Figure 15. One-Story Test Structure (E-1) EAFB

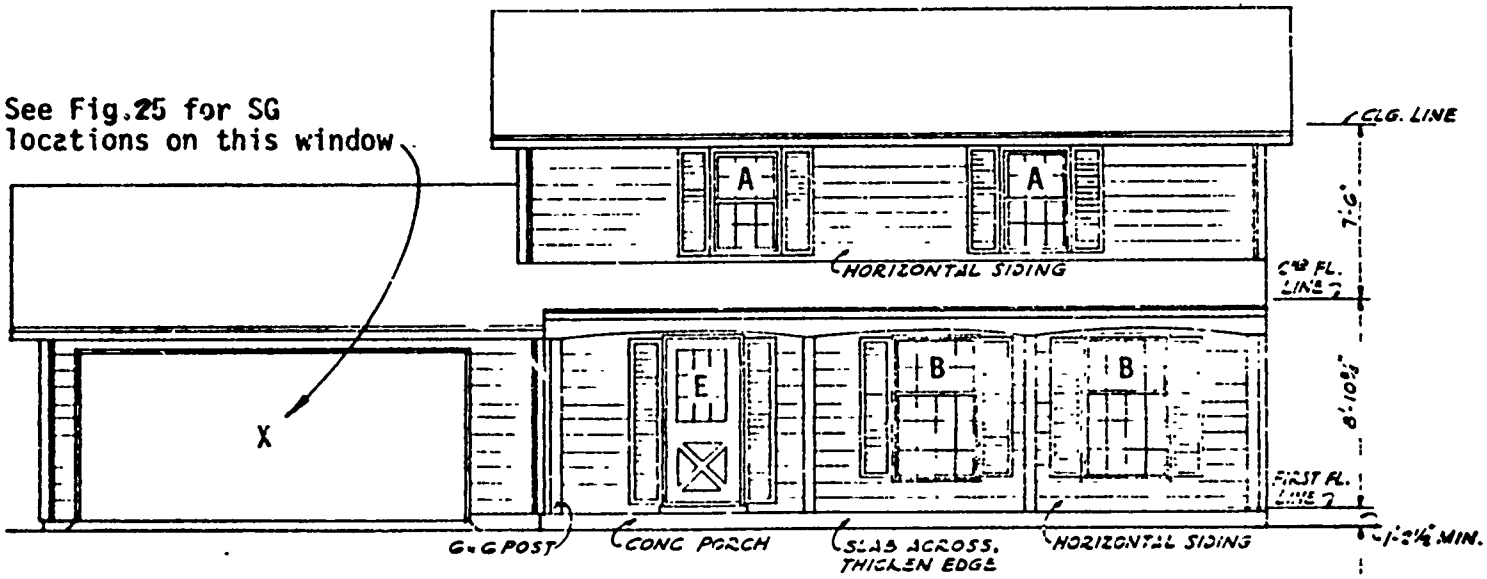

SOUTH ELEVATION

Window Schedule		
Code	Area ft²	Nominal Dimensions LxH-inches
A*	15.6	36 x 52
B*	18.0	36 x 72
C*	9.0	36 x 36
E	6.0	24 x 36
F	48.0	72 x 80
X	107.5	184 x 84

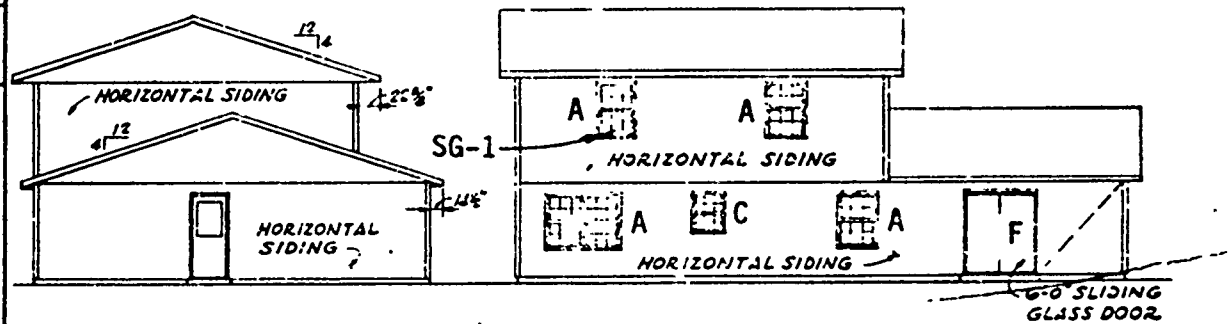

WEST ELEVATION

NORTH ELEVATION

*Double hung aluminum sash with aluminum muntins to provide number of individual lights (panes) as shown.

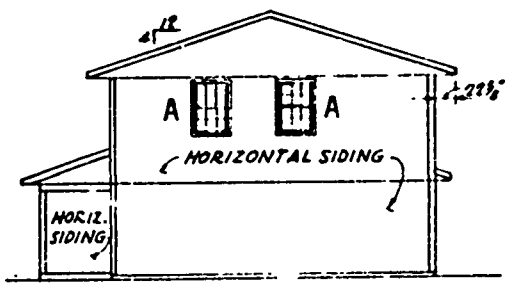

EAST ELEVATION

Figure 16. Two-Story Test Structure (E-2) EAFB

Table 8. Summary of Instrumented Windows

Window No.	Description	Length a (inches)	Width b (inches)	h (nominal)	h (actual)	Freq. f_o	Stress Factor	Area A (ft^2)	$\frac{\sqrt{ab}}{h}$
1	Sliding Door, EAFB Channel 210 Structure #1, Family Room	74.0	33.0	1/8	.120	13.00	219.00	17.0	411.8
2	Sliding Aluminum Window, EAFB Channel 211, Structure #1, Bedroom	34.0	16.0	1/8	.120	56.30	50.54	3.8	194.4
3	Garage Window, EAFB Channel 212 (Store Front Size), Structure #1	104.5	80.5	1/4	.235	5.71	255.70	58.4	390
4	Garage Window, EAFB Channel 312 (Store Front Size), Structure #2	184.0	84.0	1/4	.235	3.97	367.10	107.0	529
5	Colonial Pane, EAFB Channel 313 Structure #2, Bedroom	11.5	10.5	1/8	.115	188.10	15.78	0.84	95.6
6	Picture Window, White Sands R1 Structure W4	118.0	58.0	1/4	.218	7.92	198.00	47.0	379
7	Sliding Door, White Sands R2 Structure W4	63.0	33.0	7/32	.188	21.85	83.95	14.4	242.5

Of the Edwards data there were 102 data sets which were found to be complete and suitable for use in this study. These correspond to 102 different overflights whose readings are shown in Table 9. Note that for each overflight there are strain gauge readings from windows on five channels, internal pressure readings from two microphones, and a free field pressure reading. No readings of external pressure were made in the Edwards series. The readings shown in Table 9 form the basis of the correlation analysis which led to the statistical model.

Table 9. Summary of Edwards AFB Data

p_f	ϵ_{210}	ϵ_{211}	ϵ_{212}	ϵ_{312}	ϵ_{313}	p_{i1}	p_{i2}	T	Vertical Angle	Rise Time
2.00	9.64	8.45	18.77	38.3	6.81	1.04	.85	.183	48.4	.007
3.44	14.88	12.23	31.42	56.5	12.5	1.41	.79	.156	51.2	.0065
1.71	9.43	9.79	14.11	30.3	7.04	.69	.66	.177	52.1	.006
2.50	12.79	14.01	25.13	48.4	11.1	1.16	.95	.152	50.4	.018
1.99	8.38	5.45	12.50	23.2	5.90	.66	.55	.171	60.1	.003
3.16	13.62	13.34	23.72	41.4	25.4	1.25	1.14	.193	73.0	.006
1.70	8.38	6.01	11.54	27.2	5.17	.58	.55	.195	63.1	.0005
3.18	11.74	13.90	24.83	49.4	14.3	1.14	.69	.156	56.7	.0005
3.54	12.37	14.46	26.64	51.5	9.08	1.19	.71	.159	53.2	.006
1.70	9.94	5.62	10.90	21.1	6.59	.64	.60	.175	58.7	.014
3.17	12.82	14.31	31.06	43.6	13.2	1.08	.63	.156	50.0	.009
2.06	8.95	8.17	10.90	16.7	6.36	.6[illegible]	.52	.179	57.9	.0035
2.22	10.90	8.86	27.25	37.9	11.1	.92	.50	.147	53.9	.014
1.22	8.01	6.81	15.80	18.9	6.59	.55	.50	.166	59.0	.006
2.85	13.14	14.48	3.24	47.0	1.07	1.01	.63	.144	49.0	.002
1.76	8.98	4.09	10.90	17.4	3.27	.58	.52	.162	52.2	.030
2.63	10.90	10.05	27.79	43.6	12.0	1.06	.63	.161	60.4	.0075
2.09	8.98	4.77	10.90	18.9	6.81	.64	.60	.170	55.3	.008
3.23	13.46	11.07	34.88	48.2	12.7	1.01	.58	.148	48.9	.006
2.17	11.54	11.92	22.59	20.3	11.3	.58	.63	.169	58.4	.0015
2.70	13.78	14.99	37.06	49.3	10.2	1.06	.75	.144	48.9	.0055
4.00	15.39	18.87	34.68	53.3	10.5	1.13	.84	.153	51.1	.005
1.60	9.62	6.08	14.86	21.8	1.36	.53	.41	.140	55.5	.0085
3.44	4.75	15.30	32.70	52.8	6.98	1.08	.67	.146	49.2	.006
2.77	9.62	10.27	18.33	20.6	4.14	.54	.44	.161	51.0	.0075

Table 9. Summary of Edwards AFB Data (Continued)

P_f	ϵ_{210}	ϵ_{211}	ϵ_{212}	ϵ_{312}	ϵ_{313}	P_{i1}	P_{i2}	T	Vertical Angle	Rise Time
2.95	10.90	11.32	29.23	46.5	5.23	.97	.59	.140	48.0	.003
1.94	8.98	7.97	15.85	21.2	3.49	.47	.41	.150	54.3	.004
2.28	9.30	5.45	11.89	24.7	2.18	.73	.46	.180	60.4	.0045
3.03	10.90	11.11	29.23	49.9	5.45	1.11	.67	.155	54.4	.014
2.25	10.26	5.45	15.85	21.8	5.89	.64	.61	.176	63.6	.0175
3.80	11.22	10.45	28.24	44.2	9.59	.99	.67	.149	48.4	.012
2.04	9.62	6.71	16.84	19.5	3.49	.5[illegible]	.44	.157	51.6	.001
2.82	11.92	15.22	20.65	43.0	32.0*	1.05	2.67	.160	42.2	.0003
2.07	8.52	9.87	13.19	31.4	27.9	.84	2.16	.190	45.7	.007
2.86	12.26	14.40	22.95	44.9	27.2	1.05	2.45	.146	44.0	.004
1.88	8.17	9.46	14.92	29.5	24.5	.82	2.03	.195	42.4	.004
3.42	10.90	10.08	22.95	43.0	28.6	.99	1.78	.156	45.6	.009
1.93	9.20	6.99	17.21	27.6	22.5	.75	1.91	.182	47.3	.004
2.30	9.88	9.25	20.08	35.1	13.8	.90	2.61	.149	43.4	.005
2.67	13.08	12.37	18.69	25.6	21.8	.89	2.15	.179	51.8	.005
2.46	8.28	13.83	26.16	48.1	35.4	1.21	2.20	.153	54.1	.005
1.47	9.16	6.71	13.08	16.7	14.3	.71	1.64	.175	53.7	.023
2.58	13.08	17.40	28.65	53.9	35.4	1.30	2.61	.144	49.4	.0155
1.47	8.28	6.92	12.46	15.4	12.3	.62	1.53	.164	55.1	.0055
2.34	12.43	10.48	11.51	21.8	21.8	1.09	2.15	.218	68.7	.0075
3.04	13.95	16.14	8.78	53.2	42.2	1.33	2.69	.154	50.5	.006
2.80	13.08	13.83	28.65	53.9	34.5	1.24	2.61	.145	52.2	.002
2.90	13.52	13.83	30.52	55.1	38.2	1.24	2.56	.141	52.2	.006
2.81	14.99	10.90	26.64	53.1	32.7	.98	2.71	.151	49.2	.013
1.95	8.17	6.26	13.32	17.7	12.3	.51	1.59	.175	55.3	.002

*Channel 313 changed from colonial window to large garage window from here on.

Table 9. Summary of Edwards AFB Data (Continued)

p_f	ϵ_{210}	ϵ_{211}	ϵ_{212}	ϵ_{312}	ϵ_{313}	p_{i1}	p_{i2}	T	Vertical Angle	Rise Time
3.22	16.35	18.17	26.64	57.2	35.4	1.01	2.63	.145	57.0	.0015
1.22	7.49	4.44	9.69	16.3	10.9	.49	1.43	.167	59.0	.025
3.03	12.60	9.69	23.01	51.8	32.0	.88	2.51	.146	49.2	.010
1.51	6.81	5.85	9.69	14.3	10.2	.47	1.35	.167	54.5	.006
1.65	10.56	5.45	13.93	21.1	16.3	.64	1.97	.186	72.0	.016
1.51	10.22	5.65	12.11	19.8	14.3	.69	1.83	.177	62.8	.002
1.88	9.20	6.06	11.51	17.7	12.9	.54	1.65	.177	57.1	.009
1.73	7.83	4.04	12.11	15.0	9.54	.49	1.39	.165	58.9	.017
2.49	9.54	3.83	14.53	21.1	15.7	.59	2.01	.181	59.0	.020
2.67	13.62	9.49	24.22	50.4	26.6	.91	2.63	.148	52.2	.001
2.84	14.31	9.49	21.80	42.2	26.6	.83	1.69	.146	50.9	.005
2.66	14.11	17.82	22.75	96.7	38.3	1.01	2.47	.162	50.5	.008
1.53	9.94	8.65	18.48	81.7	25.6	.77	1.64	.154	47.7	.0085
3.44	7.69	10.03	25.59	91.3	30.8	.94	1.25	.167	50.9	.0055
2.04	11.86	5.88	21.33	87.2	28.9	.86	1.58	.163	47.5	.0295
1.48	6.73	3.81	9.48	35.4	11.5	.58	1.36	.169	56.2	.003
1.42	8.01	5.36	10.43	27.2	14.1	.55	.97	.179	56.4	.0175
2.31	11.22	7.96	18.96	70.8	23.1	.79	1.99	.157	48.0	.0145
2.40	10.90	10.55	27.25	163.5	33.4	.78	1.34	.162	46.1	.0045
1.63	8.52	6.86	15.99	43.6	13.1	.52	1.36	.168	52.8	.002
1.98	10.56	10.55	23.84	130.8	23.2	.74	1.83	.155	47.3	.008
1.25	8.86	5.45	14.99	57.2	11.6	.43	1.31	.163	59.0	.002
2.09	11.58	11.95	25.89	139.0	26.2	.83	2.01	.159	47.7	.007
5.50	13.28	8.26	32.70	234.3	34.9	.97	2.42	.160	49.4	.005
1.87	9.88	8.23	9.13	13.5	9.54	.45	.95	.074	50.3	.0035

Table 9. Summary of Edwards AFB Data (Continued)

p_f	ϵ_{210}	ϵ_{211}	ϵ_{212}	ϵ_{312}	ϵ_{313}	p_{i1}	p_{i2}	T	Vertical Angle	Rise Time
1.56	9.54	7.61	13.93	18.6	10.3	.47	.36	.079	46.6	.007
1.52	8.86	4.52	10.29	17.3	9.69	.44	.36	.079	49.4	.0095
1.39	9.54	5.76	9.69	14.7	8.48	.38	.36	.079	48.7	.008
3.75	16.17	15.84	15.14	27.6	16.7	.59	1.55	.079	62.1	.0005
1.51	7.27	5.96	8.48	14.1	8.17	.40	.95	.079	48.1	.0055
1.74	7.60	6.58	10.90	20.5	12.8	.50	.87	.092	63.5	.009
4.36	22.15	18.51	18.77	30.1	19.2	.69	1.86	.079	62.0	.004
1.31	5.95	3.91	6.06	10.3	6.81	.32	.75	.075	51.5	.008
2.25	13.01	9.67	13.93	25.0	14.7	.57	1.63	.077	63.4	.010
3.36	15.12	13.78	12.72	21.8	15.4	.55	1.59	.067	55.0	.0035
2.58	14.42	9.05	14.53	21.8	14.1	.48	1.03	.077	45.6	.005
1.51	8.17	8.23	9.69	12.2	6.81	.34	.81	.075	43.1	.0055
1.73	7.83	9.46	10.90	13.5	7.27	.40	1.13	.073	51.1	.005
1.78	4.43	5.35	18.17	20.5	8.48	.38	.69	.071	41.8	.0045
2.60	11.86	13.15	18.48	49.1	13.5	.58	1.52	.078	50.1	.0065
1.87	10.26	7.47	18.01	43.6	12.8	.48	1.09	.188	52.8	.0095
.97	5.77	3.11	10.90	27.2	7.7	.38	.62	.092	62.0	.0265
2.10	5.77	3.11	10.90	32.7	7.69	.46	1.05	.078	55.0	.007
2.41	9.62	6.57	14.22	34.1	8.98	.43	1.09	.082	59.5	.007
1.47	9.30	7.44	11.37	31.3	11.5	.43	.78	.075	54.4	.0045
1.88	10.22	7.03	11.30	70.8	13.1	.45	1.07	.076	49.3	.0055
1.61	8.17	6.98	9.69	70.8	11.6	.45	1.03	.082	51.4	.0015
2.18	10.90	8.44	8.88	70.8	13.1	.43	1.15	.076	49.6	.013
1.82	13.62	9.84	18.39	79.0	12.3	.45	1 17	.084	49.7	.010
1.88	14.31	7.91	18.39	76.3	15.3	.48	1.36	.079	55.2	.003
2.09	10.90	7.56	14.99	62.7	10.9	.45	.99	.077	53.3	.0045
2.27	11.54	5.11	14.71	29.1	9.31	.99	.94	.233	61.8	.03

IV. RESPONSE PROBABILITY DENSITY FUNCTION TECHNIQUE

All the calculations of breakage probabilities in this report are based on the response probability density function (pdf) technique. In order to understand the analysis it is essential that the concept of a probability density be fully understood. Therefore, this chapter begins with a review of that concept.

1. PROBABILITY DENSITY FUNCTIONS

For illustration, assume that a group of 402 readings have been taken, representing the breaking strengths of steel rods. The readings are then sorted according to size and the number of readings in each 250 psi interval is tabulated. The number of readings in each interval is then graphed as a bar chart as shown in Figure 17a. (If the readings were from glass rather than steel the shape of the distribution would be different, as will be discussed later.) This particular form of bar chart, showing the number of readings in each interval, is known as a histogram. The shape of the histogram in Figure 17a is the well-known bell shape which occurs often for distributions of men's heights, students' grades, and many other measurements.

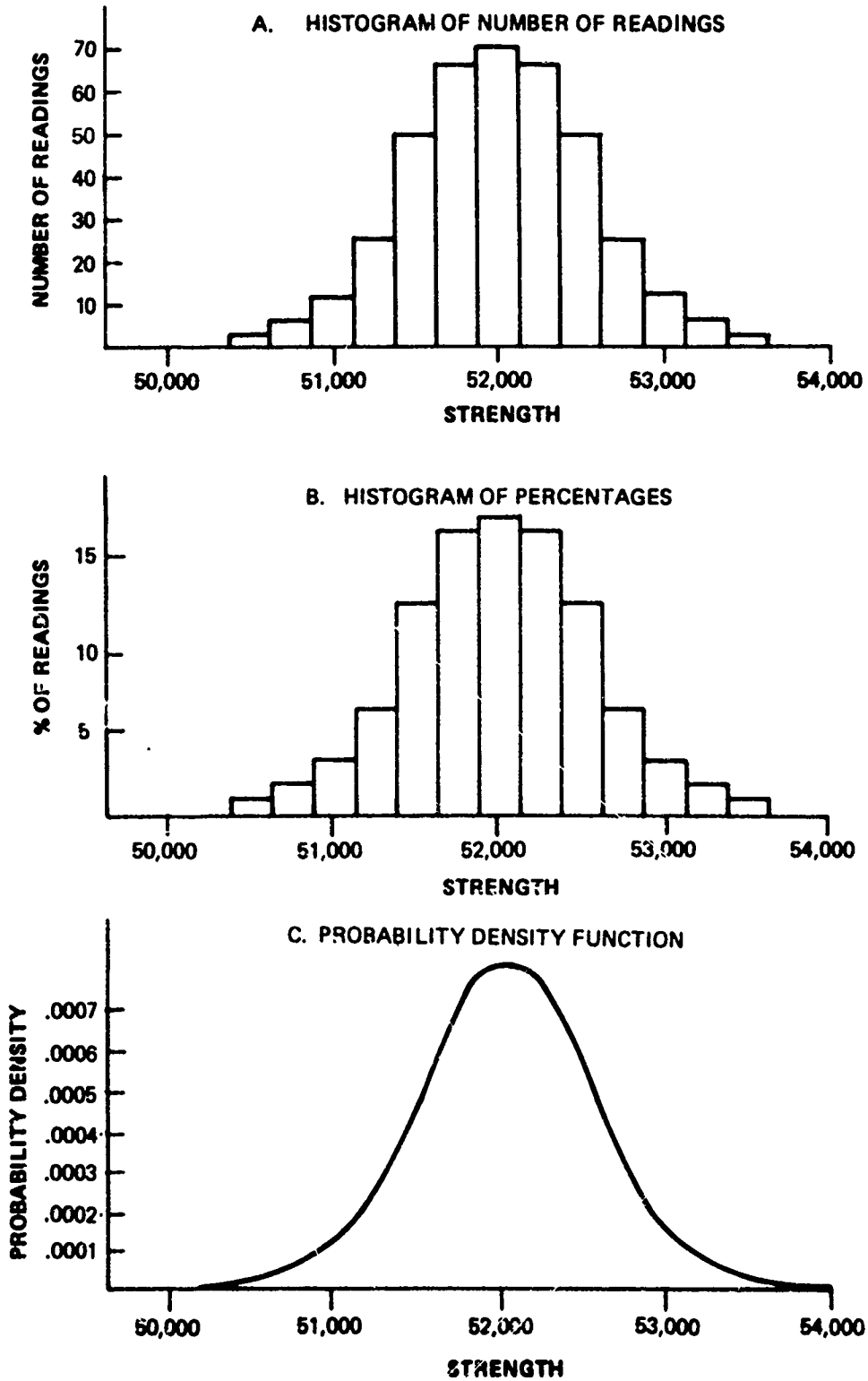

Figure 17. Example of a Probability Density Function

Now assume that for each interval shown in Figure 17a the number of readings is divided by the total number of readings for all intervals combined. This will give the slightly different histogram shown in Figure 17b. The ordinate of Figure 17b shows the percentage of the total number of readings that are in each interval. If the sample rods tested were typical of the rods being manufactured, Figure 17b could also be viewed as a histogram of probabilities. Then it could be observed from the histogram that the probability is .17 of picking a rod at random whose strength is in the interval centered at 52.0 kpsi.

Note that the histogram of Figure 17b is a discrete function. For most analyses, it is more convenient to work with continuous functions, such as the curve in Figure 17c. Note that the curve looks very much like Figure 17b. In fact, it is what would be obtained if there were a very large number of samples and the strength intervals were made smaller and smaller. The curve of Figure 17c is an example of a probability density function. The ordinate of the curve is a density in probability per unit length. For the normal curve shown (also called a gaussian density function), the probability density function is

$$f(x) = \frac{1}{\sqrt{2\pi}\sigma} \exp\left(-\frac{(x-\mu)^2}{2\sigma^2}\right), \qquad (5)$$

where μ is the mean and σ is the standard deviation. To find the probability that a stress, x, falls between two values, x_1 and x_2, merely take the definite integral of the probability density function between x_1 and x_2. Obviously the integral of a probability density function from $-\infty$ to ∞ is 1.

Now observe the probability density function of a stress from some form of random loading as shown in Figure 18. Note the wide range of values that may be expected for readings of stress from the randomly occurring loads of this type. Assume that this probability density function has been determined from a very large number of experimental values. Now suppose that another large sample of the same form of random loading is taken. The probability density functions should be almost identical for the two large samples. (If both sample sizes are infinite they will be identical.) Thus, although individual stress values are random, the shape of the density function is for all practical purposes constant. The probability that stresses will fall in a given range can be predicted with certainty.

Similar to the probability density function for stress, a probability density function for the breaking strengths of the specimens is shown in Figure 19. Again, the probability that a strength reading will be in a given range can be determined.

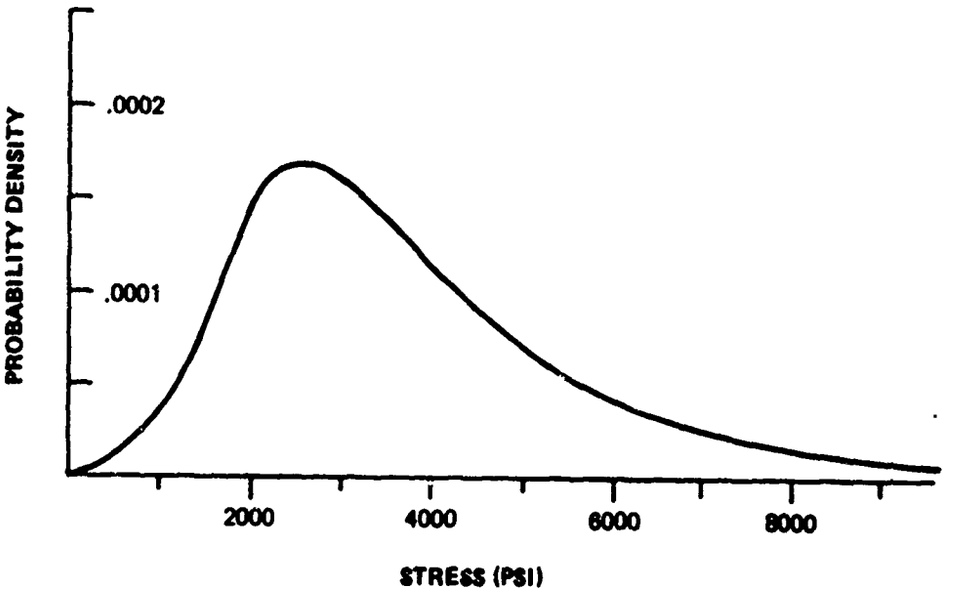

Figure 18. Probability Density Function of Stress

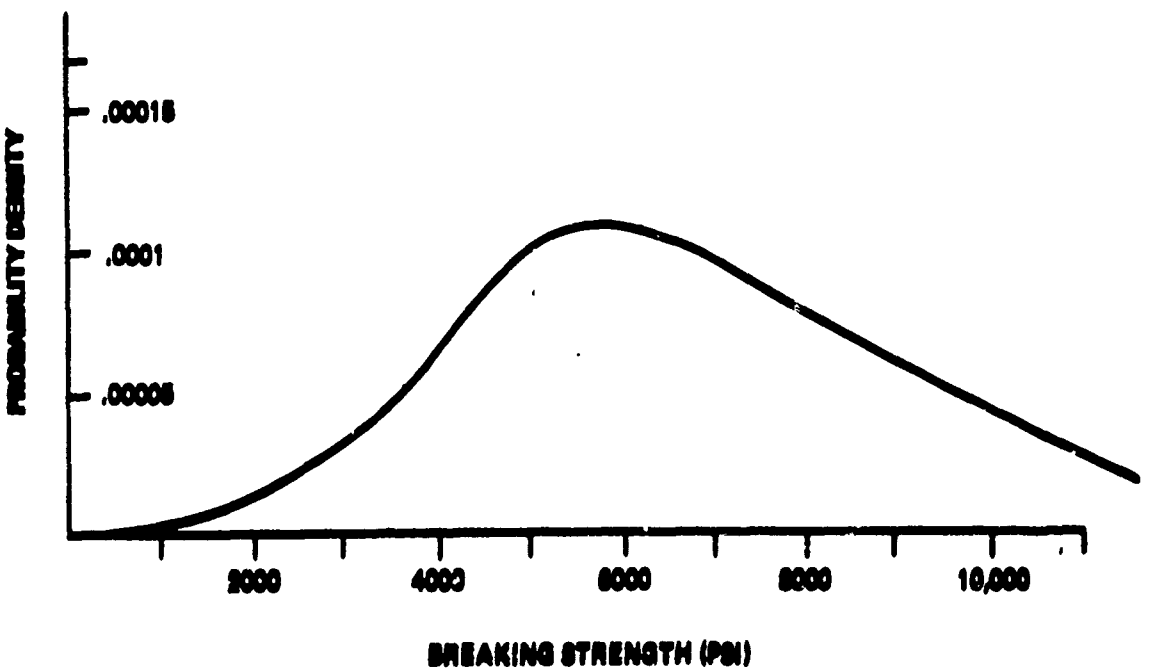

Figure 19. Probability Density Function of Breaking Strength

Now, suppose one of the stresses σ_{m_i} from the loads selected at random acts on one of the random strength samples σ_{G_j}. For this case, an effective factor of safety N_e can be defined by

$$N_{e_k} = \frac{\sigma_{G_j}}{\sigma_{m_i}} \tag{6}$$

Since the stress and strength are assumed to be statistically independent, the probability density function of the effective factor of safety can be found from the probability density functions of the stress and strength. The process for finding the probability density function of N_e in the general case is a convolution-like procedure [35], which can usually be accomplished by computer integration only,

$$F(N_e) = \int_0^\infty f_{\sigma_G}(N_e\sigma_m) f_{\sigma_m}(\sigma_m)\sigma_m d\sigma_m \tag{7}$$

Note that the factor in the integral is a joint probability density of two variables.

Considerable simplification is possible if the stress and strength probability density functions are both lognormal. The lognormal probability density function has the form

$$f(x) = \frac{1}{x\sigma\sqrt{2\pi}} \exp\left[-\frac{1}{2\sigma^2}(\ln x - \mu)^2\right] \tag{8}$$

for $x>0$ and $\sigma>0$, and $f(x) = 0$ for $x>0$. A variable is distributed lognormal if its logarithm is distributed normal.

If imposed stress and material strength are both distributed lognormal, the probability density of the effective factor of safety will then also be lognormal. This is because the logarithm of the effective factor of safety will be the difference of the logarithms of the stress and strength, and the difference of two normally distributed random variables is normally distributed with its mean equal to the difference of the means and its variance equal to the sum of the variances. The probability of breakage can then be found as the area under the curve of the probability density of the effective factor of safety, for effective factor of safety less than 1. Equivalently, this is the area under the curve of the density of the logarithm of the factor of safety to the left of zero.

The probability density functions for the effective factor of safety and its logarithm are shown in Figure 20. The easiest way to find the probability of breakage in this case is to work with the normal curve of the logarithm of N_e in Figure 20b, since the probabilities under a normal curve are a tabulated function.

The following sections will develop the probability density functions of sonic boom stress and material strength so that the above nique can be utilized.

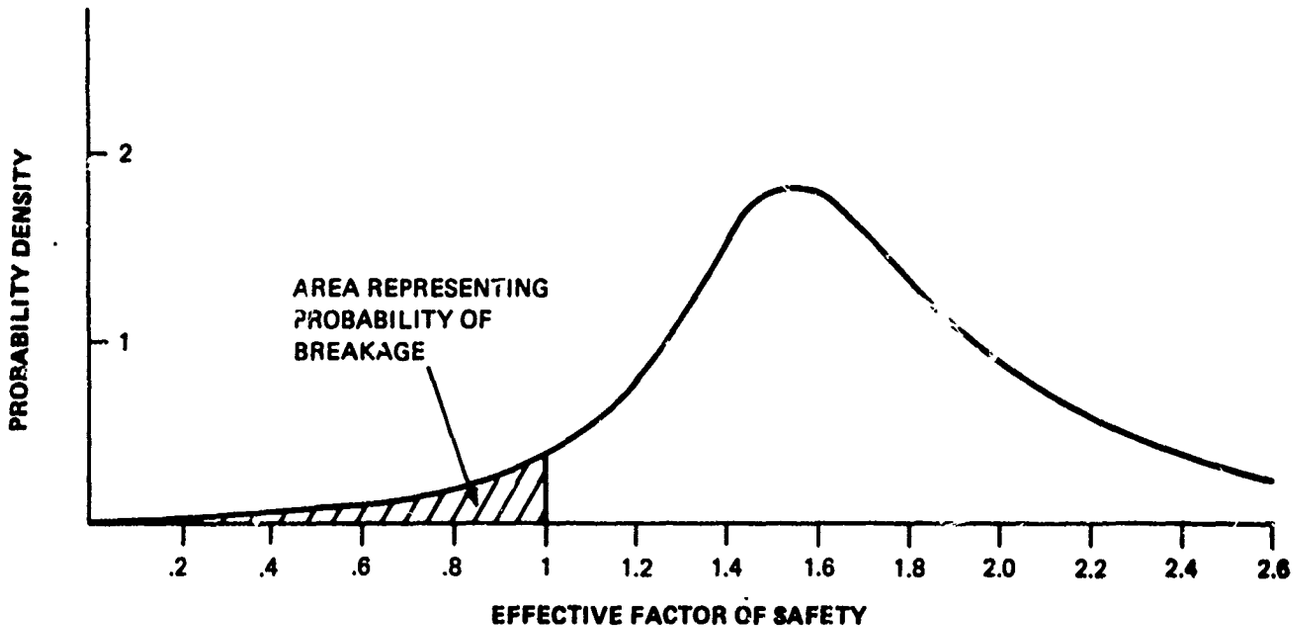

A. PROBABILITY DENSITY FUNCTION OF EFFECTIVE FACTOR OF SAFETY

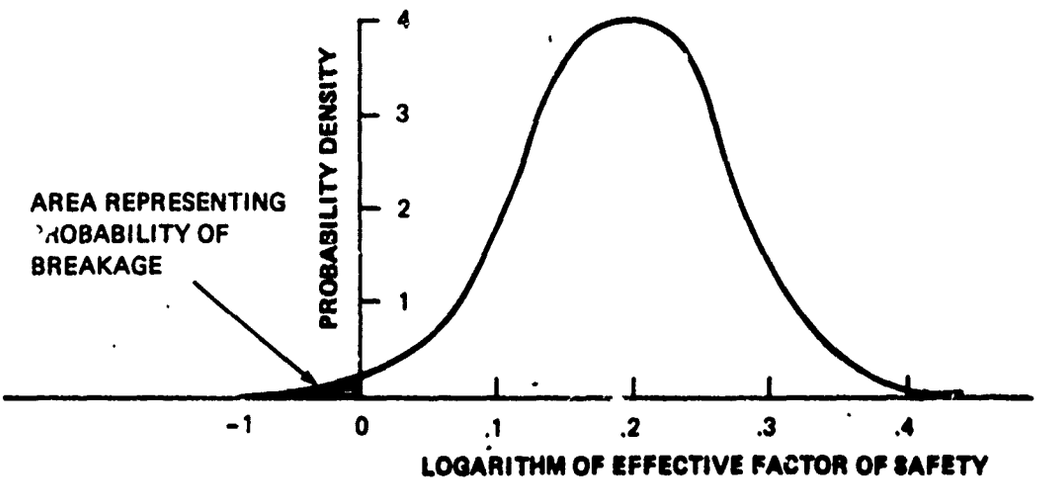

B. PROBABILITY DENSITY FUNCTION OF THE LOGARITHM OF THE EFFECTIVE FACTOR OF SAFETY

Figure 20. Probability Density Function of the Effective Factor of Safety for the Lognormal Case

2. SONIC BOOM STRESS

With the definitions of the peak overpressures and the DAF discussed in Chapter II, a correlation analysis was performed using experimental data from the sonic boom tests performed at White Sands in 1965 [29,30,33] and Edwards Air Force Base in 1966 [31,32,33]. These data consisted of values of p_f, p_e, and p_i measured from microphones and concomitant values of σ_m measured with strain gauges on the windows on the test houses.

Correlation analysis [1,4] of the Edwards data indicated that strain in the test windows correlated well with free field pressure and poorly with other variables. The correlation coefficients calculated between p_f and the strains on four windows were 0.66, 0.69, 0.69, and 0.42. All these results indicate significant correlation at the 99 percent confidence level. Correlation coefficients were also computed between the strains and the impulse $p_f T/2$, but correlations were found to be less than for the pressure p_f. Similarly correlations with wave energy $p_f^2 T/3$ were also found to be less than those with p_f. These results indicate that the free field pressure, p_f, is the correct variable to use in formulating a linear expression for stress.

Three variables that were discarded on the basis of low correlation were the internal pressure p_i, the rise time of the free field pressure waveform t_r, and the sonic boom duration T. The strains

on two windows were found to have correlations of -0.06 and +0.18 respectively with p_j/p_f. These low correlations with signs in both directions suggest that internal pressure is for all practical purposes uncorrelated with strain. The DAF's on five windows were found to have correlations with rise time of +0.20, -0.28, +0.01, and -0.06. This indicates that DAF is not correlated with rise time. Correlation analysis and examination of scatter diagrams also showed that stress is unrelated to the sonic boom duration T except in the case where a very short duration boom impinges on a very large storefront window. In this exceptional case, such as might occur from an F-104 boom, there is a lowpass filter effect. The short duration boom is ineffective in exciting the window above its natural frequency and a low DAF occurs, perhaps of the order of 0.5.

A correlation of 0.78 was found between the peak external pressure p_e and the peak free field pressure p_f. Scatter diagrams of p_e/p_f from the White Sands data indicated a marked dependence on the cosine of the flight path angle, θ. On this basis a regression analysis was performed resulting in the relation

$$\log_{10}(p_e/p_f) = .1427 \cos \theta - .1258. \qquad (9)$$

Having observed the results of the correlation analysis it was now desired to formulate a statistical relationship between the stress and the nominal overpressure. Data from the Oklahoma City sonic

boom tests of 1964 [28] indicated a correlation of 0.42 between the nominal pressure p_o and the free field pressure p_f. The dependence of external pressure p_e and free field pressure p_f had also been noted earlier as had the dependence of stress on p_f. Thus the most suitable form for the stress relation was determined to be

$$\sigma_m = p_o(p_f/p_o)(p_e/p_f)(\sigma_d/p_e)(\sigma_m/\sigma_d). \qquad (10)$$

In the above form all the ratios shown are measurable values for which data are available. The Oklahoma City tests provided 3500 values of p_f/p_o and the White Sands tests provided 900 values of p_e/p_f. The value σ_d/p_e is deterministic; it can be visualized as a stress factor F such as that given in Equation 3 for the flat plate case. The value σ_m/σ_d is the DAF, for which 500 values are available from the Edwards Air Force Base and White Sands tests.

It is readily apparent from the physical situation that the random variable factors in Equation 10 are all statistically independent. The value of (p_f/p_o) depends on the inhomogeneities in the atmos- and on the deviation of the aircraft from its planned altitude and Mach number. The random variable (p_e/p_f) depends on the geometry of the surfaces involved and their reflection coefficients. The DAF depends on window size and mounting. Since the three random variables depend on independent phenomena, they can be expected to be independent.

Using the data from the Oklahoma City, White Sands, and Edwards Air Force Base tests, histograms were computer plotted for p_f/p_o, p_e/p_f, and DAF. The results [1, 4] showed that their pdf's were to a reasonable approximation lognormal. Thus the histograms of the logarithms appeared normally distributed as did the example of (p_f/p_o) shown in Figure 21; a gaussian curve of the same mean and variance is also plotted for comparison. Thus we have verified that the stress was indeed lognormal. The next section considers the probability density function of the material strength.

3. MATERIAL STRENGTH

The breaking stress σ_G of a material can be expressed in terms of a breaking pressure p_G multiplied by a stress factor F, which depends on the loading configuration.

$$\sigma_G = p_G F. \tag{11}$$

The materials we are discussing here are brittle in nature, such as glass, plaster, and mortar. For each of these materials the question arises as to what the shape of the pdf of the breaking pressure is.

We have been able to obtain data on the shape of the breaking pressure for some of the materials and found them to be lognormal.

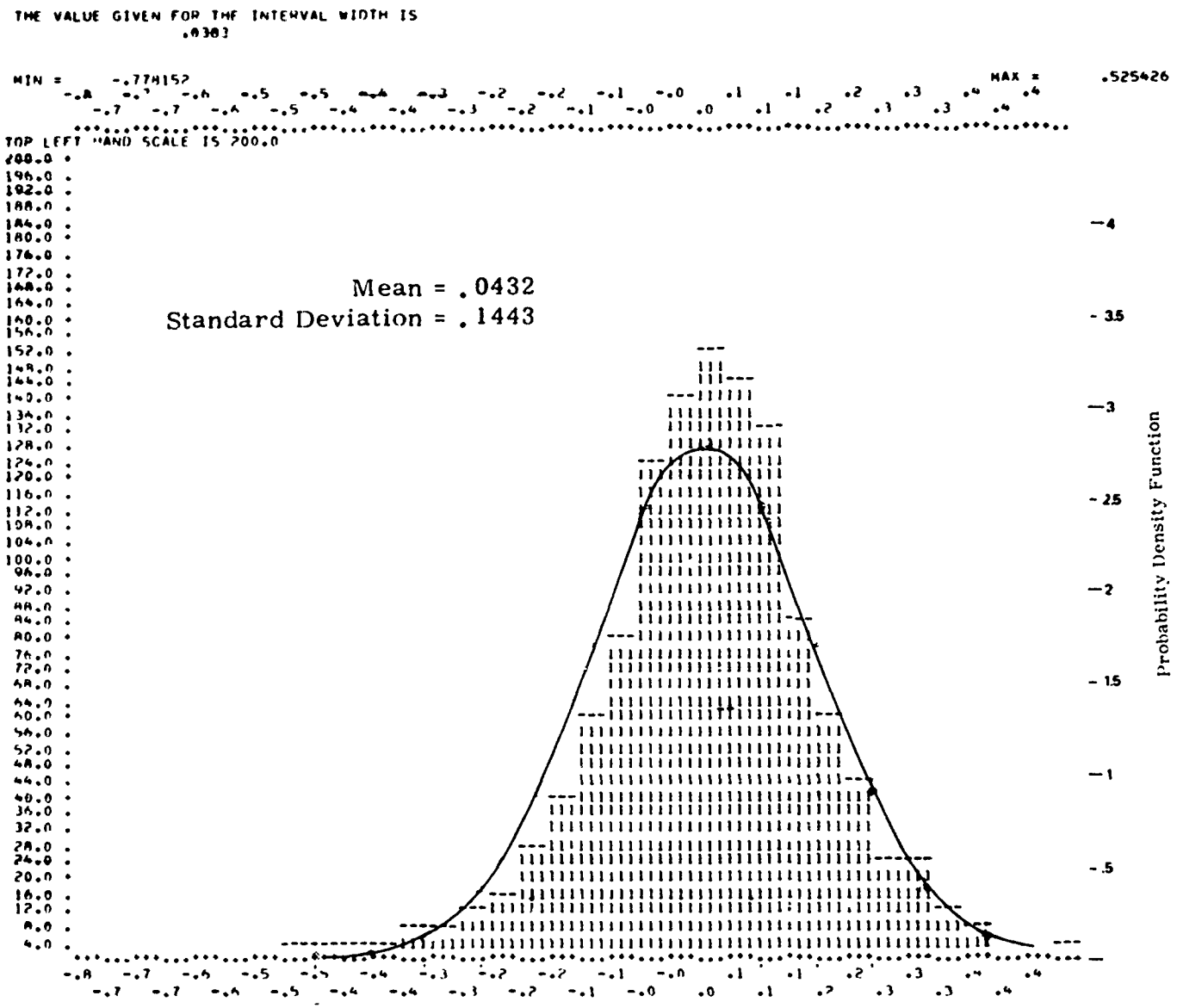

Figure 21. Experimental Probability Density Functior. of Logarithm of External Pressure/Nominal Pressure, Station 3

In our previous work on glass [1, 4] we obtained a large data base of glass breaking pressure readings from the Libbey-Owens-Ford Company [36]. By plotting the histograms of the breaking pressures we found the probability density function of the glass breaking pressure to indeed be lognormal. Similarly we obtained experimental data on the tensile strength of mortar [37, 38] and determined that the pdf is also lognormal. For other materials we have been unable to find sufficient experimental strength data to plot a histogram indicative of a pdf but on the basis of their brittle nature and their similarity to glass or mortar we have assumed their pdf's to be lognormal also.

4. PROBABILITY OF BREAKAGE

Having examined the pdf's of the stress and the strength and found them to be lognormal, the response probability density function technique can now be applied to find the probability of breakage. The effective factor of safety N_e is given by

$$N_e = \sigma_G/\sigma_m. \tag{12}$$

where σ_G is the breaking pressure of the material and σ_m is the maximum stress created by the sonic boom. Using Equations 10 and 11 for the maximum sonic boom stress σ_m and the material strength σ_G we have after taking logarithms

$$\log_{10} \sigma_m = \log_{10} p_o + \log_{10} (p_f/p_o) + \log_{10} (p_e/p_f) \quad (13)$$
$$+ \log_{10} F + \log_{10}(DAF).$$

$$\log_{10} \sigma_G = \log_{10} F + \log_{10} p_G. \quad (14)$$

Thus there results from Equations 13 and 14

$$E\{\log_{10} N_e\} = E\{\log_{10} p_G\} - \log_{10} p_o - E\{\log_{10} (p_f/p_o)\} \quad (15)$$
$$- E\{\log_{10}(p_e/p_f)\} - E\{\log_{10}(DAF)\}.$$

and

$$\text{Var}(\log_{10} N_e) = \text{Var}\left[\log_{10} (p_f/p_o)\right] + \text{Var}\left[\log_{10}(p_e/p_f)\right] \quad (16)$$
$$+ \text{Var}\left[\log_{10}(DAF)\right] + \text{Var}\left[\log_{10} (p_G)\right]$$

The pdf's of the terms involved are illustrated in Figure 22.

The mean and variance of the distribution of each logarithm were found for each case. Note that the mean must be found after taking logarithms, since the mean of the log is not equal to the log of the mean [39]. For $\log_{10} (p_f/p_o)$ the mean was found to be 0.0471 and the variance was 0.0446. For sonic booms equally likely from any flight path direction the mean of $\log_{10} (p_e/p_f)$ was -0.1251 and its variance was 0.0439. If instead only head-on booms are considered then the mean of $\log_{10} (p_e/p_f)$ is 0.0174 and its variance is 0.0308. For the remaining random variables DAF and p_G the mean and variance depend on the material configuration. The other two numbers F and p_o are deterministic.

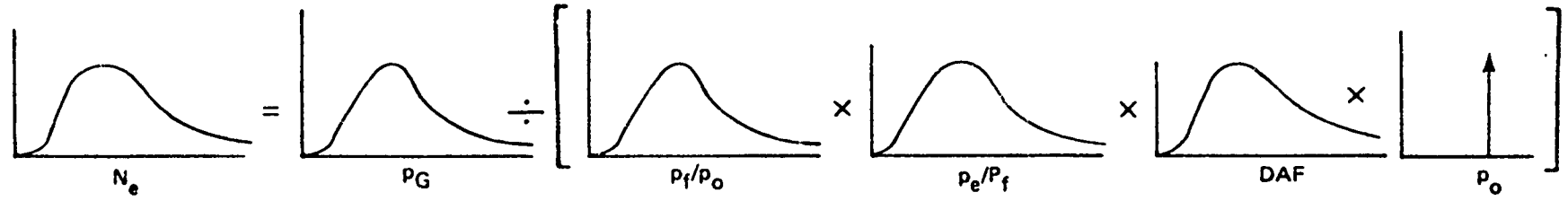

(a) N_e is the product of lognormal random variables

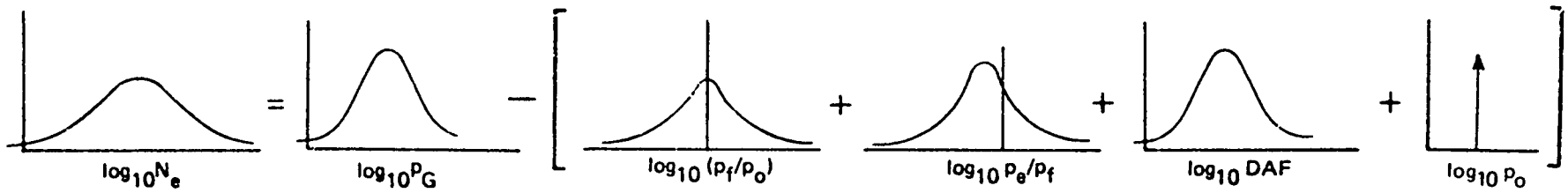

(b) $\log_{10} N_e$ is the sum of normal random variables

Figure 22. Development of Probability Density Function of $\log_{10} N_e$

Having found the mean and variance of $\log_{10} N_e$, the probability of breakage follows directly. By finding the value of

$$z = E\{\log_{10} N_e\} \Big/ \left[\text{Var}\,(\log_{10} N_e)\right]^{1/2} \qquad (17)$$

the area to the left of zero in Figure 20 can be found by entering a standard gaussian table.

This is the technique which will be used in succeeding chapters to find the probability of breakage for various materials. The next chapter will consider glass, and subsequent chapters will analyze plaster, bric-a-brac, and brick.

V. GLASS

Unlike metals, the microstructure of glass is amorphous rather than crystalline. Because of this fact, the practical design strength of glass is a surface condition property rather than a constant material property. For example, glass that is acid-etched and coated with lacquer to protect its surfaces can have an average strength of 250 kpsi. If the same glass is severely sandblasted, its average strength is reduced to 2 kpsi [40]. Because of this dependence on surface scratch condition, strength tests on seemingly identical panes of glass will show a wide scatter of values. Even if the panes of glass have received the same handling, the depth and location of minute surface scratches will be random. The exact value of breaking strength for a given pane cannot be predicted; however, the mean and variance of large lots of glass of the same size, type, and surface condition will be repeatable.

In addition to the variations due to surface scratch condition, there are also variations with loading geometry, loading rate, atmospheric moisture content, and composition. Glass exhibits a property known as "static fatigue" in that it is weaker for loads of longer duration. Static fatigue is a stress corrosion type of process that takes

place when water vapor gets into cracks during loading and aids their growth [41]. Thus for sonic boom loading, which has a duration of the order of 0.1 sec, the strengths of glass will be roughly twice those obtained in typical laboratory measurements whose loading duration is of the order of 60 sec, as shown in Figure 23.

In our study we were fortunate in being able to use a data base of unpublished static test results on 2500 lites of glass, which the Libbey-Owens-Ford Company graciously made available. The data consisted of 119 sets representing a full range of window sizes with approximately 25 readings of breaking pressure per set. Each reading was obtained by loading the glass incrementally to failure on a vacuum test fixture, with the effective load duration being approximately one minute.

Two adjustments were necessary in extrapolating from the Libbey-Owens-Ford data of new glass under static loading to the case of used glass in people's homes under sonic boom loading. First, the glass must be considered to have twice the strength under sonic boom loading as under 60 second laboratory loading because of the static fatigue effect. Counterbalancing this, a reduction of the strength must be allowed for the deterioration of the surface condition over time. After the glass emerges from the factory it suffers scratches in shipping, unpacking, handling, installing, cleaning, and

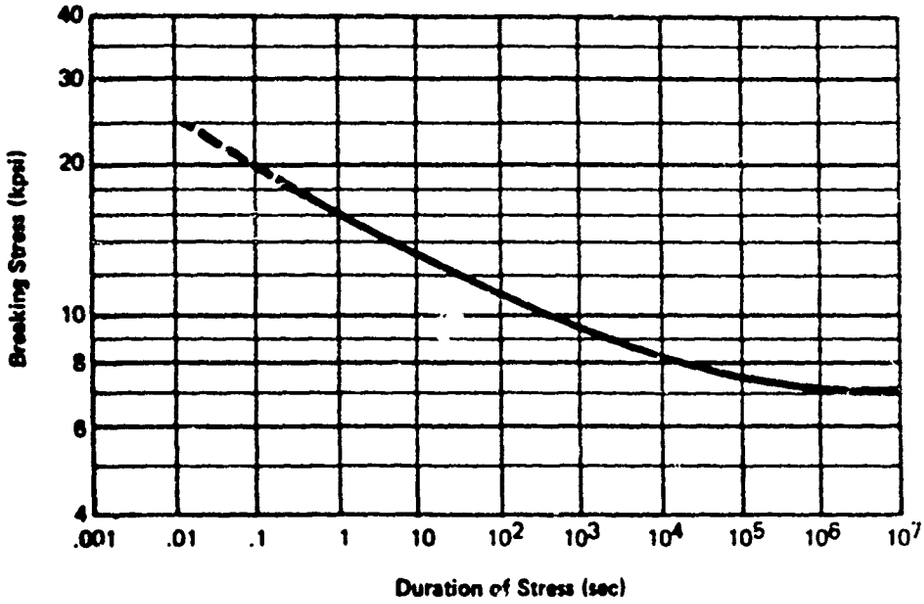

Figure 23. Stress-Time Characteristics of Glass

weathering. Although the glass is weakened by this progressive scratching over time, there appears to be no cumulative dynamic fatigue effect due to repeated sonic boom loading [42]. On the basis of comparing the only available published strength data on used glass with test results on the corresponding size of new glass [42], it was observed that the used glass appeared decreased in strength by a factor of 2, as shown in Figure 24. Thus the two factors of 2 above compensate for each other, and the strength of new glass under static loading can be assumed to be the same as that of used glass under sonic boom loading.

Computer-generated histograms [1, 4] were run for the glass breaking strength and the glass breaking pressure. Both were found to be lognormal to a reasonable approximation.

It was necessary to provide in the statistical model for the presence of already cracked glass in the window population. Although there appear to be no published test data on cracked glass, experimenters in the glass community have said that 10 percent of the strength of ordinary used glass is a good rule of thumb. On this basis the present study has assumed that the mean strength of cracked glass is one-tenth that of used glass, and that the variance of the distribution of the logarithm of its strength is the same as that of used glass. A previous study [31] found cracked glass to be

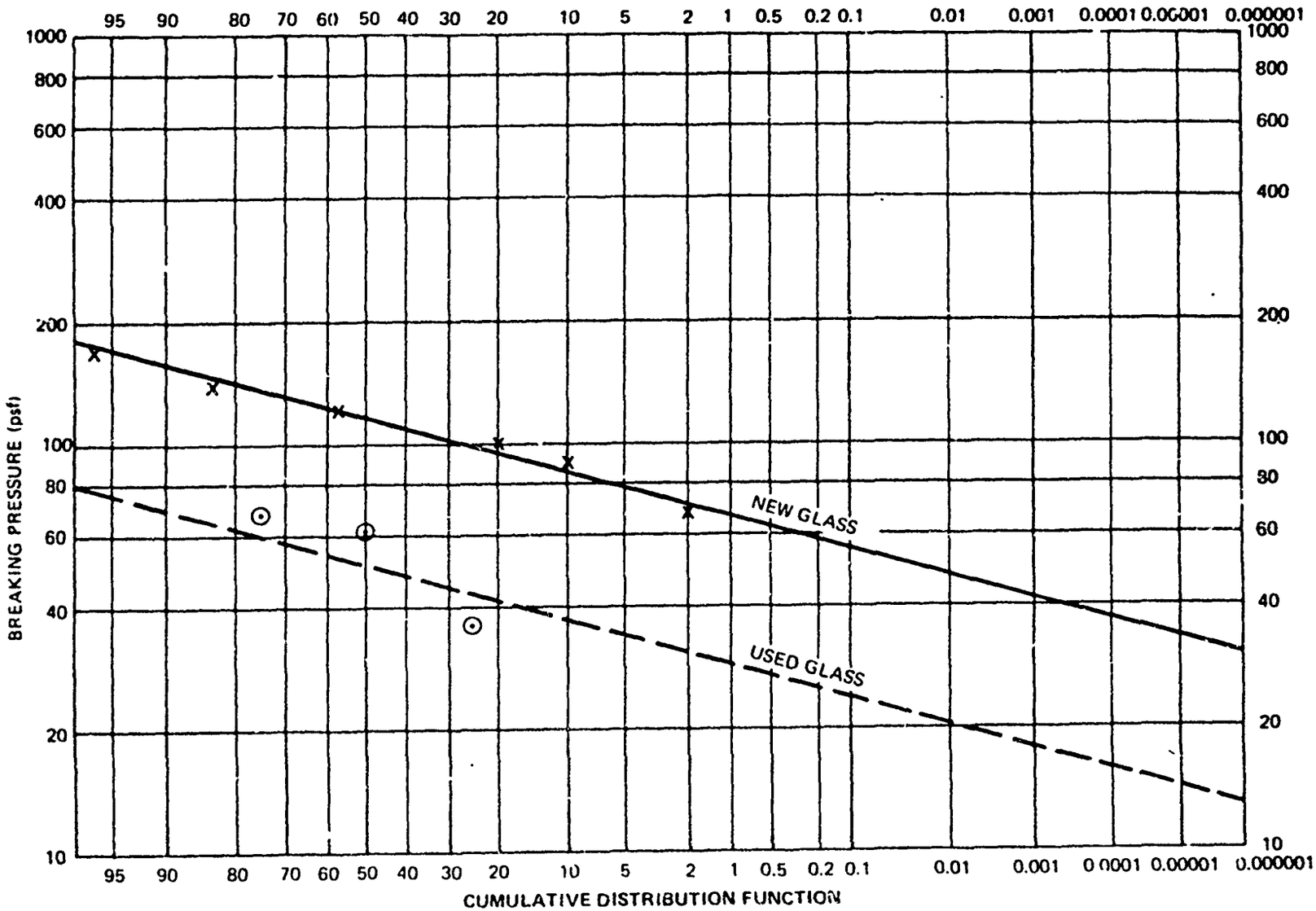

Figure 24. Comparison of Breaking Pressure Distribution of Used and New Glass

.61 percent of the population. On this basis the glass population was assumed in this study to consist of 99.39 percent good glass and 0.61 percent cracked glass. The pdf of the logarithm of strength for the entire population is shown synthesized in Figure 25. Note that in this model all glass is assumed to be either used glass in good condition or cracked glass. No provision has been made for brand new glass or for any state between cracked and good. Using this model the probabilities of breakage for the healthy glass P_H and the cracked glass P_C can then be combined into a population probability of breakage P by using the relation

$$P = 0.9939 P_H + 0.0061 P_C. \tag{18}$$

In applying the response pdf technique to predicting the sonic boom breakage probability in a group of windows, all the windows will have the same pdf's of $\log_{10} (p_f/p_o)$ and $\log_{10} (p_e/p_f)$. But the pdf's of $\log_{10}$ (DAF) and $\log_{10} (p_G)$ will, in general, be different for each window depending on its geometry. Seven typical window types for which data were available are indicated in Table 8. In this table the column headed f_o gives the natural frequency of the site, which is important only in the case where a short duration boom excites a very large window. The sixth column gives the stress factor F from Equation 3. The last column gives the value of $(ab)^{1/2}/h$; stress is roughly proportional to the square of this

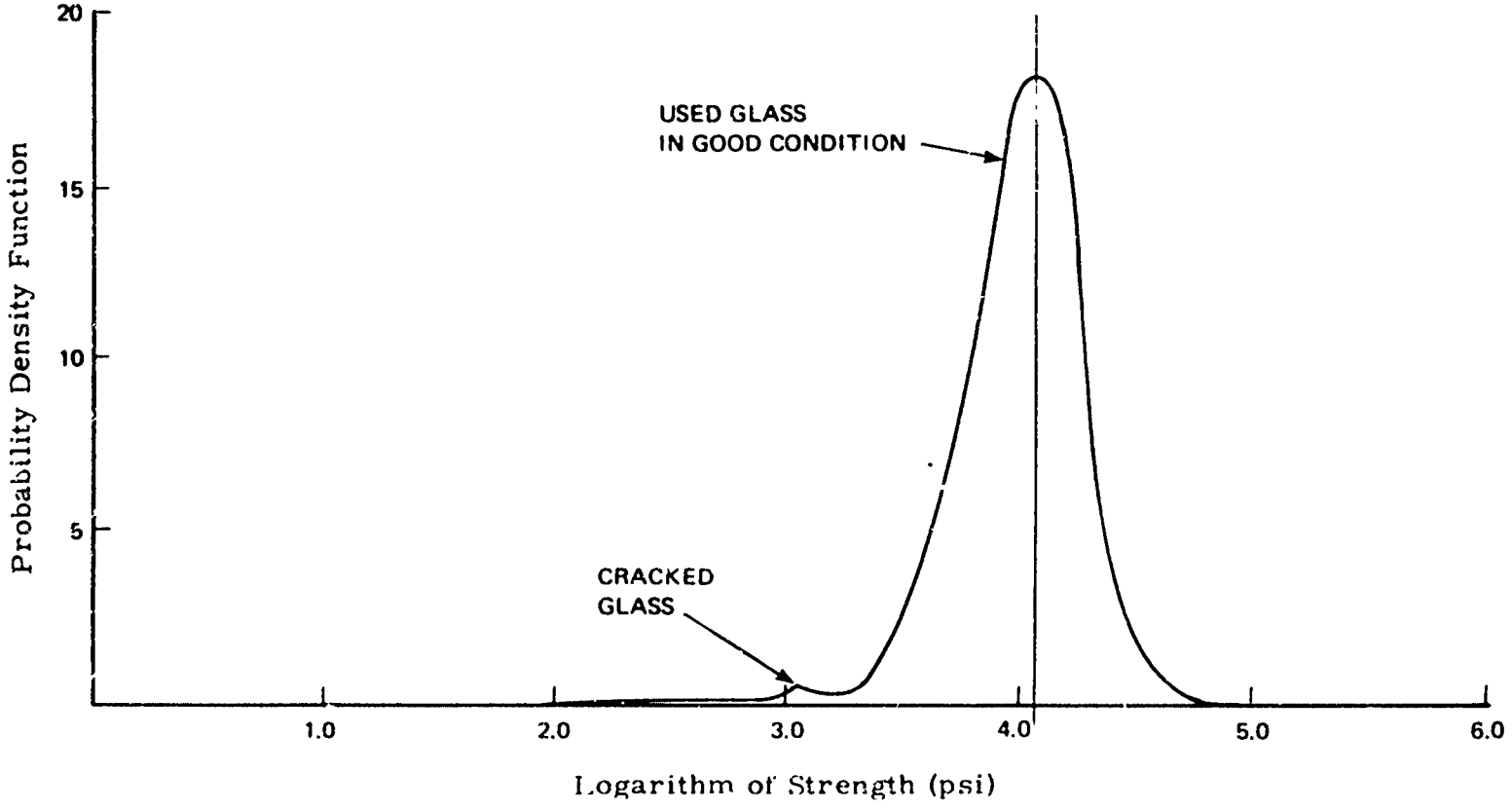

Figure 25. Model of the Probability Density Function of the Logarithm of the Breaking Strength of the Glass Population

parameter for small deflections. The means and variances of the various factors for these windows for all flight paths combined and for head-on booms are shown in Tables 10-13.

Note that for a given window size the mean of $\log_{10}N_e$ of Equation 15 decreases with increasing p_o. Probability of breakage vs. nominal overpressure p_o was plotted for the seven typical window sizes in good condition; the results were straight lines on lognormal paper. These are shown for the cases of booms equally likely from any direction and for head-on booms in Figures 26 and 27 respectively. These results agree well with sonic boom damage claims data at low overpressures of 0.6 breaks per million panes boomed at a nominal overpressure of 1 psf [43, 44]. The results also agree with NASA experiments at high overpressures [45].

Probabilities of breakage were also computed for a model window population consisting of both good glass and cracked glass using Equation 17. The results are shown in Tables 14-21 for various nominal overpressures from 1 to 100 psf with booms equally likely from any direction or head-on. The composite glass population probabilities assume equal numbers of each of the seven window types. Note that for this low overpressure the majority of breaks are likely to occur in already cracked windows.

Table 10. Mean of the Logarithm of the Effective Factor of Safety for All Flight Paths Combined

Window No.	$\log_{10}(p_f/p_o)$ Mean	$\log_{10}(p_e/p_f)$ Mean	$\log_{10}$ DAF Mean	$\log_{10} p_c$ Mean	$\log_{10} N_e$ Mean
1	.0471	-.1251	-.0118	1.7938	1.8836
2	.0471	-.1251	.2579	2.1049	1.9250
3	.0471	-.1251	-.1234	1.6878	1.8892
4	.0471	-.1251	-.1489	1.4606	1.6875
5	.0471	-.1251	.3977	2.4018	2.0821
6	.0471	-.1251	.0795	1.7652	1.7637
7	.0471	-.1251	-.0876	2.1451	2.3107

Table 11. Variance of the Logarithm of the Effective Factor of Safety for All Flight Paths Combined

Window No.	$\log_{10}(p_f/p_c)$ Variance	$\log_{10}(p_e/p_f)$ Variance	$\log_{10}$ DAF Variance	$\log_{10} p_c$ Variance	$\log_{10} N_e$ Variance	$\log_{10} N_e$ Standard Deviation
1	.0446	.0439	.0118	.0102	.1105	.3324
2	.0446	.0439	.0152	.0100	.1137	.3371
3	.0446	.0439	.0206	.0051	.1142	.3379
4	.0446	.0439	.0458	.0085	.1428	.3778
5	.0446	.0439	.0719	.0058	.1662	.4076
6	.0446	.0439	.0508	.0135	.1528	.3909
7	.0446	.0439	.0803	.0141	.1829	.4276

Table 12. Means of the Logarithm of the Effective Factor of Safety for Head-On Flight Path

Window No.	$\log_{10}(p_f/p_o)$ Mean	$\log_{10}(p_e/p_f)$ Mean	$\log_{10}$ DAF Mean	$\log_{10} p_c$ Mean	$\log_{10} N_e$ Mean
1	.0471	.0174	-.0118	1.7938	1.7411
2	.0471	.0174	.2579	2.1049	1.7825
3	.0471	0174	-.1234	1.6878	1.7467
4	.0471	.0174	-.1489	1.4606	1.5450
5	.0471	.0174	.3977	2.4018	1.9396
6	.0471	.0174	.0795	1.7652	1.6212
7	.0471	.0174	-.0876	2.1451	2.1682

Table 13. Variance of the Logarithm of the Effective Factor of Safety for Head-On Flight Path

Window No.	$\log_{10}(p_f/p_o)$ Variance	$\log_{10}(p_e/p_f)$ Variance	$\log_{10}$ DAF Variance	$\log_{10} p_g$ Variance	$\log_{10} N_e$ Variance	$\log_{10} N_e$ Standard Deviation
1	.0446	.0309	.0118	.0102	.0969	.3112
2	.0446	.0309	.0152	.0100	.1007	.3173
3	.0446	.0309	.0206	.0051	.1012	.3181
4	.0446	.0309	.0458	.0085	.1298	.3602
5	.0446	.0309	.0719	.0058	.1532	.3914
6	.0446	.0309	.0508	.0135	.1398	.3739
7	.0446	.0309	.0803	.0141	.1699	.4122

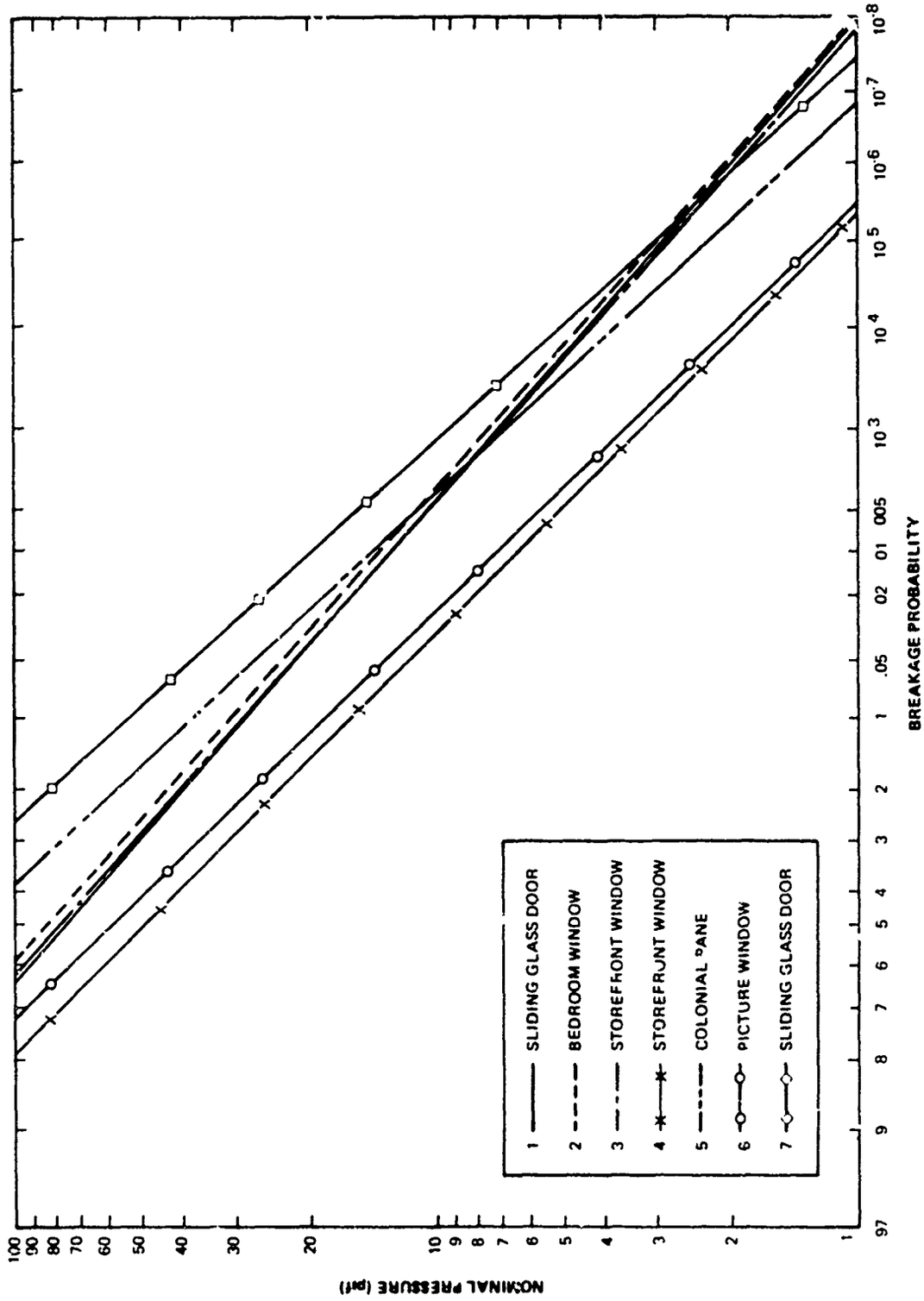

Figure 26. Breakage Probabilities for Glass in Good Condition for All Flight Paths Equally Likely

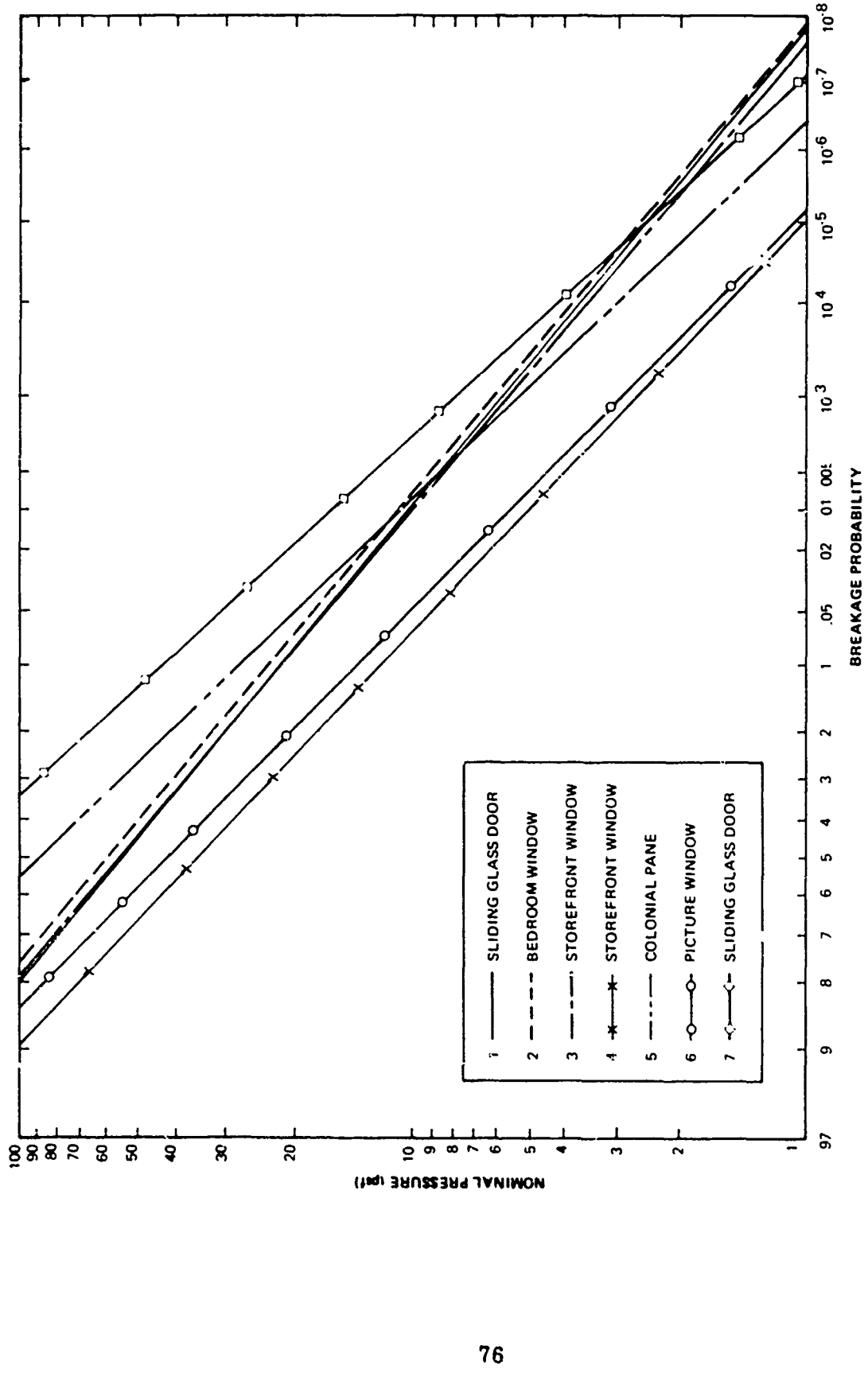

Figure 27. Breakage Probabilities for Glass in Good Condition for Head-On Flight Paths

Table 14. Probability of Glass Breakage Calculated for Model Window Population for All Flight Paths Equally Likely at a Nominal Overpressure of 1 psf

Window No.	Glass in Good Condition			Cracked Glass			Window Type Combined
	Mean $\log_{10}N_e$	z	P	Mean $\log_{10}N_e$	z	P	P
1	1.8836	5.67	$.7 \times 10^{-8}$	.8836	2.65	0040	2.44×10^{-5}
2	1.9250	5.71	$.6 \times 10^{-8}$	.9250	2.74	.0031	1.89×10^{-5}
3	1.8892	5.59	1.1×10^{-8}	.8892	2.63	.0043	2.62×10^{-5}
4	1.6875	4.47	4.3×10^{-6}	.6875	1.82	.0346	21.53×10^{-5}
5	2.0821	5.11	1.67×10^{-7}	1.0821	2.65	.0040	2.46×10^{-5}
6	1.7637	4.51	3.4×10^{-6}	.7637	1.95	.0254	15.83×10^{-5}
7	2.3107	5.41	$.3 \times 10^{-7}$	1.3107	3.07	.0010	$.61 \times 10^{-5}$

Good Glass $P_H = 1.1 \times 10^{-6}$

Cracked Glass $P_C = 0.0109$

Glass Population $P = 67.6 \times 10^{-6}$

Table 15. Probability of Glass Breakage Calculated for Model Window Population for Head-On Flight Path at a Nominal Overpressure of 1 psf

Window No.	Glass in Good Condition			Cracked Glass			Window Type Combined
	Mean $\log_{10}N_e$	z	P	Mean $\log_{10}N_e$	z	P	P
1	1.7411	5.59	$1.2X10^{-8}$	.7411	2.38	.0087	$5.13X10^{-5}$
2	1.7825	5.62	$9.8X10^{-9}$	.7825	2.47	.0068	$4.15X10^{-5}$
3	1.7467	5.49	$2.1X10^{-8}$	.7467	2.34	.0096	$5.86X10^{-5}$
4	1.5450	4.29	$8.6X10^{-6}$	.5450	1.51	.0655	$40.81X10^{-5}$
5	1.9396	4.96	$3.5X10^{-7}$	.9396	2.40	.0082	$5.04X10^{-5}$
6	1.6212	4.34	$6.9X10^{-6}$	.6212	1.66	.0485	$30.27X10^{-5}$
7	2.1682	5.26	$7.4X10^{-8}$	1.1682	2.83	.0023	$1.41X10^{-5}$

Good Glass $P_H = 2.3X10^{-6}$

Cracked Glass $P_C = .0214$

Glass Population $P = 1.33X10^{-4}$

Table 16. Probability of Glass Breakage Calculated for Model Window Population for All Flight Paths Equally Likely at a Nominal Overpressure of 2 psf

Window No.	Glass in Good Condition			Cracked Glass			Window Type Combined
	Mean $\log_{10}N_e$	z	P	Mean $\log_{10}N_e$	z	P	P
1	1.5826	4.76	$1.02X10^{-6}$	.5826	1.75	.0401	$2.46X10^{-4}$
2	1.6240	4.82	$.80X10^{-6}$	.6240	1.85	.0322	$1.97X10^{-4}$
3	1.5882	4.70	$1.31X10^{-6}$	.5882	1.74	.0409	$2.50X10^{-4}$
4	1.3865	3.67	$1.3\ X10^{-4}$	.3862	1.02	.1539	$1.07X10^{-3}$
5	1.7811	4.37	$5.5\ X10^{-6}$	.7811	1.92	.0274	$1.73X10^{-4}$
6	1.4627	3.74	$1.0\ X10^{-4}$	.4627	1.[illegible]	.1379	$9.41X10^{-4}$
7	2.0097	4.70	$1.31X10^{-6}$	1.0097	2.36	.0081	$5.07X10^{-5}$

Good Glass $P_H = 3.43X10^{-5}$

Cracked Glass $P_C = 0.0629$

Glass Population $P = 4.18X10^{-4}$

Table 17. Probability of Glass Breakage Calculated for Model Window Population for Head-On Flight Path at a Nominal Overpressure of 2 psf

Window No.	Glass in Good Condition			Cracked Glass			Window Type Combined
	Mean $\log_{10}N_e$	z	P	Mean $\log_{10}N_e$	z	P	P
1	1.4401	4.63	2.0×10^{-6}	.4401	1.41	.0793	4.86×10^{-4}
2	1.4815	4.70	1.4×10^{-6}	.4815	1.52	.0643	3.94×10^{-4}
3	1.4457	4.54	2.8×10^{-6}	.4457	1.40	.0808	4.96×10^{-4}
4	1.2440	3.45	2.81×10^{-4}	.2440	.68	.2451	1.77×10^{-3}
5	1.6386	4.19	1.5×10^{-5}	.6386	1.63	.0515	3.29×10^{-4}
6	1.3202	3.53	2.20×10^{-4}	.3202	.86	.1949	1.41×10^{-3}
7	1.8672	4.53	2.8×10^{-6}	.8672	2.10	.0179	1.12×10^{-4}

Good Glass $P_H = 7.5 \times 10^{-5}$

Cracked Glass $P_C = .105$

Glass Population $P = 7.15 \times 10^{-4}$

Table 18. Probability of Glass Breakage Calculated for Model Window Population for Head-On Flight Path at a Nominal Overpressure of 4 psf

Window No.	Glass in Good Condition			Cracked Glass			Window Type Combined
	Mean $\log_{10}N_e$	z	P	Mean $\log_{10}N_e$	z	P	P
1	1.1390	3.66	$1.4X10^{-4}$	.1390	.45	.3264	$2.13X10^{-3}$
2	1.1804	3.72	$.9X10^{-4}$	.1804	.57	.2843	$1.82X10^{-3}$
3	1.1446	3.60	$1.6X10^{-4}$	.1446	.45	.3264	$2.15X10^{-3}$
4	.9430	2.62	$4.4X10^{-3}$	-.0570	- 16	.5636	$7.81X10^{-3}$
5	1.3375	3.42	$3.2X10^{-4}$	.3375	.86	.1949	$1.50X10^{-3}$
6	1.0191	2.73	$3.2X10^{-3}$	.0191	.05	.4801	$6.11X10^{-3}$
7	1.5661	3.80	$.8X10^{-4}$	.5661	1.37	.0853	$.60X10^{-3}$

Good Glass $P_H = 1.20X10^{-3}$

Cracked Glass $P_C = .223$

Glass Population $P = 3.16X10^{-3}$

Table 19. Probability of Glass Breakage Calculated for Model Window Population for Head-On Flight Path at a Nominal Overpressure of 20 psf

Window No.	Glass in Good Condition			Cracked Glass			Window Type Combined
	Mean $\log_{10}N_e$	z	P	Mean $\log_{10}N_e$	z	P	P
1	.4401	1.41	.0793	-.5599	-1.80	.9641	.085
2	.4815	1.52	.0643	-.5185	-1.63	.9485	.070
3	.4457	1.40	.0808	-.5543	-1.74	.9591	.086
4	.2440	.68	.2451	-.7560	-2.10	.9821	.250
5	.6386	1.63	.0515	-.3614	- .92	.8212	.056
6	.3202	.86	.1949	-.6798	-1.82	.9656	.200
7	.8672	2.10	.0179	-.1328	- .32	.6255	.022

Good Glass $P_H = .105$

Cracked Glass $P_C = .895$

Glass Population $P = .110$

Table 20. Probability of Glass Breakage Calculated for Model Window Population for Head-On Flight Path at a Nominal Overpressure of 40 psf

Window No.	Glass in Good Condition: Mean $\log_{10} N_e$	z	P	Cracked Glass: Mean $\log_{10} N_e$	z	P	Window Type Combined: P
1	.1[illegible]0	.45	.3264	- .8610	-2.76	.9971	.330
2	.1804	.57	.2843	- .8196	-2.58	.9951	.289
3	.1448	.45	.3264	- .8554	-2.69	.9964	.330
4	-.0570	- .16	.5636	-1.0570	-2.93	.9983	.566
5	.3375	.86	.1949	- .6625	-1.69	.9545	.200
6	.0191	.05	.4801	- .9809	-2.62	.9956	.483
7	.5661	1.37	.0853	- .4339	-1.05	.8531	.090

Good Glass $P_H = .323$

Cracked Glass $P_C = .970$

Glass Population $P = .327$

Table 21. Probability of Glass Breakage Calculated for Model Window Population for Head-On Flight Path at a Nominal Overpressure of 100 psf

Window No.	Glass in Good Condition			Cracked Glass			Window Type Combined
	Mean $\log_{10}N_e$	z	P	Mean $\log_{10}N_e$	z	P	P
1	-.2589	- .83	.7967	-1.2589	-4.04	.9999	.798
2	-.2175	- .69	.7549	-1.2175	-3.83	.9999	.756
3	-.2533	- .80	.7881	-1.2533	-3.93	.9999	.789
4	-.4550	-1.26	.8962	-1.4550	-4.04	.9999	.897
5	-.0604	- .15	.5596	-1.0604	-2.71	.9966	.562
6	-.3788	-1.01	.8438	-1.3788	-3.68	.9999	.845
7	+.1682	+ .41	.3409	- .8318	-2.02	.9783	.345

Good Glass $P_H = .711$

Cracked Glass $P_C = .9963$

Glass Population $P = .713$

The external overpressures are somewhat higher for head-on booms than for flight paths equally likely from any direction as indicated in Equation 9. For a 1 psf head-on boom, the breakage probability calculated for the model glass population was 133 breaks per million panes boomed; for 2 psf head on, 715 breaks per million. Note that these values of P are almost twice those shown in Tables 14 and 16 for the same overpressures and flight paths equally likely from any direction. Breakage probabilities for the model population were also computed for head-on booms at higher overpressures; at 4 psf, 3,160 breaks per million; at 20 psf, 110,000 breaks per million; at 40 psf, 327,000 breaks per million; and at 100 psf, 713,000 breaks per million.

* * * * * * * * * * * *

This concludes the analysis of glass; the remaining chapters extend the response probability density function technique to plaster, bric-a-brac and brick.

VI. PLASTER

Plaster, like glass, is a brittle material which is sometimes subject to sonic boom damage. Plaster is manufactured by heating (calcining) gypsum at 300°-350°F. The calcining process drives off water vapor and changes the state of the material from dihydrate calcium sulfate to hemihydrate. The calcined gypsum can be used to form various plasters at the building site, depending on the aggregate with which it is mixed. In older construction the aggregate consisted of lime and sand. Other possible aggregates are wood fiber, vermiculite, and perlite. When the plaster and aggregate are mixed with water they form a slurry and entrapped air bubbles float out. As the plaster sets, a crystallization process takes place and the gypsum returns to its dihydrate form and bonds in the aggregate materials.

The proportioning of ingredients, the thoroughness of mixing, and the removal of air bubbles all depend on the workmanship of the individual plasterers. For this reason plaster shows considerable variation in strength.

The strength of the plaster will depend to a large extent on whether the correct amount of water is mixed in; too much or too

little will lower the strength. The key parameter in determining the mechanical properties of plaster is the water-to-plaster ratio, which is called the consistency. If too much water is added the excess will run off, leaving the set plaster weak. If too little is added incomplete hydration will take place and the resulting plaster will have places that have never gone into the crystalline form. Figures 28 and 29 [46, 48, 49] show the variation in mechanical properties.

There is also a substantial variation in tensile strength of plaster depending on the proportion of aggregate and the type of aggregate used. This variation is indicated in Table 22 [50]. Note from the table that plaster is considerably stronger in compression than in tension, so that for sonic boom push-pull loading only tension failures would be expected. From Table 22 it appears that a typical conservative figure to use for the tensile strength of plaster is 100 psi. However, the strength could get up to 350 psi.

Usually plaster is applied to a wall or ceiling in three coats. The first coat or "scratch coat" is applied directly to the lathing. Its surface is then scratched with a rough tool to provide better adherence of the following coat. The second coat, called the "brown coat," is somewhat thicker. The "finish coat" which goes over the brown coat is the one that is visible to the eye. It is often composed of "gauging plaster," a combination of calcined gypsum and lime.

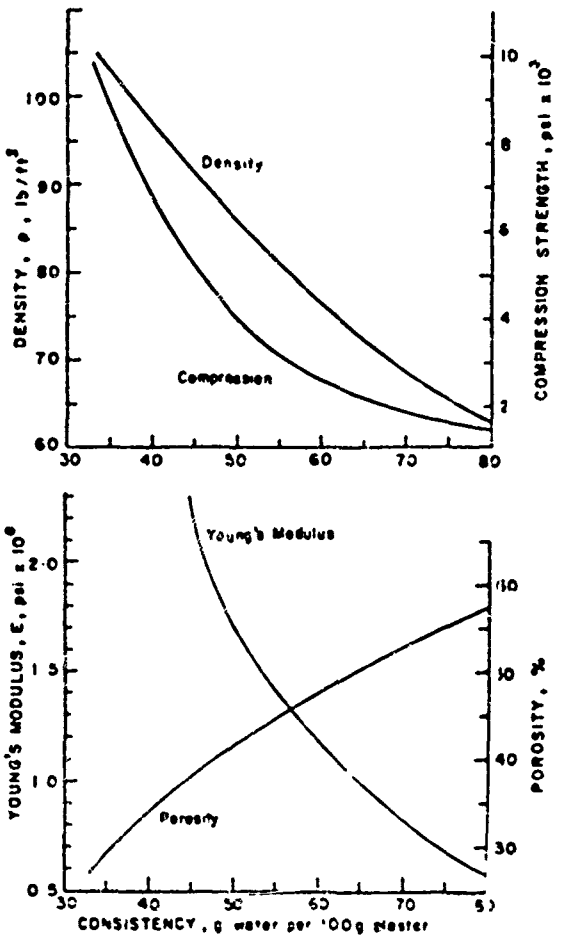

Figure 28. Variation in Mechanical Properties of Gypsum Plasters With Consistency

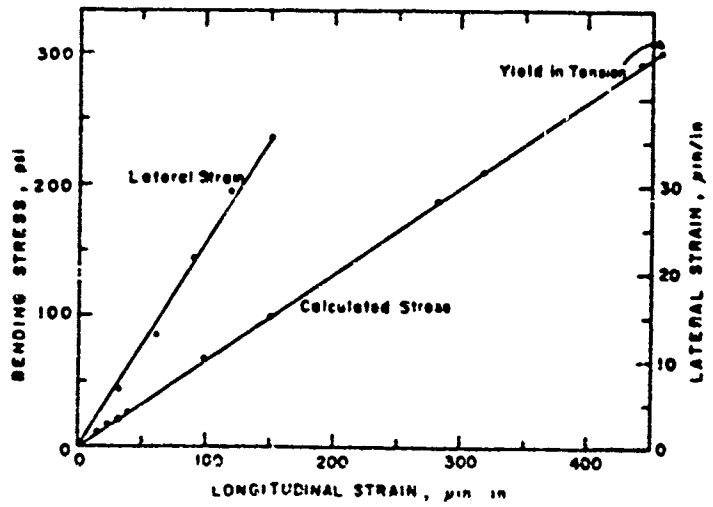

Figure 29. Stress/Strain Plot for Plaster (80 Parts Water)

Table 22. Strength of Basecoat Plaster for Mixtures With Various Aggregates

Type of Plaster and Mix*	Compressive Strength Range, Dry, psi	Tensile Strength Range, psi
Mill-Mixed Perlite Plaster	600-800	125-160
Wood Fiber Plaster		
Neat	1500-2000	320-390
Sanded 100:1	1200-1600	180-240
Gypsum Neat Plaster Mixed With:		
Sand 100:2	750-1100	140-170
100:2-1/2	650-850	120-145
100:3	550-750	100-125
Perlite 100:2	600-800	120-150
100:3	450-600	95-110
Vermiculite 100:2	400-525	90-100
100:3	250-325	75-85

*Aggregates shown in cu ft, plasters in lb

Note: Average laboratory test results; actual job strengths may vary from these data because of job conditions and methods of mixing and handling.

The total thickness for all three coats combined is usually 1/2 to 3/4 inch.

The analysis of plaster failures on buildings is much more difficult than those of glass, because plaster never appears as a lone element subjected to sonic boom as glass does. Plaster is always used in conjunction with a wall or ceiling configuration, which supplies the vast majority of the load-resisting capacity of the assembly. Each wall or ceiling configuration thus represents a different support for the plaster mounted upon it and the stress on the plaster can be expected to vary accordingly. The more the support structure deflects, the greater the stress on the plaster. Because of the many variations possible, the best that can be attempted within the scope of this study is to perform the analysis for a few configurations which seem typical.

Besides the structural variation another problem which complicates plaster failure predictions is the nature of plaster failures. Generally the overstressing of building plaster in tension merely results in hairline cracks, but not in immediate catastrophic failure. This is much different from sonic boom failure of glass where it is likely that the window will shatter, or that a highly visible crack will appear. Plaster cracks by comparison are very thin and are

difficult for the untrained observer to detect with the naked eye, especially if they occur in a ceiling. Only when a catastrophic failure occurs, such as a piece of plaster falling from the ceiling, is the damage apparent. For such a failure, where the plaster actually breaks loose and falls, it is necessary not only that it be cracked at its surface, but also that its hold on the lath structure be cracked.

Patterns of plaster failures caused by sonic booms in the White Sands tests [30] are shown in Table 23. Note from the table that almost all the observed damage consisted of hairline cracks and the extension of existing cracks. The table indicates two types of failure for plaster, diaphragm and racking. In diaphragm failure the wall or ceiling bellies out due to the sonic boom, bending the plaster on its surface. In racking failure the adjacent walls and ceiling lean forward slightly, trying to push the wall into a parallelogram shape. This results in a tearing action on the plaster at the corners of the room and near doors and windows. As seen from the table, diaphragm failures and racking failures occur at about the same overpressures. Since racking failures are much harder to treat analytically and data on them are scarce, we treat diaphragm failures only here. The results should also extend to racking failures, however, on the basis of the similarity in failure overpressures.

Table 23. Plaster Breakage at White Sands

Item and Description	Mechanism*	Bldg.	Intensity (psf)			
			Boom†	Min.	Max.	Ave.
Jacking Crack Extended (2 in)	R	W-4	-	4.8	7.4	5.9
Stucco Cracks Hairline Extended (1 in)	D	W-3	-	4.6	12.5	7.6
Old Gypboard Ceiling Crack Extended (1 in)	D	H	-	4.5	11.0	6.9
New Hairline Stucco Cracks (1 in)	R	W-3	38.0	-	-	-
Ceiling Crack Extended (1/2 in)	D	H	-	8.7	11.7	10.0
Ceiling Crack Extended (1/2 in)	D	H	-	8.2	22.4	13.7
Jacking Crack Extended (2 in)	R	W-4	-	2.4	7.6	4.7
Damaged Suspended Ceiling Spalled at Joint	D	366TAC	-	1.6	11.6	4.2
Cracks Spalled, Ceiling (2 in)	D	H	-	7.0	12.2	9.4
Ceiling Fell (8' x 8' section)	D	W-4	12.1	6.4	12.1	10.2

*R-Racking Action
D-Diaphragm Action

†By Calibrated Sound Level Intensity Meter

We performed calculations of the probability of plaster cracking from sonic boom for the six plaster configurations shown in Table 24. The entries in the table for Numbers 1 and 2 are calculated static pressures for the ceiling configuration indicated. The first ceiling has low strength plaster with a tensile strergth of 100 psi, and the second has high strength plaster with a tensile strength of 350 psi. The four plaster wall configurations shown represent experimental results from pressurizing wall sections in laboratories [51, 52]. Plaster configurations 3 and 4 failed at lower overpressures than would be expected for a typical external wall in a home, since these configurations represented party walls rather than outside walls. Configurations 5 and 6 represent the most susceptible configurations of external walls, those of wood frame houses. The fact that the failure pressures in Table 24 are so low shows the reason why plaster often fails in ordinary occurrences, such as slamming a door or hammering a nail in the wall.

A thorough search was made for data on the probability density function of the breaking strength of plaster. We reviewed the literature and contacted manufacturers, trade associations, and the National Bureau of Standards. Unfortunately no probability density function data on plaster were available, We were, however, able to find sufficient data on a similar material, mortar [37], and found

Table 24. Static Failure Pressures of Plaster Configurations

Number	Element	Configuration	Static Failure Pressure (psf)
1	Ceiling	20 ft x 15.5 ft 2 in x 8 in joists 2 ft o.c. 1/4 in wooden lath. 1/2 in plaster with 100 psi tensile strength.	11
2	Ceiling	20 ft x 15.5 ft 2 in x 8 in joists 2 ft o.c. 1/4 in wooden lath. 1/2 in plaster with 350 psi tensile strength.	39
3	Wall	10 ft height 1-5/8 in hollow steel stud 16 in o.c. gypsum lath and plaster.	15
4	Wall	10 ft height 3-5/8 in steel screw stud 1/2 in gypsum base with veneer plaster.	26
5	Wall	Wood frame, sugarcane-fiber insulating board sheathing and wood bevel siding outside, sugarcane-fiber insulating board lath and plaster inside.	50
6	Wall	Wood frame, wood fiber sheathing, wood furring strips and wood shingles outside, plaster on wood fiber lath inside.	60

its distribution to be lognormal. The fact that mortar has a lognormal distribution allows us to apply the response probability density function technique, as we did for glass, in treating brick-mortar systems later in this report. On the basis of the structural similarity of plaster and mortar, we represent the probability density function of plaster here with a lognormal probability density function having the variance of its logarithm the same as the variance of the logarithm of the breaking pressure of mortar. The variance of the logarithm of the breaking pressure of mortar was found to be .0324; this figure was thus also used here as the variance of the logarithm of the breaking pressure of plaster.

The response probability density function technique was used in analyzing the plaster configurations shown in Table 24. The resulting estimates of the probability of breakage as a function of nominal overpressure are shown in Figure 30. Note that the breakage probabilities indicated are comparable to those of glass.

In calculating the breakage probabilities of the ceiling configurations 1 and 2, different values of the mean and variance of $\log_{10}(p_e/p_f)$ were used than were used for the walls. This is done to account for the transmission loss of the boom in passing through the attic structure. For ceilings the mean of $\log_{10}(p_e/p_f) = -.1609$

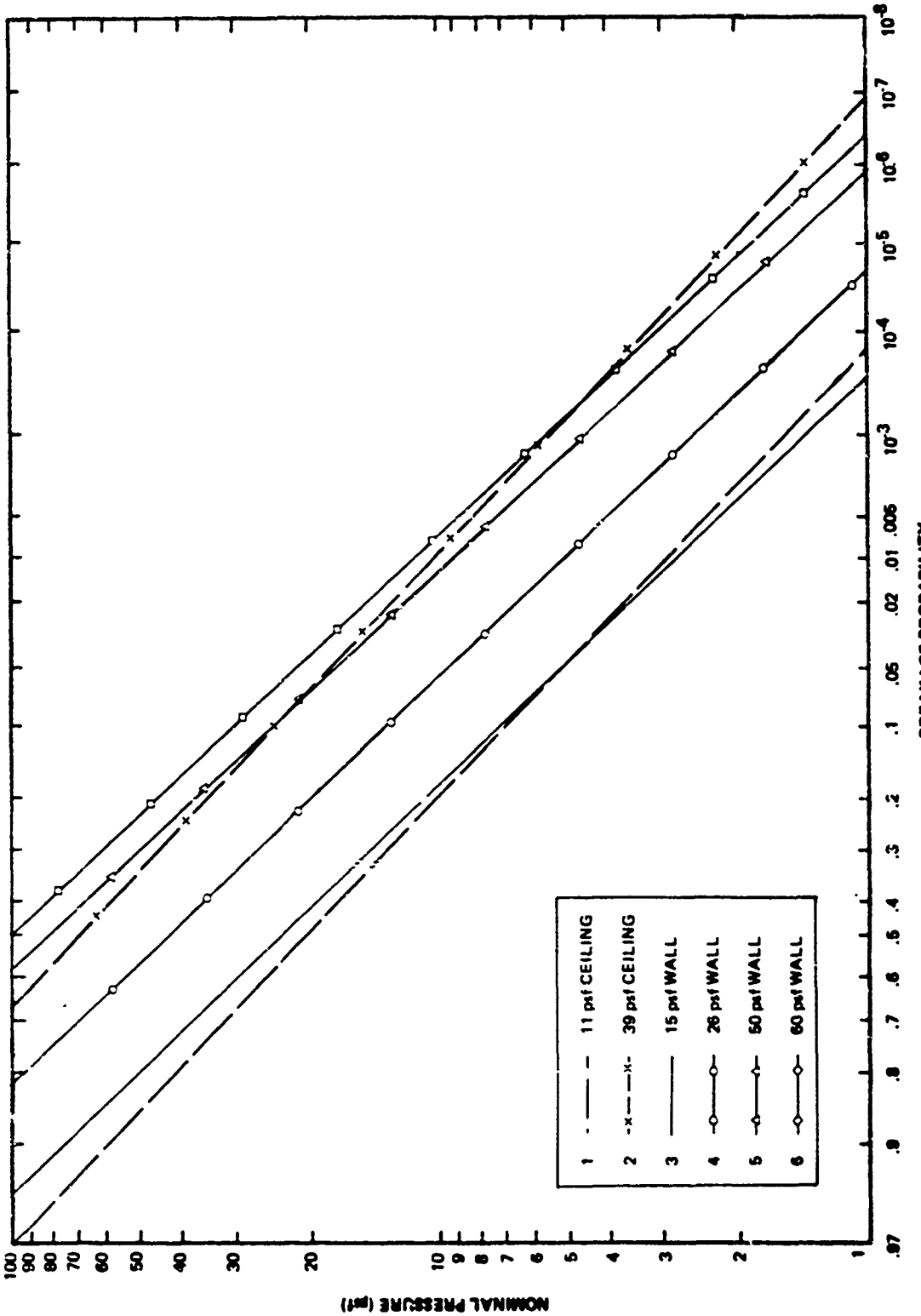

Figure 30. Breakage Probabilities for Plaster for All Flight Paths Equally Likely

and the variance of $\log_{10} (p_e/p_f) = .0029$. For the wall configurations the mean and variance of $\log_{10} (p_e/p_f)$ which were used for windows were again used. The dynamic amplification factor distribution found for the large window, Window 4, was used with the plaster calculations, since this window is comparable in size to a wall or ceiling. On the basis of the above procedures the graphs shown in Figure 30 resulted.

* * * * * * * * * * *

In summary, the estimated breakage probabilities for plaster, shown in Figure 30, are similar to the results found for glass. As in the case of glass there is a great deal of variation in the probability of breakage for the various configurations.

VII. BRIC-A-BRAC

For the purpose of this study bric-a-brac is defined as an assortment of miscellaneous ornamental articles, which sit on surfaces such as shelves or tables. Typical examples would be figurines, ashtrays, clocks, cup and saucer sets, or candlesticks. Not included in this definition are objects which hang from walls such as pictures and mirrors. The exclusion of hanging objects from this category is in keeping with earlier sonic boom claims categorization work [32].

By its very nature this type of sonic boom damage is very difficult to analyze. The objects which make up this category vary by orders of magnitude in the force needed to overturn or slide them. They also vary by orders of magnitude in their probability of breaking once they fall from their supporting surface. For one extreme, imagine a heavy steel disc paperweight sitting on a rubber mat in the middle of a table. For the other extreme, imagine a delicate saucer whose owner has balanced it on edge, precariously leaning on the wall of a narrow knick-knack shelf, with a concrete floor below. The steel paperweight would be immune to any sonic boom ever created, both in the matter of falling and also of breaking if it did fall. The precariously balanced saucer, however, would probably

break with any small disturbance such as a door slamming, a footfall, or a wind from opening a window.

The above examples point out three key factors:

- There is no "typical" piece of bric-a-brac.
- Pieces of bric-a-brac vary tremendously in their strength.
- The susceptibility of pieces of bric-a-brac to overturning or sliding off their supports depends to a large extent on how their owner places them.

It is apparent from the above discussion that bric-a-brac do not lend themselves well to a stress analysis, such as was used for glass windows. The determination of the probability of breakage of bric-a-brac will have to be based instead on claims data and on observations of bric-a-brac breakage during severe booms at White Sands. Our analysis extrapolates from these measured breakage probabilities by assuming a lognormal effective factor of safety holds, such as was observed for window glass.

The two measured breakage probabilities for bric-a-brac are indicated by the circles on Figure 31. The point at 2 psf is from the Edwards Air Force Base claims data [32]. The point at 38 psf is from the White Sands experiment.

The breakage probability shown at 2 psf of 8.8×10^{-7} was calculated by observing the ratio of bric-a-brac claims to window

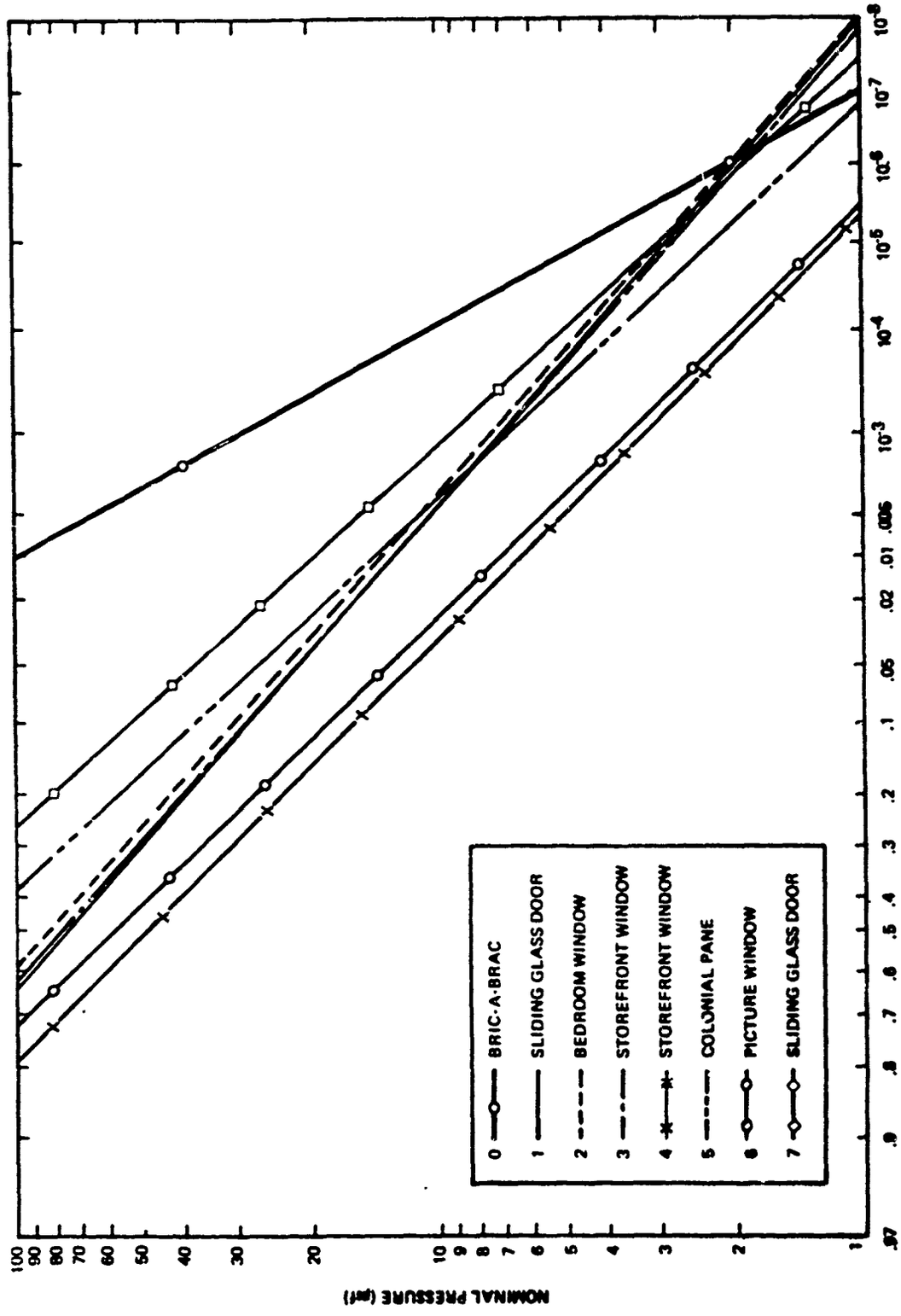

Figure 31. Breakage Probabilities for Bric-a-Brac for All Flight Paths Equally Likely

claims from the data in Table 25 to be 3/58. We also estimated that there are roughly twice the number of bric-a-brac items in an average home as there are windows, based on a count in the author's own home. We assumed the breakage probability of a typical window population to be 3.4×10^{-5}, as found in our previous studies. Thus multiplying these gave $(3.4 \times 10^{-5}) \times (3/58) \times (1/2) = 8.8 \times 10^{-7}$ as the bric-a-brac breakage probability.

The point at 38 psf indicating a breakage probability of 0.2 percent was derived from the White Sands data [30]. It was observed that 2 out of an estimated 900 pieces of bric-a-brac in the test houses were broken by a sonic boom with an overpressure of 38 psf.

In Figure 31 these two points are connected by a double line on a lognormal probability scale. This is the same scale that was used earlier in Figure 26 to display the probability of breakage of glass as a function of sonic boom nominal overpressure. The graphs for glass breakage are shown with single lines on the same graph for comparison. It can be observed from the very steep slope of the bric-a-brac line shown that the standard deviation of the effective factor of safety is much higher for bric-a-brac than it is for windows. This is as expected since, as discussed above, bric-a-brac has a much greater structural variation than does glass. The bric-a-brac line indicates that because of the very wide variation of strength and

Table 25. Damage Claim Tabulation for Edwards Air Force Base Sonic Boom Tests

Complaint Classification		Phase I								Phase II	
		June 3-12, 1966 Track at 245° Mag.		June 13-23, 1966 Track at 233° Mag.		Date Not Available		Total		Oct. 31, 1966-Jan. 17, 1967 Track at 245° Mag.	
Number	Type	Number	Percent	Number	Percent	Number	Percent	Number	Percent	Number	Percent
1	Glass - Window and/or Door	11	52.3	36	67.8	5	55.6	52	62.8	6	46.1
2	Glass - Miscellaneous	0	0	1	1.9	0	0	1	1.2	0	0
3	Plaster or Stucco - Cracks	4	19.0	3	5.7	1	11.1	8	9.6	2	15.4
4	Plaster or Stucco - Fallen	0	0	1	1.9	0	0	1	1.2	0	0
5	Structural	0	0	3	5.7	3	33.3	6	7.1	0	0
6	Fallen Object - Bric-a-Brac	1	4.8	1	1.9	0	0	2	2.4	1	7.7
7	Fallen Object - Miscellaneous	3	14.3	5	9.4	0	0	8	9.6	4	30.8
8	Miscellaneous	1	4.8	1	1.9	0	0	2	2.4	0	0
9	Noise Complaint - No Damage	0	0	2	3.8	0	0	2	2.4	0	0
10	Information Call - No Damage	1	4.8	0	0	0	0	1	1.2	0	0
	TOTAL	21	100.0	53	100.0	9	100.0	83	100.0	13	100.0

support condition there would be a breakage probability, comparable to the less susceptible glass, even at very low nominal overpressures, such as 1 psf. By the same token, however, it is unlikely that more than about 1 percent of the bric-a-brac boomed would be broken even for the highest overpressures.

* * * * * * * * * *

In summary, bric-a-brac breakage is generally less than glass for the normal range of sonic boom nominal overpressures. Estimates of bric-a-brac breakage probabilities are given by the line in Figure 31. However, it must be emphasized that the breakage probabilities for bric-a-brac exhibit large variations depending on the strength of the individual items and their support conditions.

VIII. BRICK

Brick is a far stronger material than glass or plaster and is generally not susceptible to sonic boom damage. For the sake of completeness, however, we are also considering brick in this report.

Common bricks are typically manufactured by heating rectangular prisms of clay or shale in a kiln. The processes used include the dry-press process, the stiff-mud process, and the soft-mud process [53]. In the dry-press process relatively dry clay mixes are used and the molding of bricks is done at high pressure. This results in all six surfaces being smooth and even with good uniformity among the bricks. In the stiff-mud process the clay mixture is more moist and it is extruded by a machine into a long ribbon with the cross-section of a brick. The ribbon is then cut by wires into brick-length pieces, leaving rough surfaces at the wire cuts. In the soft-mud process the brick is formed from a wet mix of clay under only slight pressure.

Various forms of kilns are used for firing the brick. In tunnel kilns the bricks are placed on cars and move slowly through the tunnel gradually reaching a temperature of about 2000°F, and then they are gradually cooled as they emerge. The tunnel kiln method of

firing results in very uniform bricks. Other kinds of kilns, however, results in more variation among bricks depending on where in the kiln the brick was fired. These other kilns include scove kilns, round kilns, continuous kilns, and permanent kilns. The brick may be classified as "top brick" from the top of the kiln, "body brick" from the center, or "bench brick" from the arches of the kiln. Variations in strength of bricks have practically no effect as far as sonic boom loading is concerned; the weak point in the brick structure is almost always the mortar.

Mortar consists of cement, lime, and sand combined in various proportions. The proportions used result in mortars with designations as M, S, N, O, and K as shown in Table 26. In general the compressive strength of the mortar increases with increasing proportions of cement. There is a trade-off, however, since mortars with more lime and less cement tend to be easier for bricklayers to apply.

For the purpose of this study we gathered data on the strength of mortars when used in wall assemblies subjected to uniform loading [37,54,55]. An analysis of the data, covering types M, N, O, and S mortars showed the probability density function of the strengths to be lognormally distributed with a mean modulus of rupture of 45.6 psi and a standard deviation of 16.9 psi. The distribution of the

Table 26. Approximate Ranges in Compressive Strength for Various Mortar Proportions and Types

Mortar Proportion [1]			ASTM Mortar Designation	Type of Lime or Cement	Approximate Compressive Strengths		
C	L	S [2]			*Min.*	*Max.*	*Average*
1	0	2-3	—	—	3800	4600	4200
1	¼	3	M	—	3000	3800	3400
1	½	4½	S	—	2300	3000	2600
1	1	6	N	Type S	1500	2400	1800
				Putty or Type N	800	1800	1200
1	2	9	O	Type S	750	1200	900
				Putty or Type N	350	750	500
0	1	3	—	Type S	125	400	200
				Putty or Type N	50	300	125
1MC	—	3	O	M.C., Type I	500	800	750
1MC	—	3	N	M.C., Type II	800	3000	1500
1	3	12	K	Type S	300	600	450

[1] C = Portland Cement; L = Lime; S = Sand; M.C. = Masonry Cement.
[2] Strength values include possible adjustment of 1:3 total cementitious-sand ratio by up to ±25%.

logarithms of the strengths had a mean of 1.6252 and a variance of .0324. On the basis of these data probability of failure of brick structures was calculated for sonic boom loading using the response probability density function technique.

The first calculation presented here should lay to rest once and for all any fears that people may have of sonic booms knocking down brick walls of homes. Table 27 from the nuclear effects literature [56] shows that it takes a pressure of 7 psi (1008 psf) to knock down a brick wall of a house. The most intense sonic booms deliberately created for test purposes were of the order of 100 psf. Even if one of these acts on the brick wall the breakage probability is 1.3×10^{-15}. With an astronomical probability like this we can say that for all practical purposes there is no chance of knocking down a brick wall of a home.

The question remains, however, of the probability of damage to other parts of more susceptible brick structures; for instance, cracking mortar on free-standing brick walls. The probability of such occurrences will be examined here using National Bureau of Standards data on tests of brick walls [57].

The four brick wall configurations analyzed are shown in Table 28. All the brick walls shown were tested by National Bureau of Standards using an air bag technique to create the pressure load.

Table 27. Conditions of Failure of Peak Overpressure-Sensitive Elements

Structural Element	Failure	Approximate Incident Blast Overpressure (psi)
Glass windows, large and small.	Shattering usually, occasional frame failure.	0.5–1.0
Corrugated asbestos siding	Shattering.	1.0–2.0
Corrugated steel or aluminum paneling.	Connection failure followed by buckling.	1.0–2.0
Wood siding panels, standard house construction.	Usually failure occurs at the main connections allowing a whole panel to be blown in.	1.0–2.0
Concrete or cinder-block wall panels 8 in. or 12 in. thick (not reinforced).	Shattering of the wall.	2.0–3.0
Brick Wall panel, 8 in. or 12 in. thick (not reinforced).	Shearing and flexure failures.	7.0–8.0

Table 28. Static Failure Pressures of Brick Wall Configurations

Number	Brick Description	Brick Width (in)	Brick Length (in)	Brick Height (in)	Modulus of Rupture (psi)	Mortar Type	Static Failure Pressure (psf)
1	Cream colored, extruded wire-cut units with 3 round cores	3.63	7.97	2.25	850	1:1:4	17.3
2	Red, extruded, wire-cut units with no cores	3.62	8.00	2.26	740	high-bond	57.6
3	Cream colored, extruded wire-cut units with 3 round cores	3.63	7.97	2.25	850	high-bond	83.5
4	Gray, extruded, wire-cut units with 5 oval cores	3.75	8.08	2.25	760	high-bond	158.4

All the walls were constructed of bricks with a nominal width of 4 inches. The static failure points indicated were when the first cracking of the mortar was observed. In each case two specimens were tested; the value shown in Table 28 is the lower of the two static failure pressures. All tests were performed on 4-foot wide by 8-foot high test panels. The mortar referred to in the table as 1:1:4 consisted (by volume) of one part of Type 1 portland cement, one part hydrated lime, and four parts sand. The mortar referred to in the table as "high-bond" contained one part (1 cubic foot) portland cement, one part (1 cubic foot) fine limestone (passing a No. 200 sieve), four parts (4 cubic feet) masonry sand, and four gallons of a polyvinylidene chloride additive called Saran̊ond.

The breakage probabilities for sonic boom loading of the four brick wall configurations were calculated using the response probability density function technique. The results are shown in Figure 32. Note that the breakage probabilities shown are generally lower than those for glass except for the 17.3 psf wall, which was not made from high-bond mortar. The results from the four wall cases shown and the house example make it appear extremely unlikely that any damage to brick structures would occur during supersonic overflights. It would be very unusual for anyone to have a free-standing 4-inch brick wall, and only one made from lower bond mortar would be more

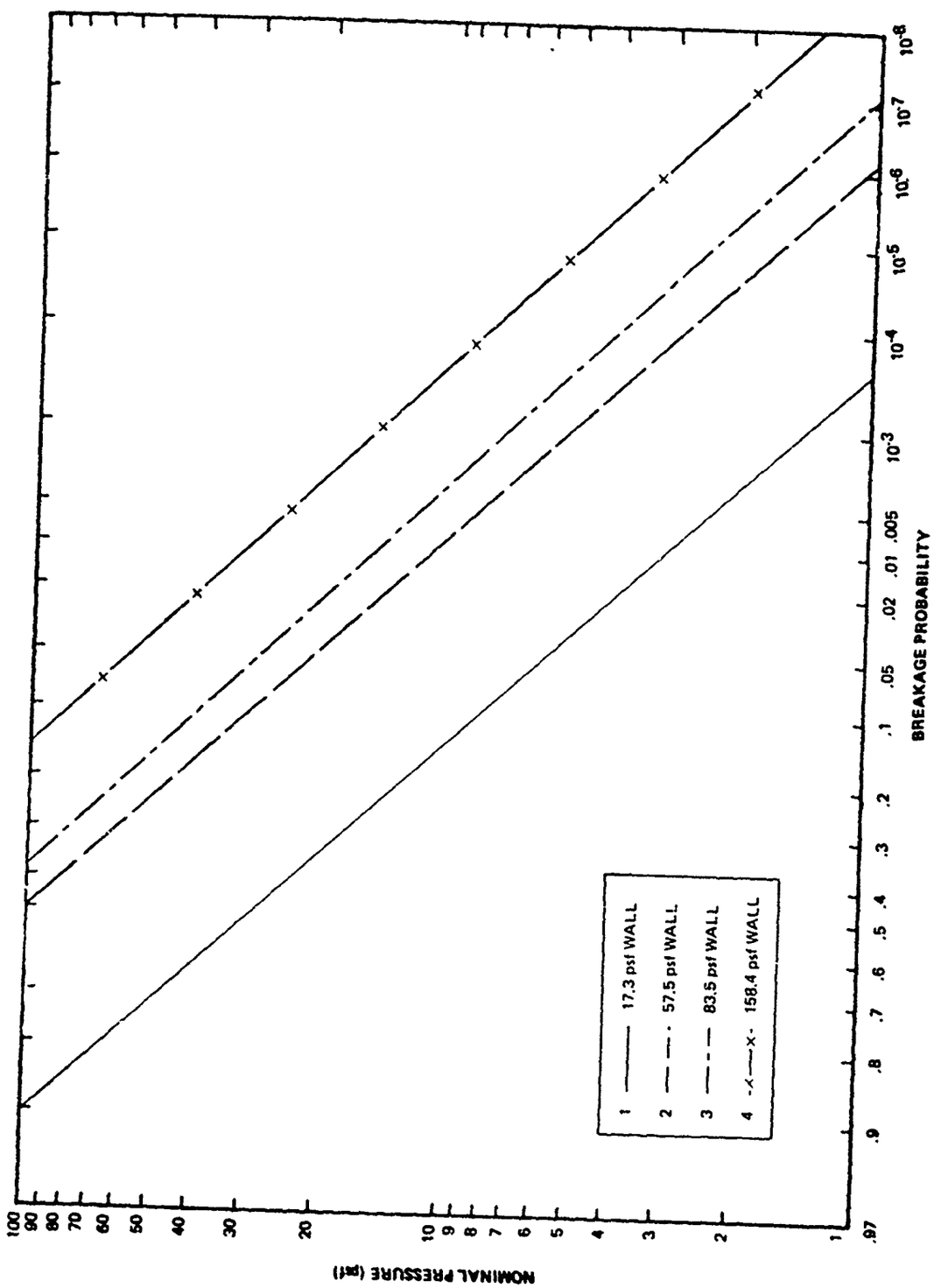

Figure 32. Breakage Probabilities for Free-Standing 4-Inch Brick Walls for All Flight Paths Equally Likely

susceptible than windows. In fact, the only damage to brick structures reported in the White Sands tests was that three bricks loosened below a window under a 38 psf boom.

* * * * * * * * * * * *

Structures made of brick are not very susceptible to sonic booms. For rare cases of free-standing brick walls the probability of breakage is generally somewhat lower than for windows.

IX. CONCLUSIONS

The analysis presented here has generally confirmed the findings from sonic boom claims experience. The most likely elements to break are windows, plaster, and bric-a-brac, and their likelihood of breaking increases with increasing overpressure.

The combined graph for the probability of breakage of glass, plaster, bric-a-brac, and brick is shown in Figure 33. It presents the results that had been shown earlier for the separate materials, except that the bric-a-brac curve has been broadened to indicate a range of probabilities at each overpressure typical of other materials. The curve for the brick wall with low strength mortar was eliminated, since it is not a very representative structure; it was merely a sample in a laboratory test rather than a real wall in use.

For sonic booms with a nominal overpressure of 1 psf, with all flight paths equally likely, the breakage probability ranges for the structural elements were as follows:

- Windows: 4×10^{-6} to 3×10^{-8}
- Plaster: 3×10^{-4} to 5×10^{-7}
- Bric-a-Brac: 1×10^{-6} to 1×10^{-8}
- Brick Walls: 6×10^{-7} to 1×10^{-9}.

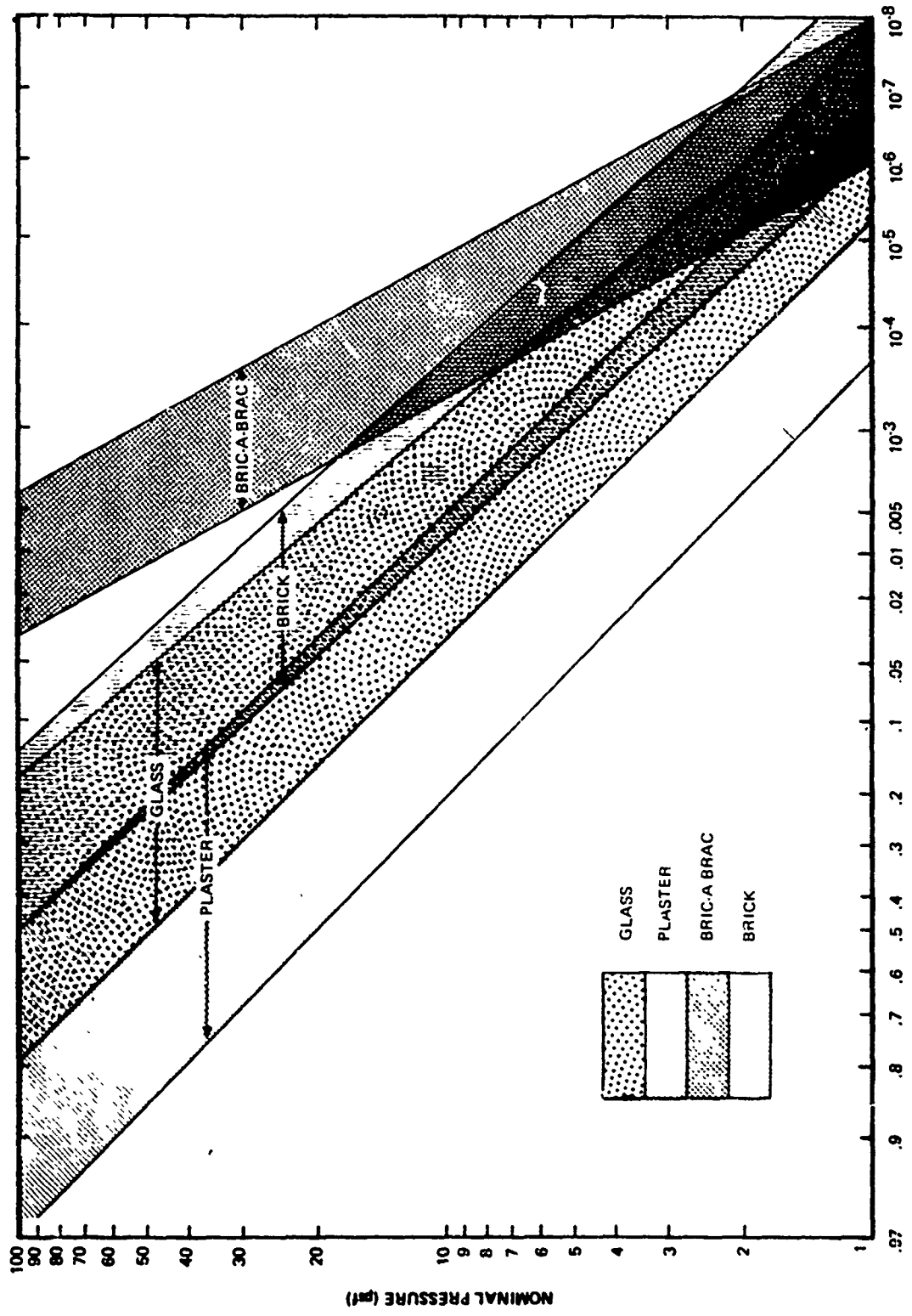

Figure 33. Ranges of Breakage Probabilities for Glass, Plaster, Bric-a-Brac, and Free-Standing Brick Walls of High-Bond Mortar

On the basis of the results of the study various measures can be suggested for reducing the probability of structural damage from supersonic overflights. These measures are summarized in Table 29 and listed below:

1. In planning flights—reducing nominal overpressures
2. In designing aircraft—
   (1) Increasing altitude capability
   (2) Decreasing weight
3. In designing window installations—
   (1) Reducing the width to thickness ratio
   (2) Reducing the lite size
   (3) Replacing cracked panes
   (4) Avoiding scratches during installation and cleaning
   (5) Placing windows so that they face away from the flight path of supersonic aircraft
   (6) Mounting windows carefully to avoid stress concentrations from direct contact with the glazer's points or looseness of the window in the sash
4. In designing plaster installations—
   (1) Stiffening walls and ceilings
   (2) Using higher strength plaster
   (3) Mixing plaster thoroughly with correct proportion of water during installation
5. In placement of bric-a-brac—avoiding precarious positioning of items near edges

Table 29. Measures to Reduce Sonic Boom Structural Breakage Rates

Material	Method	Model Parameter Affected	When Applied
All	Higher aircraft altitude	Nominal overpressure	Flight plans and plane designs
All	Decrease aircraft weight	Nominal overpressure	Plane design
Glass	Reduce window width to thickness ratio	Stress factor	Building code
Glass	Reduce lite size	Glass strength	Building design
Glass	Replace cracked panes	Percentage cracked panes	Maintenance
Glass	Avoid scratches	Glass strength	Maintenance
Glass	Face windows away from flight path	Angle of incidence	Building design
Plaster	Stiffer walls and ceiling	Breaking pressure	Building code
Plaster	Higher strength plaster	Breaking pressure	Building design
Plaster	More uniform plaster mixture	Breaking pressure	Installation
Bric-a-Brac	Avoid precarious placement	Overturning pressure	Placement
Brick	Thicker walls	Breaking pressure	Wall design
Brick	High-bond mortar	Breaking pressure	Installation

6. In designing brick walls—

(1) Using thicker walls

(2) Laying of bricks with high-bond mortar.

In conclusion, this report has estimated the probabilities of structural damage of various susceptible elements using the response probability density function technique. These probabilities were found to vary widely with the specific material configuration, but to consistently increase with increasing nominal overpressures. For all materials in good condition, breakage probabilities were found to be below .001 for a nominal overpressure of 1 psf. By using appropriate measures in aircraft design, flight planning, and material installation the probability of sonic boom structural damage can be significantly reduced.

LIST OF REFERENCES

1. Hershey, Robert L. and Higgins, Thomas H., "Statistical Prediction Model for Glass Breakage From Nominal Sonic Boom Loads," FAA Report No. FAA-RD-73-79, NTIS No. AD-763-594, January 1973.

2. Hershey, Robert L. Higgins, Thomas H., and Magrab, Edward B., "Application of the Response Probability Density Function Technique to Predicting the Probability of Sonic Boom Glass Breakage," Journal of the Acoustical Society of America, 1974.

3. Hershey, Robert L. and Higgins, Thomas H. "Design of Windows for Dynamic Loading," Sound and Vibration, March 1975.

4. Hershey, Robert L.. "Statistical Model of the Rupture of Brittle Rectangular Plates Under Loading by Transient Overpressures," Ph. D. Dissertation, the Catholic University of America, April 1973.

5. Hershey, Robert L. and Turner, Louie, "Aircraft Taxiing Noise Measurements," FAA Report No. FAA-RD-74-114, NTIS Report No. AD787-235, August 1976.

6. Hershey, Robert L., Kevala, Russ J., and Burns, Sharon L.. "Analysis of the Effects of Concorde Aircraft Noise on Historic Structures," FAA Report No. FAA-RD-75-118 NTIS No. ADA 017-082, July 1975.

7. Carlson, Harry W. and Maglieri, Domenic J.. "Review of Sonic Boom Generation Theory and Prediction Methods," Journal of the Acoustical Society of America, Volume 51, No. 2, February 1972.

8. Blume, John A., and Associates, "Structural Reaction Program National Sonic Boom Study Project," Supersonic Transport Development, Federal Aviation Agency, Washington, D.C., Prepared under Contract FA-SS-65-12, April 1965, SST-65-15, Volume 1 and Volume 2.

9. Wiggins, John H., Jr., "Effects of Sonic Boom," J. H. Wiggins Company, Palos Verdes, California, 1969.

10. Ting, L., and Pan, Y.S., "Incidence of N-Waves on Structures," Second Conference on Sonic Boom Research, NASA SP-180, May 1968, pp. 89-98.

11. Ting, L., and Kung, F., "Studies in the Diffraction of a Pulse by a Three-Dimensional Corner," Third Conference on Sonic Boom Research, NASA SP-255, October 1970, pp. 161-180.

12. Lowery, Richard L., and Andrews, Don K., "Acoustical and Vibrational Studies Relating to an Occurrence of Sonic Boom Induced Damage to a Window Glass in a Store Front," prepared under Contract No. NAS1-5813 by Andrews Associates, Inc., Oklahoma City, Oklahoma, for NASA, NASA CR-66170.

13. Wiggins, John H., Jr., "Phase A Status Report on the Theoretical Study of Structural Response to Near-Field and Far-Field Sonic Booms," under Contract No. AF49(638)-1777, Datacraft, Inc., August 3, 1966.

14. Seaman, L., "Response of Windows to Sonic Booms," Technical Report 7, Mechanics Department, Stanford Research Institute, Menlo Park, California, June 1967.

15. Crocker, M. J., and Hudson, R. R., "Structural Response to Sonic Booms," Journal of Sound and Vibration (1969), 9(3), 454-468.

16. Cheng, David H., "Some Dynamic Effects of Sonic Booms on Structural Elements," National Aeronautics and Space Administration, Langley Research Center, Langley Station, Hampton, Virginia, LWP-25, August 14, 1964.

17. Cheng, David H., "Dynamic Response of Structural Elements to Traveling N-Shaped Pressure Waves," National Aeronautics and Space Administration, Langley Research Center, Langley Station, Hampton, Virginia, LWP-47, September 15, 1965.

18. Pretlove, A.J., "Forced Vibration of a Rectangular Panel Backed by a Closed Rectangular Cavity," Journal of Sound and Vibration (1966) 3(3), 252-261.

19. Pretlove, A.J., "Acousto-Elastic Effects in the Response of Large Windows to Sonic Bangs," Journal of Sound and Vibration (1969) 9(3), 487-500.

20. Pretlove, A.J. and Bowler, J.F., "An Estimate of Sonic Boom Damage to Large Windows," Journal of Sound and Vibration (1972) 22(1), 107-112.

21. Clarkson, Brian L. and Mayes, William H., "Sonic Boom-Induced Building Structure Responses Including Damage," Journal of the Acoustical Society of America, Volume 51, No. 2, February 1972.

22. Bowles, R. and Sugarman, B., "The Strength and Deflection Characteristics of Large Rectangular Glass Panels Under Uniform Pressure," Glass Technology, Volume 3, No. 5, 1962.

23. Seely, Fred B., and Smith, James O., "Advanced Mechanics of Materials," New York, Wiley, 1952.

24. Timoshenko, S., and Woinowsky-Krieger, S., Theory of Plates and Shells, New York, McGraw-Hill, 1959.

25. Levy, Samuel, "Bending of Rectangular Plates With Large Deflections," National Bureau of Standards, No. 846, May 1942.

26. Hemp, W.S., "Elastic Direct Stresses and Deflections for Flat Rectangular Plates Under Uniformly Distributed Normal Pressure," Engineering Sciences Data Unit, 251-259 Regent Street, London, W1., R7Ad, approved for issue May 1971, Item No. 71013.

27. Timoshenko, S., and Young, D.H., "Vibration Problems in Engineering, New York, Van Nostrand, 1956.

28. Hilton, David, Huckel, Vera, Steiner, Roy, and Maglieri, Domenic, "Sonic Boom Exposures During FAA Community Response Studies Over a 6-Month Period in the Oklahoma City Area," National Aeronautics and Space Administration, NASA TN D-2539, December 1964.

29. Blume, John A., and Associates, "Structural Reaction Program National Sonic Boom Study Project," Supersonic Transport Development, Federal Aviation Agency, Contract FA-SS-65-12, SST 65-15, Volumes 1 and 2, April 1965.

30. Blume, John A., and Associates, "The Effects of Sonic Boom on Structural Behavior—A Supplementary Analysis Report," Federal Aviation Agency, SST Report NO-65-18, October 1965.

31. Kryter, Karl, et al, "Sonic Boom Experiments at Edwards Air Force Base," Stanford Research Institute, July 28, 1967.

32. Blume, John A., and Associates, "Response of Structures to Sonic Booms Produced by XB-70, B-58, and F-104 Aircraft," October 1967.

33. Lee, Lloyd A., "Additional Sonic Boom Data Related to Tests Conducted at White Sands, New Mexico, and Edwards Air Force Base," John A. Blume and Associates, August 1972.

34. Blume, John A., and Associates, "Response of Structures to Sonic Booms Produced by XB-70, B-58, and F-104 Aircraft Based on Sonic Boom Experiments at Edwards Air Force Base," October 1967.

35. Wozencraft, J.M. and Jacobs, I.M., "Principles of Communication Engineering," New York, Wiley, 1965.

36. Unpublished data from Libbey-Owens-Ford Company, August 1972.

37. National Concrete Masonry Association, "Comments on Detailed Structural Analysis for the Design of Load Bearing Concrete Masonry."

38. Copeland, R.E. and Saxer, E.L., "Tests of Structural Bond of Masonry Mortars to Concrete Block," Proceedings, American Concrete Institute, Vol. 61, No. 11, November 1964.

39. Hershey, Robert L., "Analysis of the Difference Between log Mean and Mean log Averaging," Journal of the Acoustical Society of America, Vol. 51, No. 4, April 1972.

40. Shand, E.B., Glass Engineering Handbook, McGraw-Hill, 1958.

41. Wiederhorn, S.M., "Influence of Water Vapor on Crack Propagation in Soda-Lime Glass," Journal of the American Ceramic Society, Vol. 50, No. 8, August 1967.

42. White, R., "Effects of Repetitive Sonic Booms on Glass Breakage," Wyle Laboratories for Federal Aviation Administration, No. FAA-RD-72-43, April 1972.

43. Higgins, Thomas H., "Analysis of U.S. Air Force SR-71 Sonic Boom Damage Complaints and Flight Data," presented to the Committee on SST-Sonic Boom, NAS-NRC, November 1967.

44. Higgins, Thomas H., "A Survey of Sonic Boom Community Overflight Program Overpressure Distribution, Community Reaction, and Material Failure Data Related to the Supersonic Transport," Federal Aviation Administration, April 1967.

45. Maglieri, Domenic J., et al, "Ground Measurements of Shock Wave Pressure for Fighter Airplanes Flying at Very Low Altitudes and Comments on Associated Response Phenomena," National Aeronautics and Space Administration, Langley Research Center, Technical Memorandum X-611, December 1961.

46. Leigh, Barry R. "Lifetime Concept of Plaster Panels Subjected to Sonic Boom," UTIAS Technical Note No. 191, University of Toronto, July 1974.

47. Diehl, John R., "Manual of Lathing and Plastering," National Bureau for Lathing and Plastering, 1965.

48. Soroko I. and Sereda, P.J., "Interrelation of Hardness, Modulus of Elasticity and Porosity in Various Gypsum Systems," Journal of the American Ceramic Society, Vol. 5, No. 6, June 1968.

49. U.S. Gypsum Company, "Casting With Plaster and Hydrocal Gypsum Cements," IGL Bulletin No. 350, Chicago, 1970.

50. U.S. Gypsum Company, Correspondence, April 1974.

51. Arde Associates, "Response of Structures to Aircraft Generated Shock Waves," WADC Technical Report 58-169, April 1959.

52. Wiss, Janney, Elstner and Associates, "Transverse Load Tests of Plastered Partitions for the Gypsum Association," October 1966.

53. Plummer and Reardon, "Principles of Brick Engineering Handbook of Design," Structural Clay Products Institute.

54. Fishburn, Cyrus C., "Effect of Mortar Properties on Strength of Masonry," National Bureau of Standards, Monograph 36, 1961.

55. Copeland, R. E. and Saxer, E. L., "Tests of Structural Bond of Masonry Mortars to Concrete Block," Proceedings. American Concrete Institute, Vol. 61, No. 11, November 1964.

56. U.S. Department of Defense, "The Effects of Nuclear Weapons." Table 6.6, p. 232, 1957.

57. Yokel, F. Y., Mathey, R. G., and Dikkers, R. D., "Strength of Masonry Walls Under Compressive and Transverse Loads." Building Science Series 34, National Bureau of Standards. March 1971.

LIST OF SYMBOLS

a	length of window (inches)
A	area of window (square feet)
b	width of window (inches)
$DAF = \sigma_m/\sigma_d$	dynamic amplification factor
E( )	expected value (mean) of random variable
f_o	natural frequency of window (Hz)
F	statistic used in testing for differences between groups
h	thickness of window (inches)
$I = P_f T/2$	impulse of a sonic boom signature
$I_o pos = p_f T/4$	impulse of positive half of a sonic boom signature
n	number of factors of the sensitivity random variable
N_e	effective factor of safety
p_e	peak external overpressure (psf)
p_{e1}	peak external overpressure measured on the north wall of Structure W4 (psf)
p_{e2}	peak external overpressure measured on the south wall of Structure W4 (psf)

p_f	peak free field overpressure (psf)
p_G	material breaking pressure (psf)
p_i	peak internal overpressure (psf)
p_{net}	peak net overpressure on window (psf)
p_o	nominal overpressure (psf)
p_s	static pressure (psf)
P	probability of glass breakage for the model population
P_C	probability of breakage of cracked glass
P_H	probability of breakage of glass in good condition
q	p_i/p_e internal pressure ratio
$\Delta t_o pos$	duration of the positive half of the sonic boom signature
t_r	rise time of the free field pressure waveform
T	total duration of the sonic boom signature
Var ( )	variance of a random variable
Y	Young's modulus of elasticity (psi)
z	normally distributed random variable with zero mean and unit variance
θ	flight path angle
μ	mean of random variable
ν	Poisson's ratio

ρ	mass density
σ	standard deviation of random variable
σ_d	dynamic stress (psi)
σ_G	strength of material (psi)
σ_m	Maximum stress (psi)
σ_s	static stress (psi)